2016

Wetting kinetics in forced spreading

Amer Mohammad Al-Shareef

Department: Chemical and Biochemical Engineering

WETTING KINETICS IN FORCED SPREADING

by

AMER MOHAMMAD AL-SHAREEF

A DISSERTATION

Presented to the Faculty of the Graduate School of the

MISSOURI UNIVERSITY OF SCIENCE AND TECHNOLOGY

In Partial Fulfillment of the Requirements for the Degree

DOCTOR OF PHILOSOPHY

in

CHEMICAL ENGINEERING

2015

Approved by

Parthasakha Neogi, Advisor
Muthanna H. Al-Dahhan
Baojun Bai
Gearoid Mac Sithigh
Joontaek Park

PUBLICATION DISSERTATION OPTION

This dissertation has been prepared according to the format and style used by Missouri University of Science and Technology. It consists of the following articles that have been submitted for publication as following:

Pages 18 to 37 “Force based dynamic contact angles and wetting kinetics on a Wilhelmy plate“. It has been accepted and published in *Chemical Engineering Science Journal.*

Pages 38 to 74 “Wetting kinetics of polymer solution and force based contact angles“. It is under journal review.

Pages 75 to 107 “Dynamic contact angles in liquid-liquid-solid system“. It is under journal review.

Pages 108 to 135 “Dynamic contact angles in oil–aqueous polymer solutions”. It will be submitted for journal review.

ABSTRACT

Under dynamic conditions, the dynamic contact angle (the angle that the liquid makes with the solid) of a liquid on a solid surface varies dramatically with substrate velocity from its equilibrium value. Experimental data of the dynamic contact angles for polydimethylsiloxane (PDMS or silicone oil) under air on a glass substrate coated with teflon, for water under PDMS, for solutions of the polymer polyethylene oxide (PEO) under air, for solutions of PEO under PDMS, were obtained to simulate and understand the systems of brine or brine containing a polymer displacing viscous crude. A variety of solid substrates were used other than above to displace oil with the object that the equilibrium contact angles ~ 90º. The method used was that of a plate immersed or withdrawn from a pool of liquid, and the machine (Cahn-Thermo) calculates for us the dynamic advancing and receding contact angles. The dynamic contact angles determine the basic driving forces such as capillary pressures. The data were correlated with a number of available models. In most cases, the models were developed further to fit the requirements of various cases. In general, it is necessary for the model to include fluid flow, interfacial phenomena, and rheology. Photography was used to verify cases of entrainment and instability. One object of the present work was to determine the contribution of the non-Newtonian nature of the PEO solution. For the PEO solution under oil (PDMS) no obvious signs are observed although solutions at high polymer concentrations, that is, high elasticity, show some anomalous effects. However, it is not possible to conclude that shear thinning effects will be absent in all cases since a criterion is established here that shows under what condition the above may not hold.

ACKNOWLEDGMENTS

First of all, I would like to express my sincere gratitude and deep appreciation to my adviser Professor Dr. Parthasakha Neogi for his guidance and encouragement. Over the years of my research, he has been so enthused, dedicated, patient and understanding as distinguished professor. I am so excited to work with him, and this work would not have been possible without him.

Also I would like to extend my appreciation to the Professors that served on my dissertation committee : Dr. Muthanna Al-Dahhan, Dr. Baojun Bai, Dr. Gearoid Mac-Sithigh, and Dr. Joontaek Park, for their advice and fruitful discussion.

I would like to thank the faculty and staff in chemical and biochemical engineering department at Missouri University of Science and Technology for their assistance, contribution to my research, and I would like to say my experience at Missouri S&T has been simply great.

I am thankful to Elmergib University, the Higher Education Ministry in Libya and Canadian Bureau for International Education (CBIE) for their support through the Libyan-North American Scholarship Program (LNASP).

In the end, I could not express my deepest gratitude to my parents, Salma and in memory of Mohammad, and my beloved wife, Haifa, for their unconditional support, understanding, love, and encouragement.

TABLE OF CONTENTS

Page

LIST OF ILLUSTRATIONS

Page

SECTION

PAPER III

PAPER IV

LIST OF TABLES

NOMENCLATURE

Symbol	Description
A	displaced fluid (silicone oil).
B	displacing fluid (water).
Ca	capillary number.
g	the gravitational constant, 9.8 m/sec^2
H	the length below the liquid, mm
h	the film thickness, mm
P	the perimeter P, mm
$PDMS$	polydimethylsiloxane.
PET	polyethylene terephthalate.
PVC	polyvinyl chloride.
R	viscosity ratio.
THF	tetrahydrofuran.
U	the velocity of the substrate, μm/sec.
v_r	the velocity component in r-direction, μm/sec.
v_θ	the velocity component in θ-direction, μm/sec.
W	the weight of the plate, mg.
x	the vertical direction, mm
γ	surface tension, (mN/m)
γ_{LV}	liquid-vapor surface tension, (mN/m)
γ_{SL}	solid-liquid surface tension, (mN/m)
γ_{SV}	solid-vapor surface tension, (mN/m)
μ	viscosity, cp.

μ_o	zero shear viscosity of the polymer, cp.
μ_B	viscosity of the displacing fluid, cp.
μ_A	viscosity of the displaced fluid, cp.
π	constant (3.1415)
θ	the contact angle, degree
α	dynamic contact angle, (degree)
λ	equilibrium contact angle (degree)
$\lambda_a°$	advancing equilibrium contact angle, (degree)
$\lambda_r°$	receding equilibrium contact angle, (degree)
ρ_L	the density of the liquid, kg/m^3
ε	singularity, the ratio of micro length scale to the macro length scale.
π_e	the spreading pressure.

1. INTRODUCTION

1.1. EQUILIBRIUM CONTACT ANGLE

One of the daily observations is that the raindrops fall and then spread on the automotive windshield. This phenomenon is known as spontaneous spreading of water droplets and the wetting physics here follows the Young–Dupré equation Eq. (1.1)

$$\gamma_{LV} \cos\lambda = \gamma_{SV} - \gamma_{SL} \tag{1.1}$$

Eq. (1.1) can be viewed as force balance in the horizontal direction as shown in Figure 1.1. It can also be obtained by minimizing free energy of the system. Equilibrium contact angle λ is also known as static contact angle. Figure 1.1 illustrates three different behaviors of the liquid on the solid surface, the first one from the left shows small contact angle or hydrophilic surface and the liquid preferentially wets the surface of the solid at $\lambda < 90°$, in the middle where $\lambda = 90°$ it is called hydrophobic surface or non-wetting liquid, the last one which shows bead or a complete sphere that is known as super hydrophobic surface where the wetting of the surface is impossible (Miller & Neogi, 2007; Adamson & Gast, 1997). The case of $\lambda = 0°$ is that of a wetting liquid. In this case the drop has no equilibrium configuration.

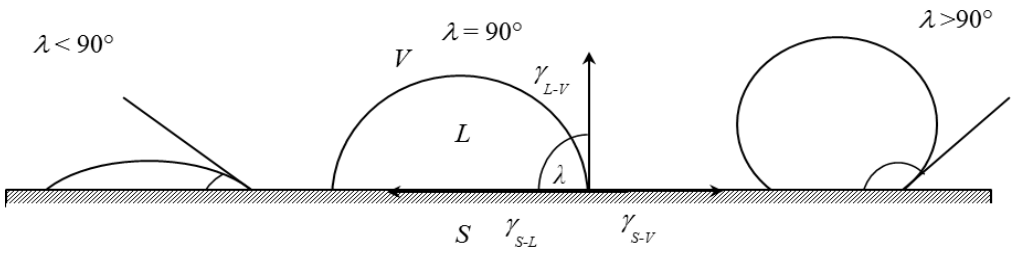

Figure 1.1. Different behaviors of drop on a solid surface

1.2. CONTACT ANGLE HYSTERESIS

Contact angle hysteresis is one of the most important phenomena in the pre-dynamic wetting for liquid droplets on modified or unmodified substrates. There are two well-known features in the hysteresis, the first one is the advancing static contact angle λ_a which defines the maximum contact angle achievable before the contact line starts to move forward and the other one is receding static contact angle λ_r the minimum contact angle achievable before the contact line starts to retract, and shows $\lambda_a > \lambda_r$. The common factors that cause hysteresis are, surface roughness, surface contamination, surface heterogeneity, and the adsorption of the liquid on the solid surface (Miller&Neogi, 2007).

1.2.1. Tilting Surface Method. This case is similar to the raindrop resting on the windshield which is an inclined surface; the gravity deforms the drops which form an asymmetric shape. When the droplet starts to slide on the tilted surface the contact angle in the front will reach to the maximum that is advancing static contact angle as shown in Figure 1.2 and the contact angle in the back shows the minimum that is receding static contact angle.

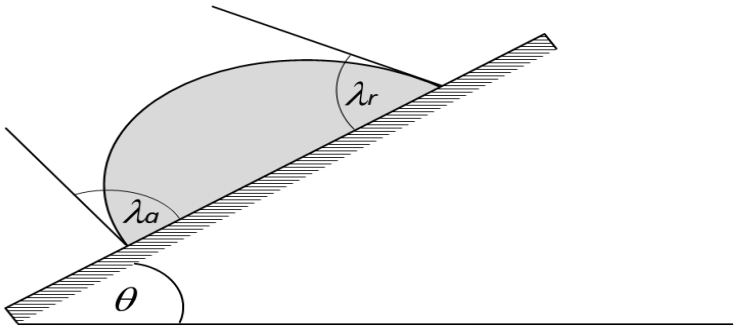

Figure 1.2. Gravity driven droplet of liquid on an inclined surface.

1.2.2. Increased and Reduced Volume Method. Another method also can be used here where a liquid drop is deposited on a horizontal flat surface. It is used to measure the contact angle hysteresis by adding or removing the liquid using a syringe. In advancing, it is required to add the liquid using syringe. As a result the volume will increase and the advanced static contact angle will be seen as in Figure 1.3A. On the other hand, in receding case, the liquid drop will be sucked out using the syringe as illustrated in Figure 1.3B, and the volume of the drop will be reduced to the minimum level and receding static contact angle can be observed, and follows $\lambda_a > \lambda_r$ and the contact angle hysteresis here is the difference between the two.

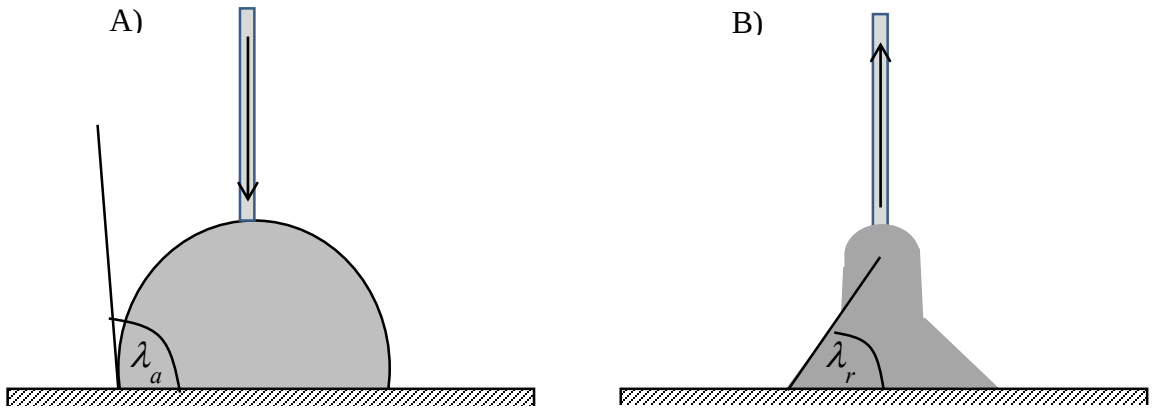

Figure 1.3. A) Advancing static contact angle B) Receding static contact angle, both on horizontal flat surface by adding and removing liquid volume respectively.

1.3. SURFACE TENSION FORCES

When a liquid drop is resting on horizontal flat solid surface, the shape of the drop is determined by the surface tension of the liquid. For example, the interactions of the water molecules in the drop are different according to their locations either in the bulk or at the surface. The adjacent molecules interact with each other in the bulk in all directions and the net force is zero, unlike the molecules at the surface that do not have neighbors as that in the bulk. This is the main reason in rearrangement of the forces among the molecules at the liquid surface resulting in increased surface energy. Those intermolecular forces work as bridge between liquid molecules as shown in Figure 1.4, the surface tension of the liquid is responsible for the shape of the interface.

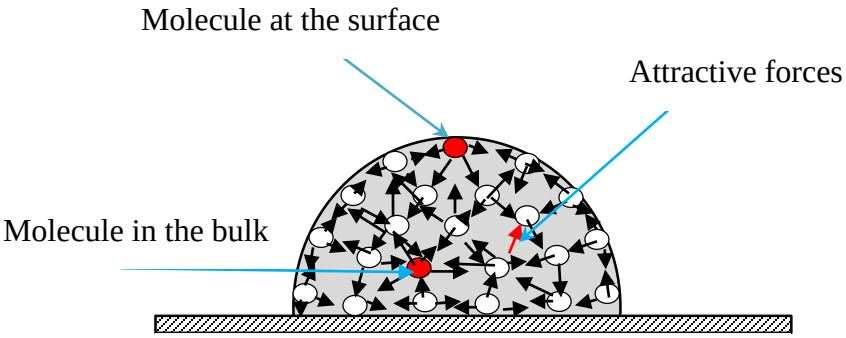

Figure 1.4. Interactions of the molecules at the surface and in the bulk of the liquid drop.

1.4. PRECURSOR FILM

When a small droplet of wetting liquid is deposited on a solid surface there are at least three to four regions that appear along the contact line as illustrated in Figure 1.5, Macroscopic front, wedge region, transition zone, and precursor film and the latter is a very thin film ahead of the wedge region (Derjaguin, 1940). The thin film has an added potential in form of disjoining pressure Π which is a function of local film thickness h, measurable as long as $h < 0.1\mu m$. Disjoining pressure arises out of wall effects on the thermodynamic potential. Frumkin (1938) and Derjaguin (1940) showed that

$$\cos\lambda = 1 - \frac{1}{\gamma_L}\int_{h_o}^{\infty} \Pi(h)dh \tag{1.2}$$

where $\Pi(h)$ refers to the disjoining pressure as a function of the equilibrium film thickness h, and the film thickness of the precursor film h_o has to be determined from other constraints, the alternate to Eq. (1.2) is to rewrite Eq. (1.1) but this time to γ_{sv} is added another term dealing to the disjoining pressure (Brochard-Wyart et al., 1991).

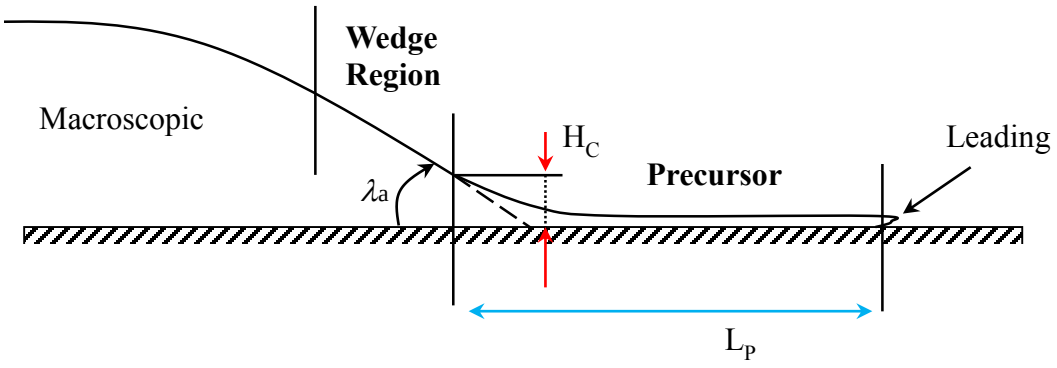

Figure 1.5. A spreading of wetting liquid on the solid surface shows the locations of the wedge region, transition zone, and precursor film.

1.5. DYNAMIC CONTACT ANGLES

1.5.1. Non-Equilibrium Contact Angles. If a small drop of liquid is placed on horizontal solid surface and is allowed to spread, then the contact angle observed is the dynamic contact angle $\alpha_a > \lambda_a$. Drop is less than 10μl so that gravity is not important and microscopy is used to take measurements. Blake (1993) assumed that Eq. (1.1) was not valid in non-equilibrium situations, etc. Bascom et al. (1964) showed a profile like Figure 1.5 where the film thickness drops very steeply near the contact line and then levels off to subtend zero contact angle at the contact line in keeping with the fact that a wetting liquid was being investigated.

1.5.2. Wilhelmy Plate Method. The classical measurement of the dynamic contact angles were obtained photographically based on the profile and the shape of the meniscus in capillary tube (Fermigier & Jenffer, 1991) or by using the Wilhelmy plate (Gutoff & Kendrick, 1982).

In the present work, the technique is force based, and also can be used to measure the surface tension and interfacial tension. Dynamic contact angle is different from equilibrium contact angle $\alpha_a > \lambda_a$ and $\alpha_r < \lambda_r$. A vertical plate is made of platinum or glass and brought in contact with the liquid. The Cahn microbalance device detects weight of the plate, buoyancy force, and the wetting force, and there are some input parameters needed here such as surface tension, width and the thickness of the plate. The Cahn machine calculates the advancing and receding dynamic contact angles, the total net force on the plate is illustrated in Eq. (1.3)

$$F = W - HP\rho_L g + P\gamma\cos\alpha \tag{1.3}$$

the first term from the right is *W*, that is the weight of the plate and *H* is the distance travelled by the plate in the liquid, *P* is the perimeter, ρ_L is the density of the lower phase, *g* is the acceleration, and γ is the surface tension. The second term describes the buoyancy force, and the third term the wetting force. Figure 1.6 and 1.7 describe one cycle for the Wilhelmy plate measurements (I) The force per wetted length is set to be zero and the substrate is plunged into the liquid surface. (II) The jump denotes the capillary effect, but it is difficult to quantify. However, we know the equation of line in (III) which is backed to obtain the jump $P.\gamma.\cos\alpha$, so that the plate is travelling further and the buoyancy force is increased. However, the total net force is decreased. (IV) The plate is dragged out of the liquid and returned to the original location. Figure 1.8 shows actual data from Cahn machine using Wilhelmy plate.

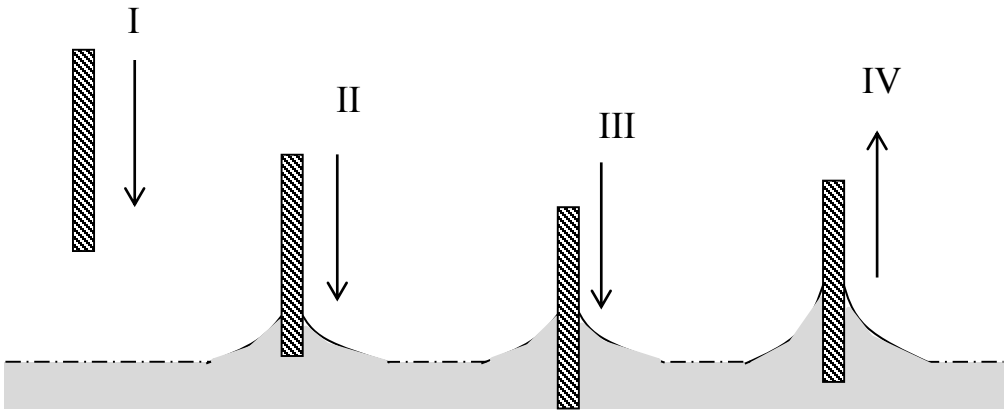

Figure 1.6. Wilhelmy plate pulled (in or out) the pool of liquid at constant plate velocity.

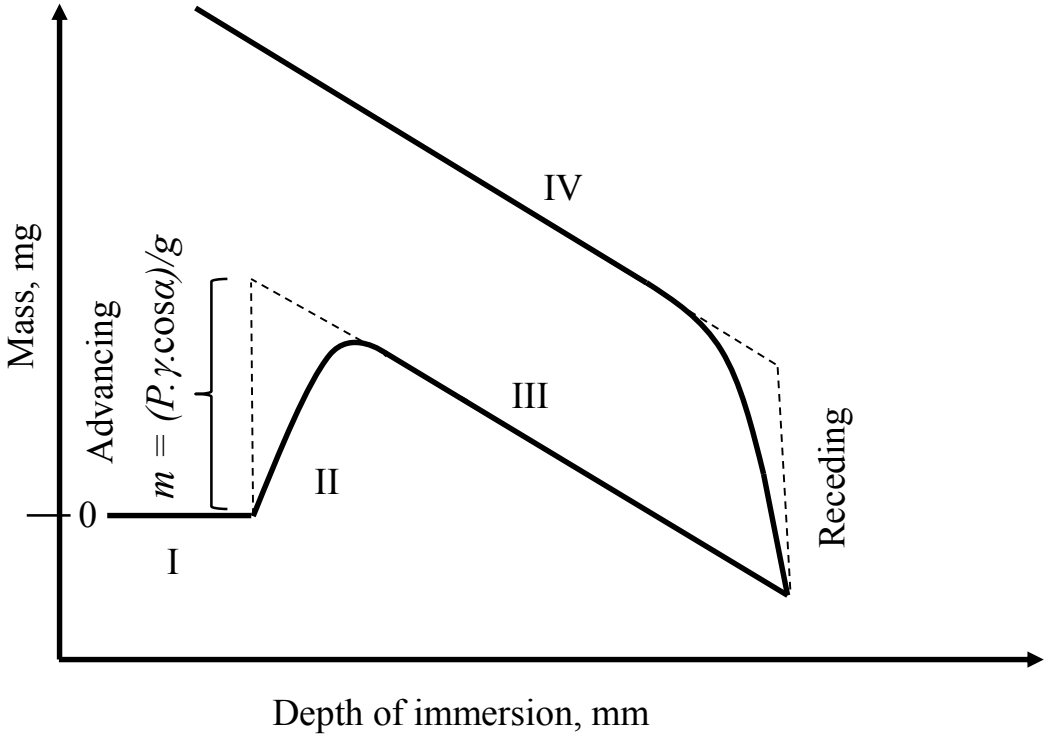

Figure 1.7. Force versus distance through travelling of the plate at constant velocity.

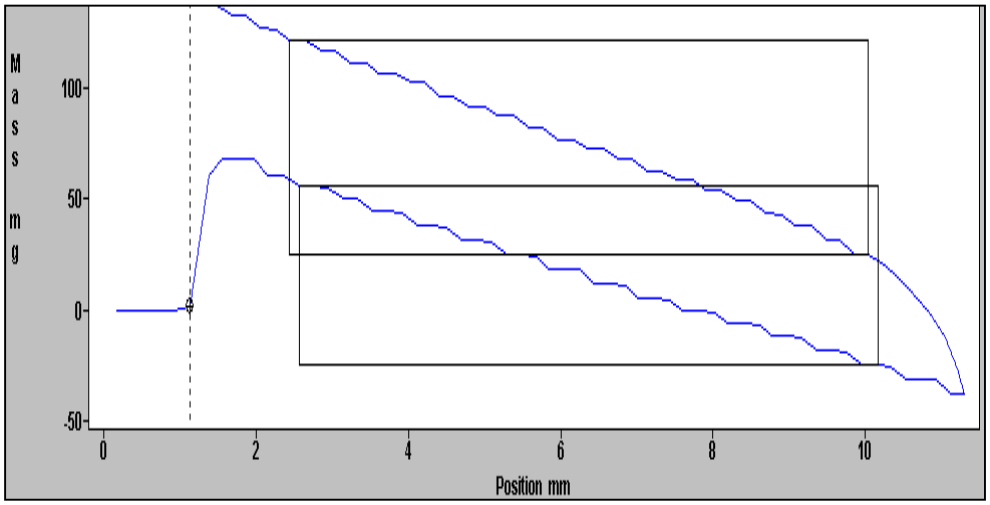

Figure 1.8. Actual data using force based Wilhelmy plate.

1.5.3. Advancing and Receding Dynamic Contact Angles. Figure1.9 shows all the contact angles as a function of the velocities. λ_a and λ_r are the advancing equilibrium contact angle and the receding equilibrium contact angle respectively, and the difference is what is often called the contact angle hysteresis. In the Figure below α_a and α_r are the advancing and receding dynamic contact angles respectively under dynamic conditions (Miller & Neogi, 2007).

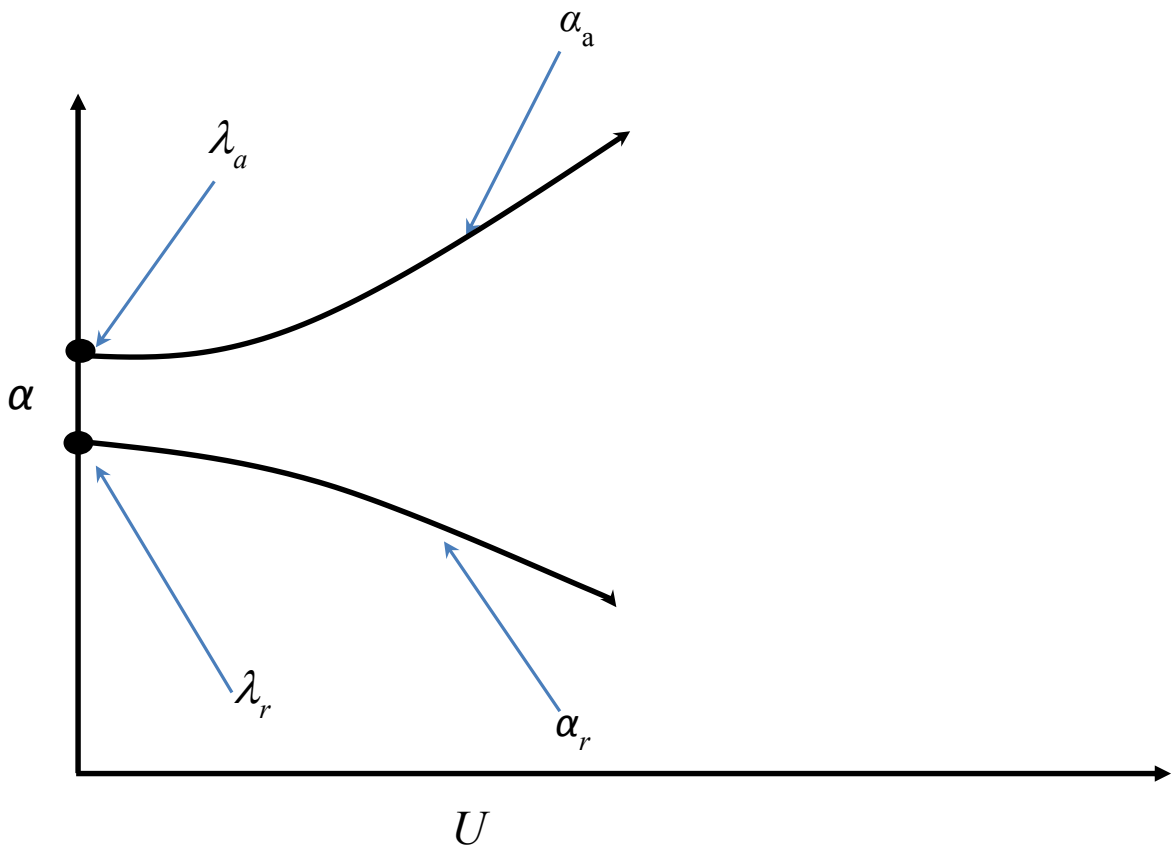

Figure 1.9. Advancing and receding dynamic contact angles versus the velocity of the substrate

1.6. ENTRAINMENT

Entrainment is one of the common problems that arise in various applications of chemical and petroleum industries. In simple words the entrainment occurs when the advancing fluid invades and entrains the receding fluid at sufficiently large displacing velocities. For instance, oil entrainment by water or gas flooding in the reservoir that causes some oil left behind. However, that entrainment decreases the oil recovery and reduces the efficiency of the oil production from petroleum reservoirs.

Entrainment in receding contact angles has been explained by de Gennes (1986) and has been verified experimentally by Quéré (1991). de Gennes shows a fold in the plot of α versus *Ca* in the receding contact angles, this fold has a nose which is the limit of the minimum receding contact angle. Therefore, there is no solution beyond this limit and entrainment takes place. This gives rise to dip coating which is the basic coating flow (Miller & Neogi, 2007). On entrainment, Cahn Thermo shows the dynamic contact angles to be zeros. Quéré (1991) shows that the entrainment occurs only at critical velocity as predicted by de Gennes (1986). The coating thickness as a function of plate velocity has been given by Landau and Levich (1942).

Entrainment in the advancing case also happens. First, the advancing contact lines α reaches 180°, this is followed by a period of instability (Blake & Ruschak, 1979), and then entrainment takes place at the highest velocity.

1.7. HYDRODYNAMIC THEORY (HD)

Theoretical investigations have been studied on the hydrodynamic theory in the form to make a relationship of the dynamic contact angle to the capillary number in two different scenarios. In the first, lubrication theory approximation is used under which the

flow field is given by $v_x(z)$ only, in other words, the lubrication theory approximation shows that the only significant term is $\frac{dv_x}{dz}$ and it will be discussed later. The equations of motion and continuity are solved together with a slip or cut-off boundary condition to eliminate the contact line singularity. This gives us a small length scale ε, the dimensionless slip or cut-off length. It is now possible to solve for the profile shape and hence the dynamic contact angle using matched asymptotic expansions using ε as the small quantity. The extrapolation of the outer solution to the interface is α (Neogi & Miller, 1982, 1983).

However, it is also possible to work with the velocity profile in terms of local film thickness h. Then using an energy balance the viscous dissipation in the wedge is equated to the surface work done (less an equilibrium contribution) (de Gennes, 1984). The velocity profile is used to calculate the viscous dissipation using $h = \alpha.x$ at this stage. On equating the viscous dissipation to surface work an expression for α in terms of capillary number is obtained.

In the other scenario, a wedge of much larger angle is considered where the lubrication theory cannot be applied. The wedge angle is at equilibrium, λ, and it is perturbed to find α from the profile (Cox, 1986).

1.8. APPLICATIONS IN ENHANCED OIL RECOVERY

We are interested here in problems in recovering crude petroleum oil from underground reservoirs. In the first stage of oil recovery (primary) the oil is displaced from the reservoir into the wellbore and up to the surface under its own pressure. In the second stage, an external fluid such as water or gas is injected into the reservoir through injection wells that have fluid communication with the production wells. The purpose of secondary

oil recovery is to maintain reservoir pressure and to displace hydrocarbons towards the wellbore. The most common secondary recovery technique is waterflooding (Craig, 1971). After the secondary oil recovery process has been exhausted, about two-third of the original oil in place (OOIP) is left behind. Most of the enhanced oil recovery (EOR) methods aim at recovering some of this oil (Green & Wilhite, 1998). The reasons for the instability to recover the crude oil fall into two categories, macro and micro.

1.8.1. Macroscale Oil Displacement. There are mechanisms operating at the macro-level category. The reservoir is stratified with some strata having high permeabilities and some having low permeabilities. The brine flood displaces the oil in the high permeability zones leaving oil in the low permeability zones untouched (Bai et al., 2007a; Bai et al., 2007b). Even in a reservoir of uniform permeability, uniform displacement can breakdown. When displacing fluid is less viscous than the crude, the less viscous fluid penetrates the oil in places. This feature which is called viscous fingering, and is shown schematically in Figure 1.10. Viscous fingering will lead to poor sweep efficiencies (Neogi, 1987) and here the ratio of viscosities of the two fluids is called the adverse mobility ratio.

To remedy this situation, a polymer is added to thicken the brine. Currently the favored polymer is partially hydrolyzed polyacrylamide (HPAM). Foams are gaining favor for imparting stability to a drive as they are less expensive than polymer and can be effective. Different types of polymers have been studied and here we investigate new trend of special kind of polymers which provide new features in terms of the elasticity and other rhological properties .

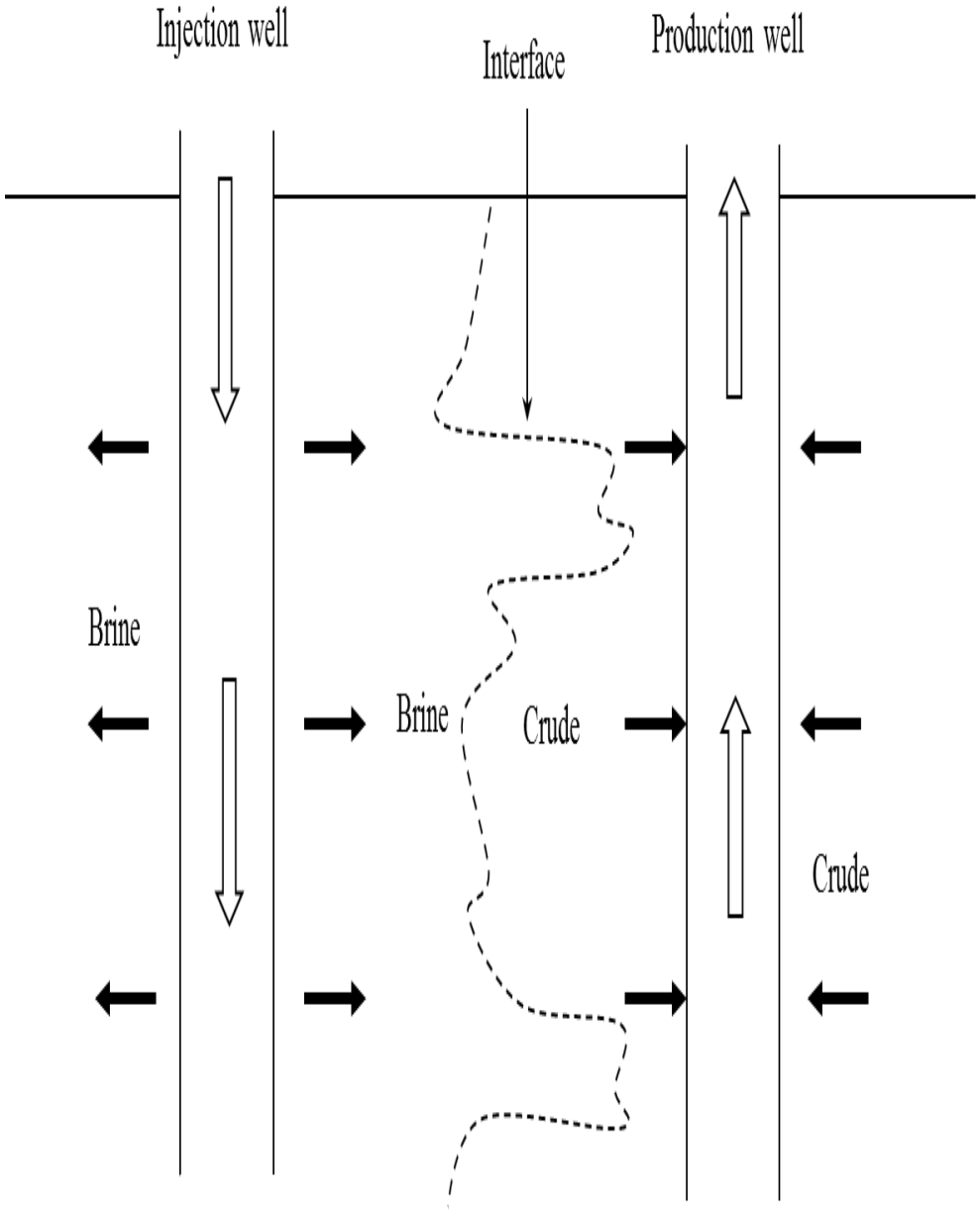

Figure 1.10. Instability in form of viscous fingering is shown schematically

1.8.2. Microscale Oil Displacement. In the micro category effects of oil-water interfacial tension (IFT) give rise to oil residing in pores and crevices from which it cannot be dislodged under even large applied pressures (Stegemeier, 1977; Slattery, 1974). As the smallest pore sizes go down to 0.1 μm or less. It is not surprising that IFT will become very important. The key quantity is the oil that is left behind after a sweep, S_{or} the fraction residual oil. It is plotted against the capillary number $Ca = \mu U/\gamma$ of the displacing fluid where μ is the viscosity of the displacing fluid, γ is the IFT and the velocity U varies in its definition, but in all cases Ca represents the ratio between viscous and surface tension forces.

The key is that S_{or} falls with increasing Ca. If the capillary number defined with a velocity given by Darcy's law $U = \frac{k}{\mu}\frac{\Delta p}{L}$ is used where k is the permeability. Water flooding is confined to below $Ca = 10^{-6}$, usually at 10^{-7}. For EOR, Ca is at 10^{-3} to 10^{-4}. The value of S_{or} is 0.005 at a Ca little higher than 10^{-2} (Foster, 1973). Obviously EOR methods that aim at reducing IFT will succeed in reaching a high value of Ca. Thus, high values are reached as miscibility is approached.

A pore doublet model is one of the conceptual models for oil entrapment in porous medium, Figure 1.9 illustrates pore doublet model, two phase flow in simple geometry and two adjacent pores of different diameters. The crude oil represents the non-wetting fluid and the brine is the wetting liquid and the latter is used to displace and push the oil ahead, the displacement is carried successfully in the small size while entrapment happens in the large pore. The pore geometry, ratio of capillary to viscous forces, and contact angle are most effective parameters in oil displacement in such models.

In the pore double model illustrated in Figure 1.11. The equation in the Figure below shows that the smaller pore diameter the larger capillary pressure as a result of that the oil displacement takes place in the small pore and the entrapment occurs in the large one, this phenomenon is well known in water wet reservoir only. In previous studies, dynamic contact angle α_1 in capillary pressure equation was set as equilibrium contact angle λ and that contradicts the concept of the fluid flow under dynamic conditions.

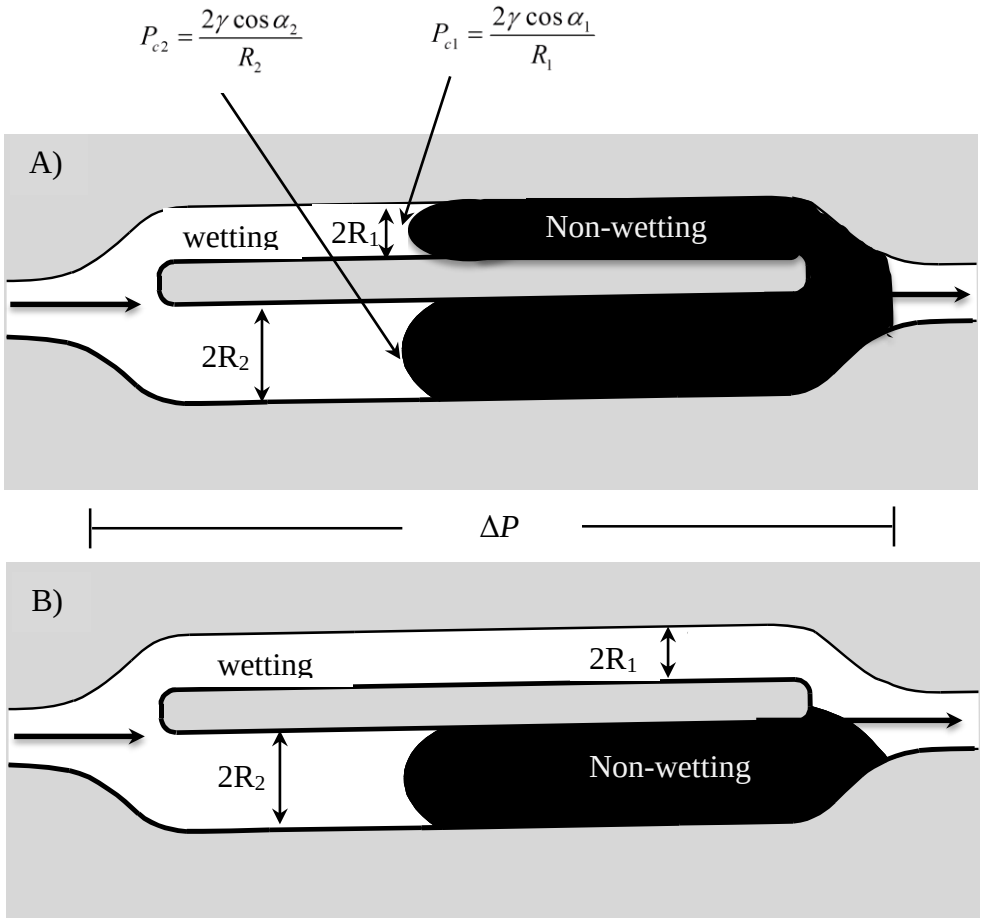

Figure 1.11. Pore doublet model. A) Pre-Oil Entrapment. B) Post-Oil Entrapment, above oil entrapment scenario takes place in the water wet reservoir only.

1.9. PRESENT STUDY

This dissertation consists of various sections which are extensively covering the subject of dynamic contact angles, here we introduce these sections and briefly discuss them, the details and the literature review are included in the following individual sections. The main reason of conducting such research is to shed light on theory and experiments of the dynamic contact angles because of its importance in the industrial and petroleum applications such as enhanced oil recovery, coating flow problem, lubrications, and inkjet printing.

In paper I, we have measured dynamic contact angles as a function of capillary number for a Newtonian liquid-air system, where the upper phase is the air and the lower phase is silicone oil (PDMS) with different viscosities 100, 200, 350, 500, 1000 cSt. The technique is the Wilhelmy plate force based. de Gennes' theory (1984) and creeping flow system by Huh and Scriven (1971) were used to correlate the dynamic contact angles as function of the capillary number. For the first time, a successful mathematical model dHS (de Gennes' Huh Scriven) was derived and the only one unknown is the cutoff length obtained from fitting to the experimental data. In the receding dynamic contact angles, the liquid entrained on the solid surface at sufficiently large speed of the substrate and high molecular weight of silicone oil.

In paper II, since most of the liquids in chemical industries are non-Newtonian fluids, we have selected two polymers, low and high molecular weight polyethylene oxides. In this section, we have studied the effect of the shear thinning behavior and elasticity on the dynamic contact angles under air. The three- parameter Ellis model has been used to fit the rheological data to obtain shear thinning power *n*, characteristic shear stress and the

zero shear viscosity. We have calculated the viscous dissipation in the wedge and equated it to the surface work under lubrication theory approximation, and at low polymer concentrations the fitted *n* conforms to the power law *n* measured using Haak rheometer. However, the remaining three concentrations at larger polymer concentrations show the fitted power *n* to be quite different and very low. This present theory shows that the elastic effect becomes important at larger polymer concentrations that reduce the dependence on capillary number.

In paper III, PDMS-water system has been used in this section which is similar to water flooding in oil recovery where the water displaces oil over the solid surface. The force tesniometer device is used to measure the excess force needed to plunge a vertical plate into a liquid-liquid interface or pull it out. This force is used to calculate the dynamic contact angle. We have used polydimethylsiloxane (PDMS) with different viscosities for the upper phase and water for the lower phase. An algebraic model was put together for the first time when both phases are liquids and it is called mdHS (modified de Gennes' Huh Scriven) here to predict dynamic contact angles in PDMS-water system. The mdHS and Cox theories were compared to the experiments on the dynamic contact angles. The receding contact angles showed significant scatter.

In paper IV, (PDMS-PEO aqueous) system is similar to the polymer flooding, the aqueous polymer PEO is displacing oil in the petroleum reservoir. Besides, mdHS and Cox's were used for comparison with experimental data. In this section, we found a good fit to the flow polymer displacing oil dominated by the zero shear viscosity of the shear thinning polymer. The last part in this dissertation provides the reader a conclusion for this study and recommendations for future research.

PAPER

I. FORCE BASED DYNAMIC CONTACT ANGLES AND WETTING KINETICS ON A WILHELMY PLATE

Amer Al-Shareef [a], P. Neogi[*a], Baojun Bai [b]

[a]*Department of Chemical and Biochemical Engineering*

[b] *Department of Geological Science and Engineering*

Missouri University of Science and Technology

Rolla, Missouri 65409-1203

ABSTRACT

A Wilhelmy plate method has been used here to measure the dynamic advancing and receding contact angles using a force balance method. The liquid phase here was silicone oils of different viscosities and the substrate was a cover glass coated with a perfluorinated polymer. A model for such a system for comparison against the data was based on the de Gennes' theory that the rate of viscous dissipation is equal to the rate of surface work. In this analysis the region in the immediate vicinity of the contact line is cutoff and the dynamic contact line actually refers to a slope of the wedge-like in the bulk liquid. de Gennes' original model has been extended here to cover larger contact angles. The comparison with the experimental data has shown the good agreement for both advancing and receding contact angles. Data over an extensive range have been provided for the first time that such detailed agreement can be established. In addition, when the speed of the plate is increased, the receding contact angle decreases with increasing capillary numbers but did not show any receding contact angle less than 30°. This sudden stop conforms to de Gennes' result that there is a minimum receding contact angle below

which entrainment takes place. In the entrained systems, the force method shows the dynamic contact angles to be zero. Photographs were taken of the dynamic meniscus to illustrate the onset of entrainment. The experimental results are supportive of de Gennes' model, and disagree with many conjectures on where the receding contact lines are entrained, or whether the dynamic contact angle is due to the failure of the equilibrium, etc.

NOMENCLATURE

Symbol	Description
W	the weight of the plate, mg.
g	the gravitational constant, 9.8 m/sec2
H	the length below the liquid, mm
P	the perimeter P, mm
Ca	capillary number.
R	viscosity ratio.
U	the velocity of the substrate, μm/sec.
α	dynamic contact angle, (degree)
γ	surface tension, (mN/m)
θ	the contact angle, degree
μ	viscosity, cp.
π	constant (3.1415)
λ	equilibrium contact angle (degree)
ρ_L	the density of the liquid, kg/m3
ε	singularity, the ratio of micro length scale to the macro length scale.

1. INTRODUCTION

When a flat plate is partially immersed into a pool of liquid with a horizontal upper surface, the total force needed to keep the plate immobile can be related to the weight of the plate, buoyancy forces and the surface tension γ. The balance makes it possible to calculate the surface tension, which is the basis of the Wilhelmy plate method for measuring surface tension. When the liquid is non-wetting, γ is replaced with $\gamma.\cos\lambda$ where λ is the equilibrium contact angle. Of these two, one has to be known independently to exploit the force balance.

It is also possible to measure forces under dynamic conditions. When the plate is plunged into the liquid, the liquid advances on the plate and the contact angle measured is the advancing dynamic contact angle α where $\alpha > \lambda$. When the plate is being withdrawn, the liquid is receding, and the receding dynamic contact angle α is less than λ. This is shown schematically in Figure 1.1. The force on the plate is

$$F = W - HP\rho_L g + P\gamma\cos\alpha \qquad (1)$$

where W is the weight of the plate and H is the length below the liquid. The second term on the right represents buoyancy forces. The procedure measures terms individually or as partial sums and returns the value of α provided the value of perimeter P and surface tension γ have been fed in.

In principle, if we can solve the fluid mechanical problem then it should be possible to predict α. However, the problem is difficult to solve in its entirety and many approximate solutions are available, making comparisons between theory and experiments difficult. Some issues have arisen that need to be addressed.

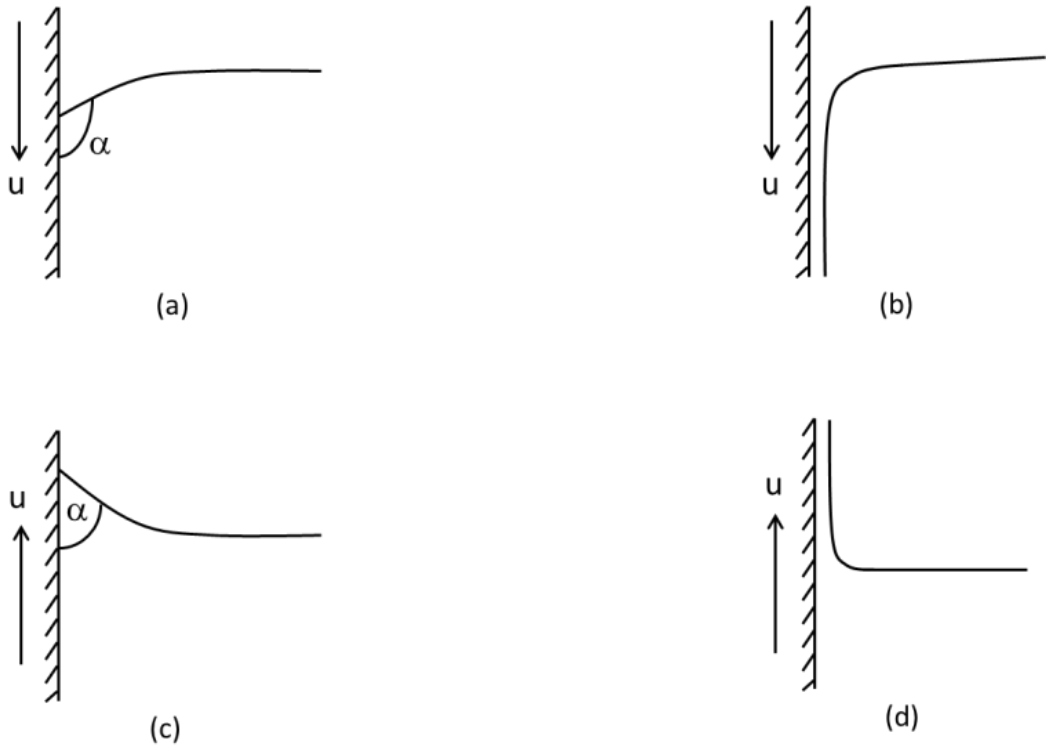

Figure 1.1. (a) the nature of the advancing dynamic contact angle on a plate and (b) to entrainment at higher plate velocities. Next are (c) the nature of the receding dynamic contact angle and (d) subsequent entrainment at higher plate velocities.

The advancing dynamic contact angles increase with plate velocity to 180° (Gutoff and Kendrick, 1982), but air entrainment, shown schematically in Figure 1.1, takes place at about 20% higher velocities (Blake and Ruschak, 1979). The region in between is marked by a serrated contact line (Blake and Ruschak, 1979; Burley and Kennedy, 1978; Benkreira and Ikin, 2010).

In case of receding contact line, the contact angle should decrease to zero with increasing plate velocity, but de Gennes' theory (1986) suggests that the lowest value reached is $\lambda/\sqrt{3}$ after which the liquid is entrained. In particular, the velocity at which entrainment takes place is $U \propto \lambda^3$. This has been verified by Quéré (1991). However,

others (Hopf and Geidel, 1987; Eggers, 2004, 2005) disagree with this mechanism and suggest that with increasing velocities, α reaches zero and it is only then that entrainment takes place.

These features are summarized schematically in Figure 1.2. de Gennes' results show that beyond a critical capillary number $Ca = \mu U/\gamma$ the solution fails. Here μ is the liquid viscosity. This is taken to mean that entrainment occurs. On the other hand the solution can smoothly reach zero.

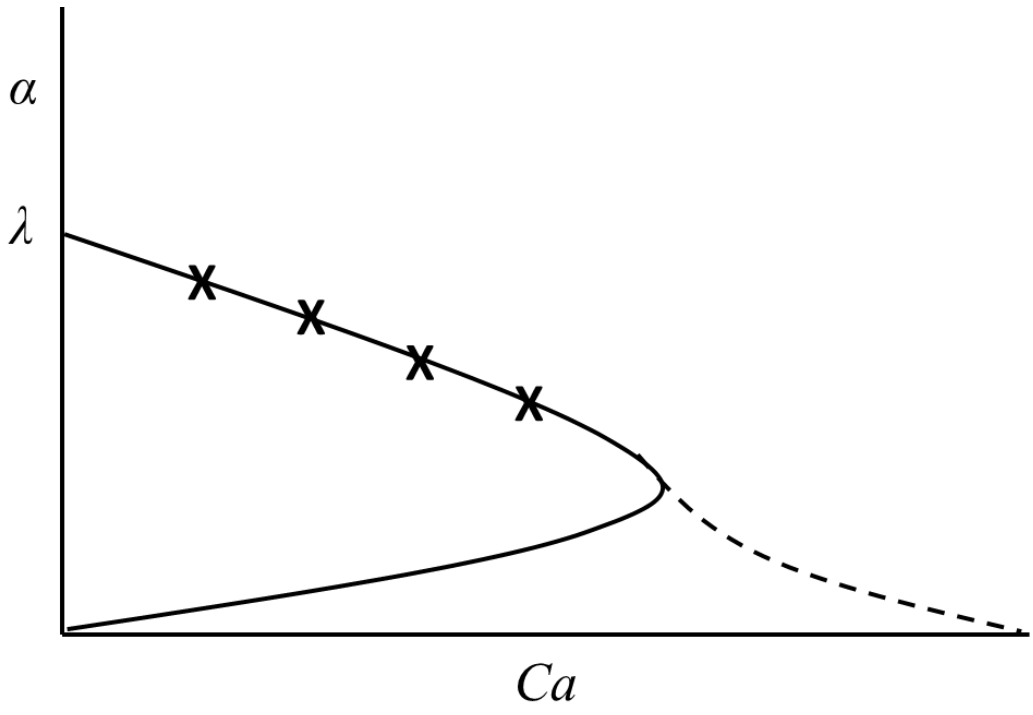

Figure 1.2. The receding dynamic contact angles as a function of capillary number. The crosses are generally where the data are. The fold is de Gennes' theory (de Gennes, 1986) and the dashed line is the Hopf-Geidel-Eggert theory (Hopf and Geidel, 1987; Eggers, 2004, 2005) .

In this case that is the point of entrainment. It appears that most of the data are on the top branch that cannot be used to discriminate between the two models. At larger capillary numbers, zero contact angles are observed, but it is not clear that this implies that entrainment has taken place. This is a key feature under investigation here.

de Gennes' theory (1984,1985) considers the energy balance in the wedge and shows the rate of viscous dissipation to be equal to the rate of surface work. For calculating viscous dissipation, a thin and flat film with a small value of α was chosen. Lubrication theory applies, under which only the velocity in the tangential direction is important and it varies mainly in the normal direction. The solution for the velocity profile obtained when the plate was being withdrawn tangentially so that the contact line was stationary and used to calculate the viscous dissipation. It showed correctly that the tangential velocity $U \propto \alpha^3$, Hoffmann-Voinov-Tanner rule (Kistler, 1993). However, singularities were encountered and eliminated by using a cutoff in the contact line region. This is the bulk region of the wedge which is characterized by α, and a thin precursor film ahead which moves at a faster velocity (Bascom et al., 1964) under molecular forces. Since it moves faster than the bulk, cutting it off does not produce complications as the film will not exert back pressure. Brochard-Wyart and Gennes (1992) extended the analysis to non-wetting liquids. They later looked at a special case (Brochard-Wyart and Gennes, 1994) where lubrication theory could not be used and the viscous dissipation was calculated using a solution to the fluid mechanical problem given by Huh and Scriven (1971). Neogi (2010a) extended the treatment to include higher values of α and found that up to $\alpha \sim 70°$ could be explained by the theory even though the solution by Huh and Scriven (1971) does not satisfy the normal stress balance at the interface.

He has also considered shear thinning fluids (Neogi and Ybarra, 2001; Neogi, 2010b) and vaporizing contact lines (Ybarra and Neogi, 2004) all using the basic idea of de Gennes.

For the liquid-air system studied here it is possible to use Huh and Scriven (1971) solution to calculate the viscous dissipation in a closed form (and the numerical integration by Neogi (2010a) is not necessary). The result of the energy balance for a non-wetting liquid using this result and those from Brochard-Wyart and de Gennes (1992) is

$$\gamma(\cos\lambda - \cos\alpha).U = \mu U^2 \ln\left|\frac{1}{\varepsilon}\right|.\frac{2\sin^2\alpha}{\alpha - \sin\alpha\cos\alpha} \qquad (2)$$

where $\varepsilon = \ell / L$ and ℓ is the microscopic cutoff length described earlier and L is the macroscale. Eq. (2) holds for the advancing contact line. For small values of α and λ (Brochard-Wyart and Gennes, 1992) result that $(\alpha^2 - \lambda^2)\alpha \propto Ca$ is obtained and which becomes the Hoffman–Voinov–Tanner rule when $\lambda = 0°$. For the receding case, the two cosines are interchanged so that the resulting capillary number emerges as positive. The left hand side of Eq. (2) is the surface work that arises from the dot product between surface forces and the vector U, hence the origin of cosine α . Out of this work done, the work due to the spreading pressure is subtracted off and attributed to the cutoff region and hence the origin of the cosine λ there. The difference in the left hand side should be not construed as the difference between the "micro" and "macro" contact angles as they do not originate from such a concept.

Given below are descriptions of the experiments conducted to measure the dynamic contact angles on a Wilhelmy plate. Neogi (2010a) has shown earlier that the dynamic contact angles from the force balance method (Wilhelmy plate) and the energy balance method (de Gennes) are the same. Another result from the hydrodynamic study was that

whereas the macroscale dynamic contact angles in both force and energy balances hold together, the results from visual observations are less clear. The data reported are more extensive than in previous works, making it possible for us to address the issue of entrainment in receding contact lines as well as some key questions on dynamic contact lines. Below is Figure 1.3. shows a schematic of liquid entrainment in receding case.

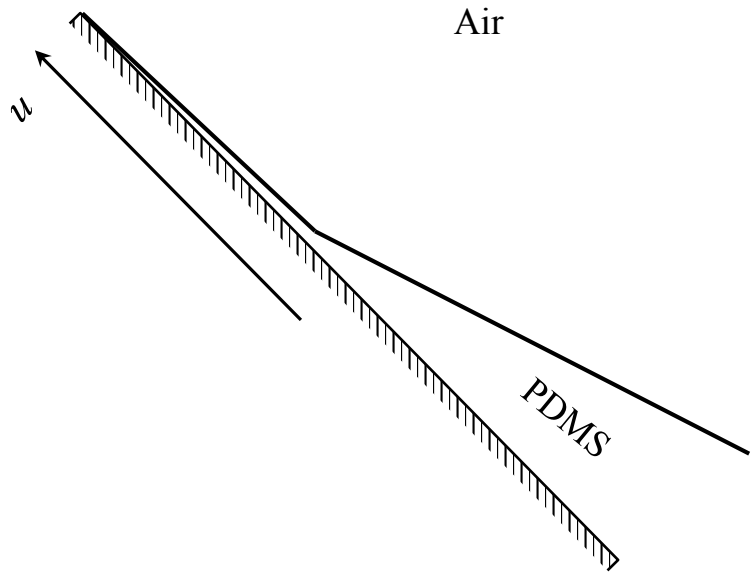

Figure 1.3. Schematic shows PDMS entrained on solid surface at receding dynamic contact angles.

2. EXPERIMENTAL

Experiments were conducted with Dow Corning silicone fluids of high viscosities, from 100 centiStokes (cSt) to a 1000 cSt. Substrates were glass cover slips which were first washed in isopropyl alcohol – KOH solution and then in distilled water. They were then dipped in about 0.3 wt% solution of a perfluorinated polymer in a perfluorinated solvent (3M), both supplied by du Pont. The cover slips were dried and microscopy was unable to detect a structure at 1.0 μm resolution. However, the equilibrium contact angle of silicone oils jumped from 0° for bare glass to 54° for the coated glass as illustrated in Figure 2.1. Ranabothu et al. (2005) report 49° for a similar system.

The viscosities were measured using a Brookfield viscometer and the surface tension through a Wilhelmy plate that operated on a Cahn electrobalance (Thermo Cahn DCA 300) using the fact that the liquids wet clean glass. The equilibrium contact angles were measured using a Ramé-Hart contact angle goniometer. The results are given in Table 2.1.

Table 2.1. Properties of the liquids

Silicone oil	**γ , mN/m**	**μ , mPa.s**	**λ°**
100 cSt	21.53	95	54
200 cSt	22.13	192	55
350 cSt	22.30	336	56
500 cSt	23.95	485	55
1000 cSt	23.96	970	57

The Cahn balance has five speeds 42, 82, 164 and 328 μm/s , up or down. It was also made to travel 15 mm into the liquid. The dynamic contact angles are reported automatically and were read off.

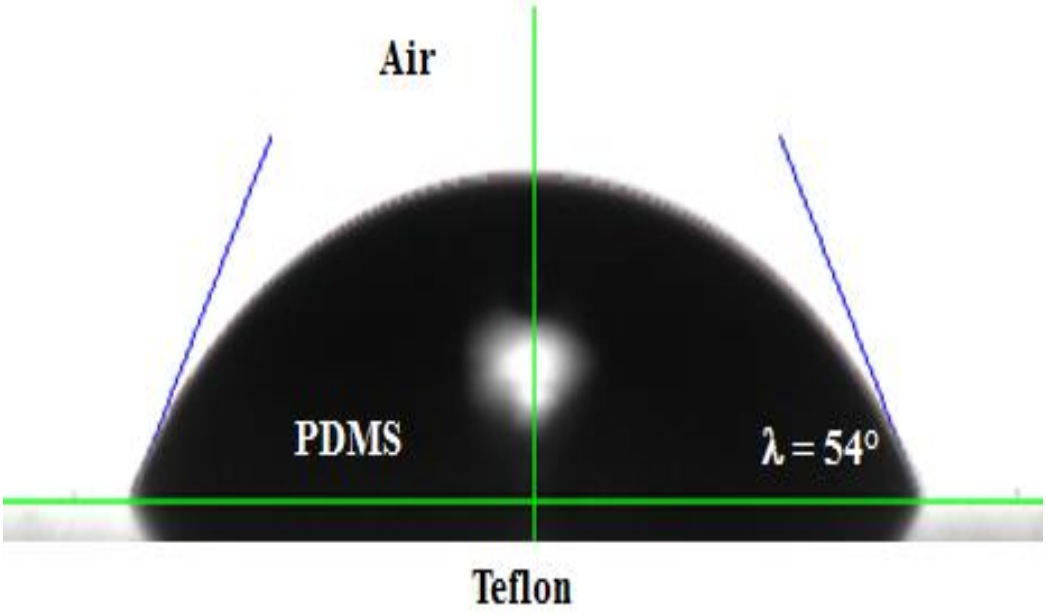

Figure 2.1. A drop of silicone oil (PDMS) deposited on a horizontal flat plate, Teflon coated, showing the equilibrium contact angle.

3. RESULTS AND DISCUSSION

The results of dynamic contact angles as the function of the capillary number are shown in Figure 3.1. The top locus of points refers to the advancing case and the bottom to the receding case. The advancing case looks uncomplicated, and Eq. (2) can be rearranged to write

$$Y(\alpha) = (\cos\lambda - \cos\alpha)(\alpha - \sin\alpha\cos\alpha)/(2\sin^2\alpha) = Ca\ln\left|\frac{1}{\varepsilon}\right| \tag{3}$$

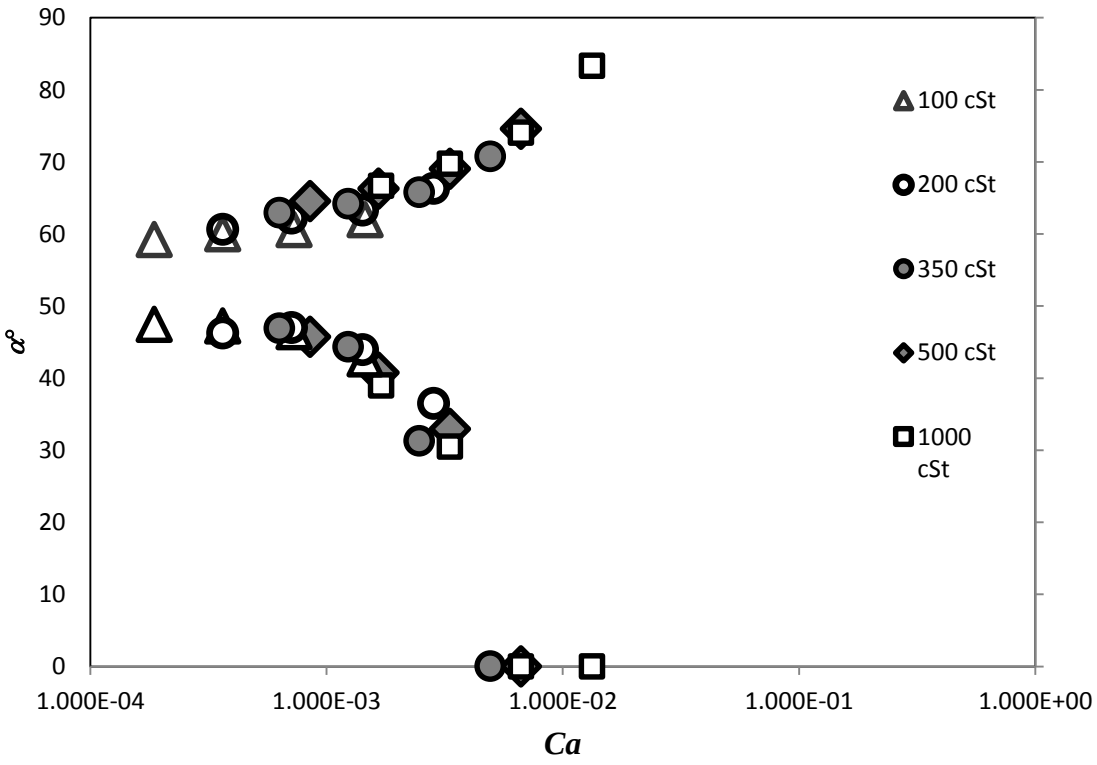

Figure 3.1. The force based dynamic contact angle data on Wilhelmy plate as a function of capillary number for a number of silicone oils.

Figure 3.2. has been plotted in the form of *Y* versus *Ca* using λ =54°. (The value for the liquid with the smallest viscosity has been taken here, as the rate of advance, for the viscous liquids near equilibrium is very low and the more viscous liquids could still be advancing to an equilibrium value that is lower than reported). Very clearly an intercept is seen. The right hand side of Eq. (3) becomes in this case *Ca*21.786 + 0.0337. The fitted value of $\ln\left|\frac{1}{\varepsilon}\right|$ is similar to values found earlier (Neogi, 2010a) but larger than the anticipated results.

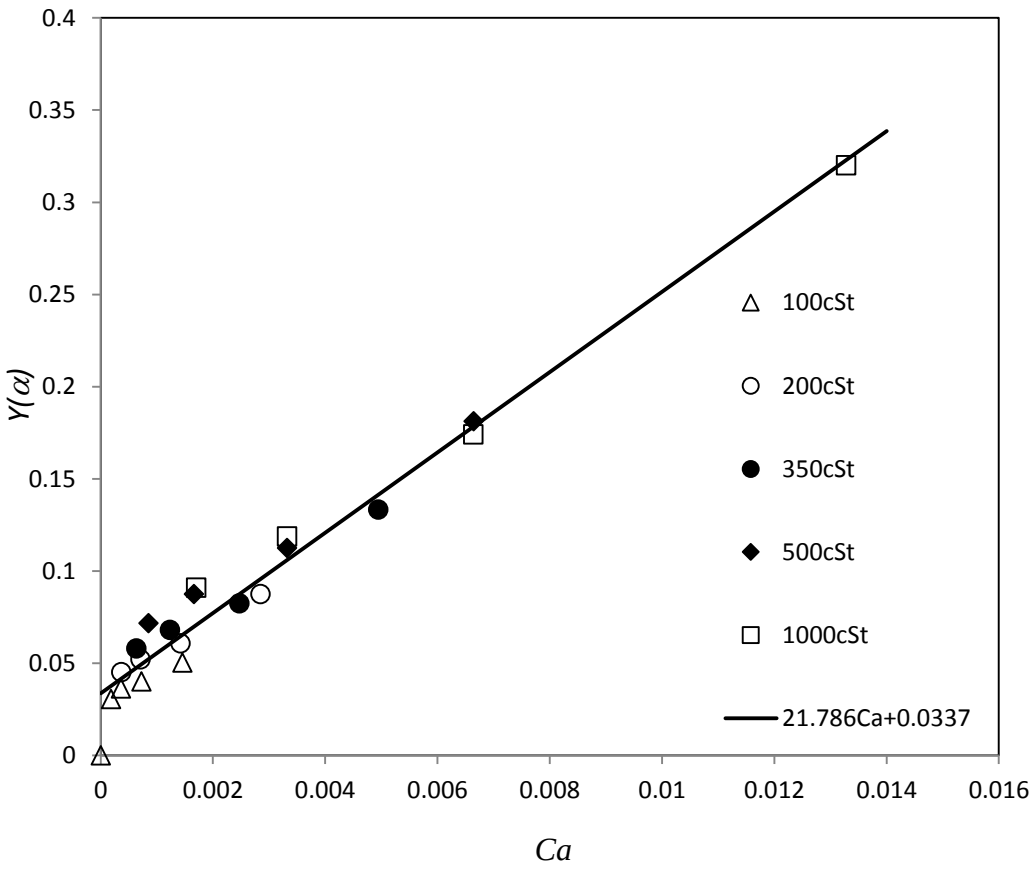

Figure 3.2. Advancing contact angles versus capillary number with a best linear fit containing an intercept. $Y(\alpha)$ has been calculated for Eq. (3) using the data.

The problem with an intercept is that the data point of $\alpha = 54°$ for $Ca = 0.0$ cannot fall on such a line. The intercept could be due to the accumulated effect of transients and such a feature has been seen in spontaneous spreading (Lin et al., 1996). It needs the intercept to fall to zero as this point is approached. There is probably a better explanation for the intercept. During the experiment, the force in Eq. (1) is reported as a function of time. As the value of the extent of plate immersed H changes linearly with time for a constant value of the plate velocity U, the measured force changes linearly with time as well. This change is noted by the machine to extrapolate the value to $H = 0$ and hence calculate to α. However, the reported change with time, is seen to be linear but very shaky, may change the effective value of U by a small amount which will show up as the intercept.

A feature that is important in theoretical consideration is, here and in a related experiment, the effect of inertia can be seen (Cox, 1998; de Ryck and Quéré, 1996). Order of magnitude estimates show that no inertia will be observed for liquid viscosities greater than 40 mPa.s, which all the liquids used here, satisfy. Thus, the locus of advancing contact angle in Figure 2.1., as well Eq. (3), constitutes the inertialess asymptote. Further, it is possible to show from Eq. (3), that $\alpha = 180°$ is reached only when $Ca = \infty$. In the experimental results by Blake (1993) show that as the liquid viscosity increases the capillary number at which 180° is reached also increases, and eventually the largest viscosity liquid provides a very large such velocity, though not infinite.

For the receding contact angles, we have ignored all cases where $\alpha = 0°$, as according to us entrainment has happened. A sign change is introduced in the definition of Y in Eq. (3) and Figure 3.3. shows that again Y is linearly dependent on Ca but clearly

there is an intercept. (For the same equipment and oils that wet the surface, Keller et al., (2007) show zero intercept for one fluid and negative intercept for the other). The slope of 10.857 is much lower than for the advancing case. This suggests that the cutoff lengths are different for the advancing and receding case.

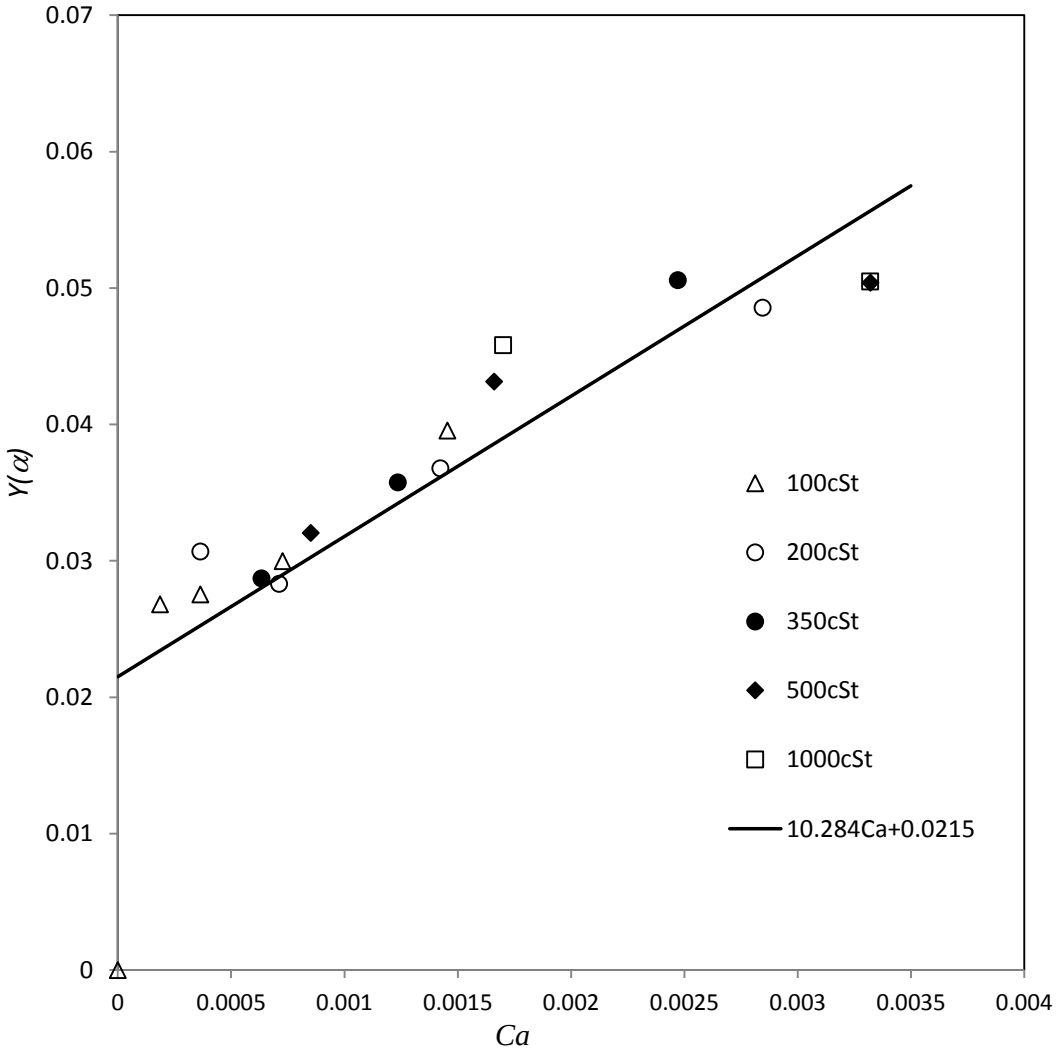

Figure 3.3. Receding contact angles versus capillary number with a best linear fit containing an intercept. $Y(\alpha)$ has been calculated for Eq. (3) with reversed signs and using the data.

Most importantly, the receding contact angle data of Figure 3.1. look like they have been terminated abruptly. de Gennes' approximate analysis for small α (and the present values are not all small) tells us that the value of α cannot fall below 30°, which they do not in Figure 3.1. Thus, 30° is the nose of the fold in Figure 1.2.

In Figure 3.4., we have photographs to show some of the phenomena discussed here. Two cases of the 350cSt fluid have been photographed from the edge to correspond with Figure 1.1. These are the first point in Figure 3.1. where the dynamic contact angle is zero and the last point where it is not, both with increasing *Ca*. As seen in the photograph, the shape and meniscus do not change when the dynamic contact angle is not zero, and the height of the meniscus keeps increasing when the dynamic contact angle is zero. That is, in the latter case, entrainment has happened.

Use of force based measurements on a Wilhelmy plate is not new (Ranabothu et al., 2005; Keller et al., 2007) but the data, particularly for the receding case are sparse or not recorded. The fully populated data as reported here is central to the good comparison with the upgraded theory. Because of the success in quantifying the experimental data, it is clear that the concept of the dynamic contact angle as different from the actual contact angle (de Gennes, 1985, 1984; Neogi and Miller, 1983, 1982) is justified, and that of the dynamic contact angle as deviation from equilibrium (Blake, 1993) is questionable.

We have not seen the single tooth observed by Blake & Ruschak (1979) for the receding contact line. However, we see that the liquid withdraws from the edge and the contact lines on the sides are straight lines that slope against the edges. These two lines when extrapolated would form a triangle that is the saw tooth. Such withdrawn edges in receding systems have been seen by Snoeijer et al. (2006), but it is not clear if there are

conditions under which the two will intersect to form a triangle. In the case of advancing contact lines, the contact angles are so far removed from 180° that no serrated contact lines are expected.

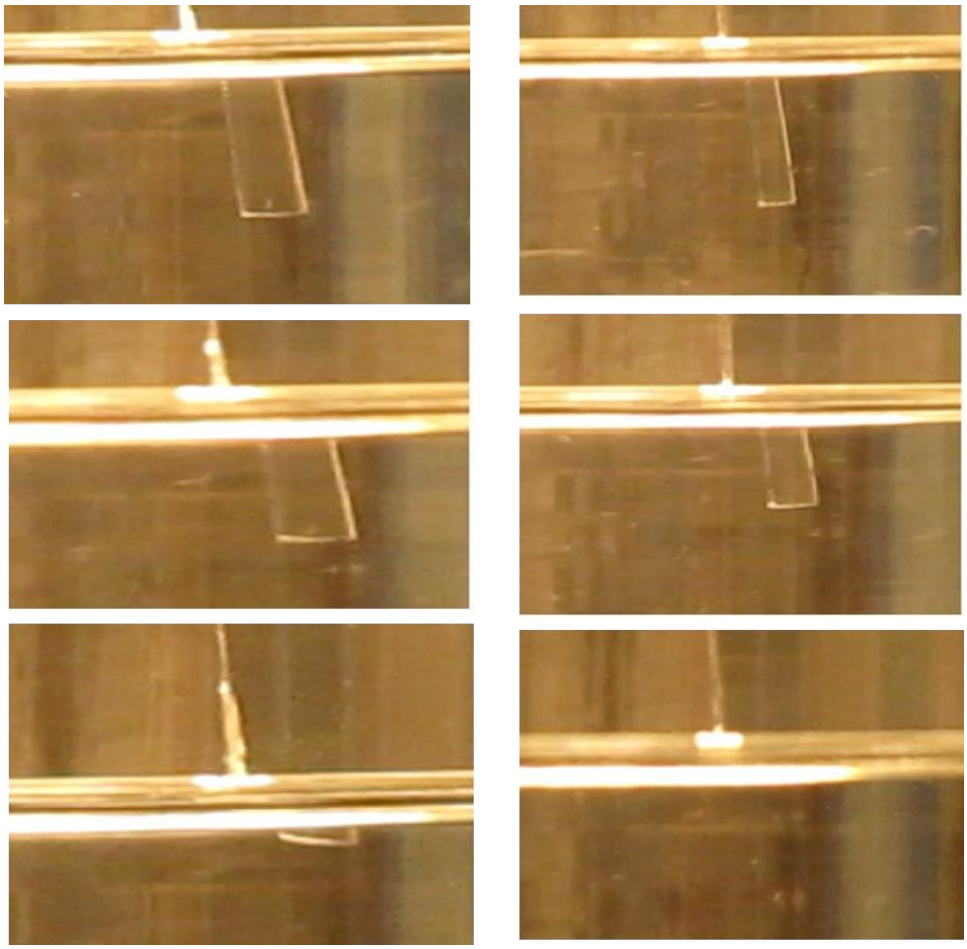

Figure 3.4. View of the meniscus from the side similar to Figure 1.1. The liquid is 350 cSt, and in the velocities correspond to the first case of 0° and the last case of non-zero contact angle (~ 30°) both from the left in Figure 3.1., in the first and second columns respectively. The bright area is the meniscus with some reflection from the substrate. From top to bottom are with increasing times. For the 0° case on the left, the size of the meniscus keeps increasing steadily with time and the developed thickness remains constant. We conclude that this is an entrained case. For the non-zero contact angle case on the right, the size of the meniscus does not change with time. Total time span in both is ~ 1 min and the relative vertical displacement between the meniscus and the camera changes with time.

4. CONCLUSION

The dynamic contact angles measured here all conform to the de Gennes' model including entrainment seen in the receding case, where de Gennes' model has been extended by us to cover larger contact angles. There is no indication that for the receding contact lines, the contact angles smoothly drop to zero with increasing velocities where entrainment takes place. Instead there is a jump to entrainment from a predicted point. There are also no saw teeth in the contact lines in the full range of receding lines and in a limited range of advancing lines.

REFERENCES

Bascom, W., Cottington, R., Singleterry, C., 1964. Dynamic surface phenomena in the spontaneous spreading of oils on solids, in: Gould, R. (Ed.), Contact Angle, Wettability, and Adhesion. American Chemical Society, Washington, D. C., pp. 355–380.

Benkreira, H., Ikin, J.B., 2010. Dynamic wetting and gas viscosity effects. Chem. Eng. Sci. 65, 1790–1796. doi:10.1016/j.ces.2009.11.019

Blake, T.D., 1993. Dynamic contact angles and wetting kinetics, in: Berg, J.C. (Ed.), Wettability. Marcel Dekker, Inc., New York, pp. 251–309.

Brochard-Wyart, F., Gennes, P. de, 1994. Spreading of a drop between a solid and a viscous polymer. Langmuir 10, 2440–2443.

Brochard-Wyart, F., Gennes, P. de, 1992. Dynamics of partial wetting. Adv. Colloid Interface Sci. 39, 1–11.

Burley, R., Kennedy, B.S., 1976. An experimental study of air entrainment at a solid/liquid/gas interface. Chem. Eng. Sci. 31, 901–911.

Cox, R.G., 1998. Inertial and viscous effects on dynamic contact angles. J. Fluid Mech. 357, 249–278.

de Gennes, P.G., 1986. Deposition of Langmuir-Blofgett layers. Colloid Polym. Sci. 264, 463–465.

de Gennes, P.G., 1985. Wetting: statics and dynamics. Rev. Mod. Phys. 57.

de Gennes, P.G., 1984. The dynamics of a spreading droplet. C. R. Acad. Sci.,Ser. II Mec., Phys., Chim., Sci. Terre Univers 298, 111–115.

De Ryck, A., Quéré, D., 1996. Inertial coating of a fibre. J. Fluid Mech. 311, 219–237.

Eggers, J., 2005. Existence of receding and advancing contact lines. Phys. Fluids 17, 1–10. doi:10.1063/1.2009007

Eggers, J., 2004. Hydrodynamic theory of forced dewetting. Phys. Rev. Lett. 93, 1–4. doi:10.1103/PhysRevLett.93.094502

Gutoff, E.B., Kendrick, C.E., 1982. Dynamic contact angles. AIChE J. 28, 459–466.

Huh, C., Scriven, L., 1971. Hydrodynamic model of steady movement of a solid/liquid/fluid contact line. J. Colloid Interface Sci. 35, 85–101.

Hopf, W.Geidel, T., 1987. The dynamic contact angle I. Dependence of the receding contact angle on velocity in the surfactant-contammg three-phase system. Colloid Polym. Sci 1084, 1075–1084.

Keller, a. a., Broje, V., Setty, K., 2007. Effect of advancing velocity and fluid viscosity on the dynamic contact angle of petroleum hydrocarbons. J. Pet. Sci. Eng. 58, 201–206. doi:10.1016/j.petrol.2006.12.002

Kistler, S.F., 1993. Hydrodynamics of Wetting, in: Berg, J.C. (Ed.), Wettability. Marcel Dekker, Inc., New York, pp. 311–429.

Lin, C., Ybarra, R., Neogi, P., 1996. Three-and two-dimensional effects in wetting kinetics. Adv. Colloid Interface Sci. 67, 185–204.

Neogi, P., 2010. Large dynamic contact angles. Chem. Eng. Sci. 65, 708–712. doi:10.1016/j.ces.2009.09.024

Neogi, P., 2010. Dynamic contact angles of shear thinning fluids. AIChE J. 56, 3284–3285. doi:10.1002/aic

Neogi, P., Miller, C. a, 1983. Spreading kinetics of a drop on a rough solid surface. J. Colloid Interface Sci. 92, 338–349. doi:10.1016/0021-9797(83)90156-X

Neogi, P., Miller, C.., 1982. Spreading kinetics of a drop on a smooth solid surface. J. Colloid Interface Sci. 86, 525–538. doi:10.1016/0021-9797(82)90097-2

Neogi, P., Ybarra, R.M., 2001. The absence of a rheological effect on the spreading of small drops. J. Chem. Phys. 115, 7811. doi:10.1063/1.1415455

Quéré, D., 1991. On the minimal velocity of forced spreading in partial wetting. C. R. Acad. Sci., Paris , Ser. II.

Ranabothu, S.R., Karnezis, C., Dai, L.L., 2005. Dynamic wetting: hydrodynamic or molecular-kinetic? J. Colloid Interface Sci. 288, 213–221. doi:10.1016/j.jcis.2005.02.074

Snoeijer, J.H., Delon, G., Fermigier, M., Andreotti, B., 2006. Avoided critical behavior in dynamically forced wetting. Phys. Rev. Lett. 96, 1–4. doi:10.1103/PhysRevLett.96.174504

T. D. Blake & K. J. Ruschak, 1979. A maximum speed of wetting. Nature 282, 489–491.

Ybarra, R.M., Neogi, P., 2004. Dynamic contact angles under evaporation. J. Chem. Phys. 120, 5755–5760. doi:10.1063/1.1649932

II. WETTING KINETICS OF POLYMER SOLUTIONS AND FORCE BASED CONTACT ANGLES

Amer Al-Shareef [a], P. Neogi[*a], Baojun Bai [b]

[a]*Department of Chemical and Biochemical Engineering*

[b] *Department of Geological Science and Engineering*

Missouri University of Science and Technology

Rolla, Missouri 65409-1203

ABSTRACT

In the present study, we investigate the effect of the shear thinning behavior and elasticity of polymer solutions on the dynamic contact angles. Under dynamic conditions, the contact angle of a liquid on a solid surface, changes significantly with the substrate velocity from its equilibrium value. The dynamic contact angles for polyethylene oxide (PEO) solutions of two molecular weights $3x10^5$ and $4\ x10^6$ have been measured using a polyethylene terephthalate (PET) plate. This is a Wilhelmy plate technique but one that provides force based dynamic contact angles. We have used the three- parameter Ellis model to fit the rheological data to obtain shear thinning power *n*, characteristic shear stress and the zero shear viscosity. We have calculated the viscous dissipation in a wedge and equated it to the surface work, all calculated under lubrication theory approximation, and obtained cases of contact angles changing with rheology. For the cases of three concentrations of polymer solutions at low polymer concentrations, the fitted *n* coincides with the power law *n* measured using Haak rheometer. However, the remaining three concentrations at larger polymer concentrations show the fitted power *n* to be quite different and very low. The present theory indicates that the elastic effect becomes

important at larger polymer concentrations that reduces the dependence on capillary number, that is, reduces *n* keeping with the experimental observations. The theory also indicates why the dynamic contact angles follow power law in this instance instead of showing Newtonian behavior with zero shear viscosity when the shear thinning effects are considered.

NOMENCLATURE

Symbol	Description
A	displaced fluid (silicone oil).
B	displacing fluid (water).
Ca	capillary number.
h	the film thickness, mm
R	viscosity ratio.
U	the velocity of the substrate, μm/sec.
v_r	the velocity component in r-direction, μm/sec.
v_θ	the velocity component in θ-direction, μm/sec.
x	the vertical direction, mm
α	dynamic contact angle, (degree)
γ	surface tension, (mN/m)
γ_{LV}	liquid-vapor surface tension, (mN/m)
γ_{SL}	solid-liquid surface tension, (mN/m)
γ_{SV}	solid-vapor surface tension, (mN/m)
θ	the contact angle, degree
μ	viscosity, cp.
μ_o	zero shear viscosity of the polymer, cp.
μ_B	viscosity of the displacing fluid, cp.
π	constant (3.1415)
λ	equilibrium contact angle (degree)
$\lambda a°$	advancing equilibrium contact angle, (degree)
$\lambda r°$	receding equilibrium contact angle, (degree)

ρ	the density of the liquid, kg/m3
ε	singularity, the ratio of micro length scale to the macro length scale.
π_e	the spreading pressure.

1. INTRODUCTION

A liquid drop makes an equilibrium contact angle λ on a solid surface given by Young-Dupré equation

$$\gamma_{LV} \cos\lambda = \gamma_{SV} - \gamma_{SL} \tag{1}$$

where γ is the surface tension and L, S and V refer to the liquid, solid and vapor. These are shown schematically in Figure 1.1 for a drop lying on a solid surface and the contact angle λ is subtended at the contact line[1]. Under dynamic conditions when the solid is moved tangentially, the contact angle becomes the dynamic contact angle α. For the advancing case, $\alpha > \lambda$ and for the receding case $\alpha < \lambda$ as shown schematically in Figure 1.2. The substrate velocity U is expressed as the capillary number $Ca = \mu U/\gamma$ and the knowledge of α as a function of capillary number is of some importance in oil recovery where most often just λ is seen to be used[2]. At sufficiently large velocities, entrainment can happen. For the advancing contact lines air is entrained and for the receding contact lines a uniform layer of liquid is coated on the emerging solid surface. This is the basic coating flow[1].

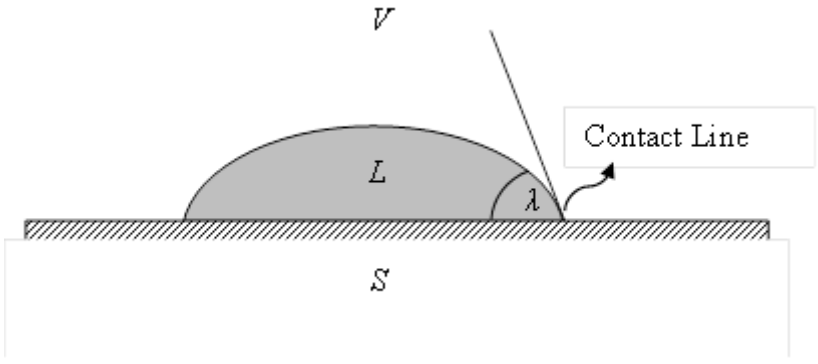

Figure 1.1. A view of the liquid droplet at rest on the substrate. The equilibrium contact angle and contact line are shown.

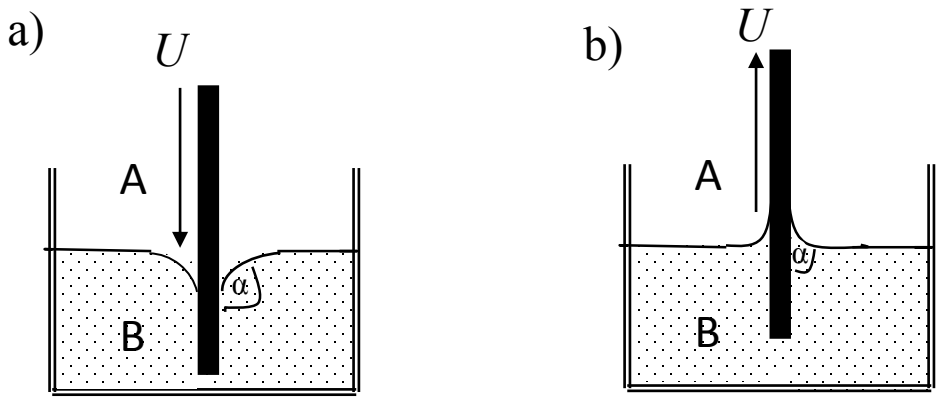

Figure 1.2. Dynamic contact angles with Wilhelmy plate a) advancing and b) receding.

Of interest here is the case where we have an aqueous polymer solution as one of the fluids and for simplicity air is another. The non-Newtonian nature of the polymer solution is divided into two parts. One part is that the viscosity is shear thinning which is often expressed through Ellis equation

$$\frac{\mu_o}{\mu} = 1 + (\frac{\tau}{\tau_{1/2}})^{q-1} \tag{2}$$

where μ is the dynamic shear viscosity (Pa.s) and μ_o is the zero-shear viscosity. τ is the shear stress and $\tau_{1/2}$ and q are system parameters. At large shear stresses (or shear rates), Eq. (2) becomes that of power law with

$$\mu \sim K\dot{\gamma}^{n-1} \tag{3}$$

where $\dot{\gamma}$ is the shear rate, and the consistency index $K = \mu_o^{1/q}\tau_{1/2}^{1-1/q}$ and $n = 1/q$. The other part of non-Newtonian behavior is the viscoelasticity and is often expressed using Criminale-Ericksen-Filbey equation for the stress[3] .

$$\boldsymbol{\tau} = -p\boldsymbol{I} + \mu\dot{\boldsymbol{\gamma}} - \frac{1}{2}\Psi_1\dot{\boldsymbol{\gamma}}_{(1)} + \Psi_2\dot{\boldsymbol{\gamma}}.\dot{\boldsymbol{\gamma}} \tag{4}$$

where $\boldsymbol{\tau}$ is the total stress tensor, $\boldsymbol{I}$ is the unit tensor, p the pressure, and Ψ_1(Pa.s^2) and Ψ_2 are the first and second normal stress coefficients respectively. The rate of deformation tensor is

$$\dot{\boldsymbol{\gamma}} = \nabla\boldsymbol{v} + (\nabla\boldsymbol{v})^{\mathrm{T}} \tag{5}$$

where $\boldsymbol{v}$ is the velocity. Further,

$$\dot{\boldsymbol{\gamma}}_{(1)} = \frac{\partial\dot{\boldsymbol{\gamma}}}{\partial t} + \boldsymbol{v}.\nabla\dot{\boldsymbol{\gamma}} - (\dot{\boldsymbol{\gamma}}.\nabla\boldsymbol{v} + (\nabla\boldsymbol{v})^{T}.\dot{\boldsymbol{\gamma}}) \tag{6}$$

A rheometer is used to obtain μ and Ψ_1 after Ψ_2 is assumed to be zero. Criminale-Ericksen-Filbey model has worked well in a related problem of coating flows[4]. There is some independence on how μ in Eq. (4) is determined, we choose Ellis' model and in one instance take μ to be a constant.

Nieh et al.[5] measured the spreading rates of a small drop of polystyrene in dibutylphthalate spreading on a glass surface, but no shear thinning character was seen. Instead of fluid mechanical solution to quantify the dynamic contact angle, de Gennes[6] started with an energy balance where the viscous dissipation was balanced by surface work. Later Neogi and Ybarra[7] used the method given by de Gennes[6] to show that the wetting kinetics of a shear thinning fluid modeled by Ellis equation was primarily due to the zero shear viscosity μ_o. Thus, it would act as a Newtonian liquid. The data of Seevaratnam et al.[8] were replotted by Neogi[9] to show that the data now followed Newtonian behavior. Neogi and Ybarra[7] also suggested that the elastic part had no role to play. The model used lubrication theory approximation where the liquid wedge is thin and flat. Barone[10] and Rafaï et al.[11] verified both these results experimentally but in a later paper Rafaï and Bonn[12]

suggested that the elasticity had some role. Wei et al.[13,14] found little effect of elasticity on dynamic contact angles.

The data that still continue to work against this effectively Newtonian behavior are the data of Carré and Eustache[15] which show that their wetting kinetics data have non-linear dependence on capillary number which can be explained by using power law for the viscosity.

Before looking at the more useful case of polymer solutions displacing oil, it is necessary to first clarify how the polymer solutions behave during dynamic wetting. We are presenting such data using Wilhelmy plate that gives us force based dynamic contact angles. This kind of contact angle data have been shown to be more in accordance with those obtained by de Gennes' method of balancing viscous dissipation with work[9]. The data of Seevaratnam et al.[8] were obtained on a Wilhelmy plate using conventional technique of photographing the profile to measure the contact angle. In the force based method, the force on the plate is measured to calculate the vertical component $\gamma.\cos\alpha$. It appears here that the details of the profile immediately near the contact line do not have much impact on the measured value of α.

Finally in this section, we note that some effect of heterogeneity in the polymer solution near that contact line is expected. Nieh et al.[5] observed that even though the solvent was wetting, the polymer solution was non-wetting. Ybarra et al.[16] suggested (as had some before them) that polymer molecules showing random coils cannot reach the contact line corner as shown schematically in Figure 1.3. When the coil size is small or overlaps among coils take place, the polymer does reach this corner which is then pried open by osmotic pressure. We do not know how this feature changes during flow. Since some of the

experiments conducted had particles besides polymers in the fluid, it should be pointed out that particles have been known to form structures near the contact line in both static[17] and dynamic[18] configurations.

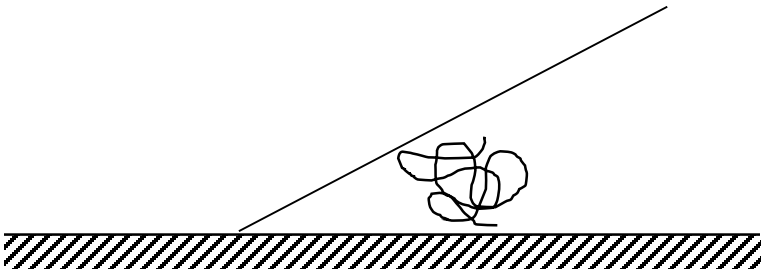

Figure 1.3. Polymer molecule finds it difficult to squeeze into the narrow corner of the wedge.

Below, we first consider existing models and extend them to better suit polymer solutions. This is followed by our experiments on polyethylene oxide (PEO) solutions. This work in keeping with the work of de Ryck and Quéré [4] on coating flows we have chosen polymers of large polymer molecular weights and large concentrations to increase the elastic effects. Their coating flow experiments indicate thickening of the liquid film profile, which needs investigation in the dynamic contact angle case.

2. MODELS

2.1. NEWTONIAN LIQUIDS

Consider a plate partially submerged in a Newtonian liquid and the plate advances steadily into the liquid with a constant velocity U. The contact angle is α as shown in Figure 2.1. If the values of U and α are small then lubrication theory approximation can be used, under which only the velocity in the tangential direction x is important and varies mainly in the normal direction z. The equations of motion become

$$0 = -\frac{\partial p}{\partial x} + \frac{\partial \tau_{zx}}{\partial z} \tag{7}$$

$$0 = -\frac{\partial p}{\partial z} \tag{8}$$

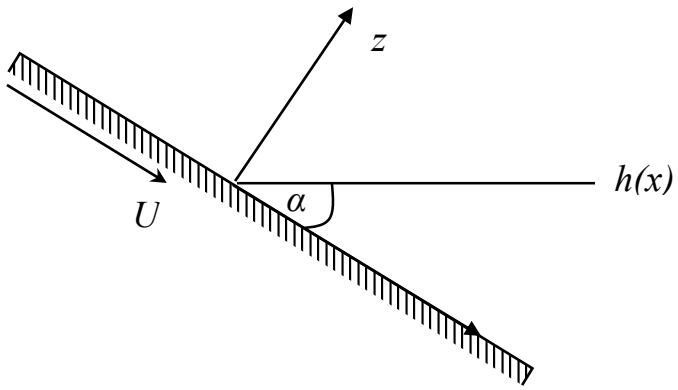

Figure 2.1. Schematic shows the advancing process when the plate is plunged into a pool of liquid with velocity U and α is the dynamic contact angle confined between the three phases near the contact line.

Since pressure is not a function of *z*, Eq. (7) can be integrated once subject to the boundary condition that $\tau_{zx} = 0$ at *z* = *h*, the local film thickness. Substituting the constitutive equation

$$\tau_{zx} = \mu \frac{\partial v_x}{\partial z} \tag{9}$$

the resulting equation is integrated once to obtain the velocity profile which is subject to $v_x = U$ at *z* = 0. This is again subject to a condition that the flow rate is zero to obtain the unknown pressure gradient

$$\frac{\partial p}{\partial x} = \frac{3\mu U}{h^2} \tag{10}$$

This allows one to calculate the viscous dissipation per unit volume $\mu\left(\frac{\partial v_x}{\partial z}\right)^2$ which integrated from *z* = 0 to *z* = *h*, to get an intermediate result

$$\phi = Uh\frac{\partial p}{\partial x} \tag{11}$$

Eq. (10) is substituted into Eq. (11). The local film thickness *h* is approximated as $h = \alpha.x$ in and integrated from $x = \ell$ to *x* = *L*. Here ℓ is the micro length scale used to cutoff the region in vicinity of the contact line to exclude the contact line singularity and *L* is the macro length scale. This viscous dissipation is equated to the surface work to get

$$U.\gamma(1-\cos\alpha) = \frac{3U^2\mu}{\alpha}\ln\left|\frac{1}{\varepsilon}\right| \tag{12}$$

where the left hand side is the surface work done and a dot product between surface tension forces and the velocity. A reference value (equilibrium) has been subtracted off. On the right hand side, the small quantity $\varepsilon = \ell/L$. The logarithmic dependence shows

the lack of sensitivity of the results on the length scales. Eq. (12) was obtained by de Gennes and for small values of α becomes the Voinov-Hoffman-Tanner rule[19] that $U \propto \alpha^3$. For non-wetting liquids, Brochard-Wyart and de Gennes[20] obtain

$$U.\gamma(\cos\lambda - \cos\alpha) = \frac{3U^2\mu}{\alpha}\ln\left|\frac{1}{\varepsilon}\right| \tag{13}$$

which is rearranged to read

$$(\cos\lambda - \cos\alpha) = \frac{3Ca}{\alpha}\ln\left|\frac{1}{\varepsilon}\right| \tag{14}$$

2.2. POWER LAW LIQUIDS

If the viscosity is chosen to be given by power law Eq. (3), the result is

$$\cos\lambda - \cos\alpha = (\frac{Ca}{\alpha})^n \left(\frac{\tau_{1/2}}{\gamma}\right)^{1-n} \frac{(\frac{1}{n}+2)^n}{(1-n)} L^{1-n} \tag{15}$$

where ε, the lower limit of integration over the length, has been set to zero wherever possible. Eq. (15) is the result of Carré and Eustache[15]. It turns out that this problem has no contact line singularity. However, the results are dependent on the macrolength scale. Since $0 < n < 1$ for a shear thinning fluid, the dependence on L can be re-expressed through

$$L = \left(\frac{\gamma}{\tau_{1/2}}\right)\ln 1/\varepsilon' \tag{16}$$

Eq. (15) takes a more conventional look into Eq. (17)

$$\cos\lambda - \cos\alpha = (\frac{Ca}{\alpha})^n [ln1/\varepsilon']^{1-n} \frac{(\frac{1}{n}+2)^n}{(1-n)} \tag{17}$$

However, ε' now has a very different meaning from the conventional cutoff length or slip length[21, 22].

2.3. ELLIS MODEL

Eq. (2) encompasses both Newtonian and power law models. If this is used for the viscosity then the expression for the pressure gradient changes from the simple Eq. (10) to

$$1 = X + \frac{X^q}{(q+2)H^{q-1}} \tag{18}$$

where $X = (h^2 / 3\mu_o U)\partial p / \partial x$ and $H = h / h_o$ and $h_o = 3\mu_o U / \tau_{1/2}$ which has been obtained by Neogi and Ybarra[7]. When the first term on the right hand side in Eq. (18), is important the result is

$$X \simeq 1 \tag{19}$$

The pressure gradient can be found and substituted into Eq. (11) eventually leads on integration to the Newtonian fluid case of Eq. (14). If the second term in Eq. (18) is important

$$X \simeq (q+2)^{1/q} H^{1-1/q} \tag{20}$$

This limit leads to the power law case of Eq. (17) and $(1-1/q)$ is positive. It is apparent that a general solution to Eq. (18) is needed, which appears impossible. In Eq. (18), if $X \to 0$, the first term on the right hand side vanishes, but the second term need not vanish if $H \to 0$. Thus an alternate way to look at Eq. (20) is to say that it is valid for small values of *H*. Similarly as $X \to 1$, the second term has to be zero or $H \to \infty$. A simple interpolation between two limits is, $\frac{1}{X} = \frac{1}{1} + \frac{1}{(q+2)^{1/q} H^{1-1/q}}$ (21)

This allows us to calculate the pressure gradient, which is substituted into Eq. (11) and integrated over x between limits. It turns out that the integral has no singularity at $x = 0$ and the result is

$$U\gamma(\cos\lambda - \cos\alpha) = \frac{3\mu_o U^2}{(1-1/q)} \ln[1+\left(\frac{\alpha L}{h_o}\right)^{1-1/q} (q+2)^{1/q}] \tag{22}$$

where the right hand side is the viscous dissipation. If L is very large, then it reduces to

$$(\cos\lambda - \cos\alpha) = \frac{3Ca}{\alpha} \ln L \tag{23}$$

Eq. (23) has been obtained by Neogi and Ybarra[7]. There is no contact line singularity. If h_o is large in Eq. (22), then the expansion of the logarithmic term leads to Eq. (17).

If we equate the right hand sides of Eqs. (19) and (20) we get

$$h^* = h_o.(q+2)^{\frac{1}{1-q}} \tag{24}$$

As local wedge thickness h exceeds h^*, Newtonian behavior changes to power law behavior.

2.4. VISCOELASTIC BEHAVIOR OF FLUIDS

For viscoelastic fluid the equation of motion becomes

$$0 = -\frac{\partial p}{\partial x} + \frac{\partial}{\partial x}[\Psi_1(\frac{\partial v_x}{\partial z})^2] + \frac{\partial}{\partial z}[\mu \frac{\partial v_x}{\partial z}] \tag{25}$$

The model for Ψ_1 is

$$\Psi_1 = N(\frac{\partial v_x}{\partial z})^{2n-2} \tag{26}$$

where N is a constant. Neogi and Ybarra[7] assumed that under lubrication theory approximation, the variation in the tangential direction can be ignored. That is the second

term on the right hand side can be set to zero, and hence there are no elastic effects. If however, we say that Ψ_1 is very large (a feature that we incorporate in our experiments), then this term could be small but not negligible. In that case, a perturbation expansion for small values of the middle term can be made[23]. Eq. (26) is valid for instance at small shear rates where viscosity can be approximated as the zero shear viscosity μ_o. Thus Eq. (25) becomes

$$0 = -\frac{\partial p}{\partial x} + N\frac{\partial}{\partial x}[(\frac{\partial v_x}{\partial z})^{2n}] + \mu_o \frac{\partial^2 v_x}{\partial z^2} \tag{27}$$

Thus, at first the middle term is ignored and the resulting equation solved subject to the boundary conditions to get

$$\frac{\partial v_x}{\partial z} = A(z-h);\ A = \frac{3U}{h^2} = -\frac{1}{\mu}\frac{\partial p}{\partial x} \tag{28}$$

This velocity gradient is now substituted in the middle term in Eq. (27) to get

$$0 = -\frac{\partial p}{\partial x} + N3^{2n}U^{2n}\frac{\partial}{\partial x}[(h-z)^{2n}\left(\frac{1}{h^{4n}}\right)] + \mu_o \frac{\partial^2 v_x}{\partial z^2} \tag{29}$$

Eq. (29) is solved by first differentiating the middle term by parts to bring out the term containing *z* and then integrating twice subject to the boundary conditions to get $\frac{\partial v_x}{\partial z}$ and v_x. Then the velocity is integrated over *z* get the flow rate which is set to zero. It gives us an expression for $\frac{\partial p}{\partial x}$ which is inserted into the previous expression for $\frac{\partial v_x}{\partial z}$ and the viscous dissipation per unit volume is calculated as $\mu_o\left(\frac{\partial v_x}{\partial z}\right)^2$. First integration is with respect to *z*, the second integration is over *x* between the two limits. The result on equating to surface work is

$$\cos\lambda - \cos\alpha = \frac{3Ca}{\alpha}\ln\frac{1}{\varepsilon} - \frac{2.3^{2n}}{\alpha^{2n-1}(1-2n)}\,\frac{8n^2+18n+9}{(2n+1)(2n+2)(2n+3)}\,Ca.De \qquad (30)$$

where Deborah number $De = \dfrac{\bar{\Psi}_1 U}{\mu L}$ and the estimate of the first normal stress difference is given by $\bar{\Psi}_1 = N\dfrac{U^{2n-2}}{L^{2n-2}}$. Since *CaDe* is of the order of U^2 or U^{2n}, we take it to be small.

The interesting conclusion is that the first normal stress difference leads only to a normal stress which should not affect the viscous dissipation. However, it affects the velocity distribution, such that the velocity gradient and the viscous dissipation are affected.

The results of de Ryck and Quéré [4] show that the first normal stress difference makes the films thicker, which could reduce viscous dissipation. Thus at large values of Ψ_1, the dynamic contact angle changes less with increasing velocities.

It is important to note that the term $(1-2n)$ is being assumed to be positive. Now, $n(=1/q)$ is usually less than 0.5 but not always so. Consequently we have reworked Eq. (30a) for $n = 1/2$ to get

$\cos\lambda - \cos\alpha = \left[\dfrac{Ca}{3\alpha} - \dfrac{5}{12}Ca.De\right].\ln\left|\dfrac{1}{\varepsilon}\right|$ which still shows that elastic effects cut down the dependence of α on velocity. Here $De = N/\mu_o$.

As mentioned previously, the lubrication theory approximation confines us to cases of small α and small *Ca*. Nevertheless there are instances where the agreement is still good at higher values of α and *Ca* (as will be seen below).

Similarly, the method of de Gennes has an assumption that at the end one has to take the profile to be linear. Nevertheless, previous comparison with experiments has been good[24]. We hope that when the above results do not quantitatively agree with the experiments, they are still good enough to shed some light on the observations.

3. EXPERIMENTAL

The substrate was cut from sheets of polyethylene terephthalate (PET) to be used in Cahn Thermo to form the Wilhelmy plate. The sheets were found to be sufficiently smooth under microscope (40X magnification) and used as such. Cahn Thermo moves the plate up or down at 42, 82, 164 and 328 μm/s. When it moves into the liquid by cutting through the liquid-air interface, the force measured is used to calculate α if the values of the perimeter of the plate, surface tension and specific gravity are supplied. The machine is essentially a balance and the liquid in the beaker is moved up or down at fixed velocities. For an air-liquid interface, the plate weight in air is set to zero. When the plate moves into the liquid a jump in weight is measured along with a base line drift due to change in buoyancy. The base line is calculated from the velocity of travel, time taken, the height of travel and the specific gravity of the liquid. When the buoyancy forces are subtracted off, the jump left is perimeter times $\gamma.\cos\alpha$. Since the value of surface tension is supplied, α is returned by the machine. The system is begun first with the plate advancing with the lowest speed and then receding with the same. This is repeated with the next highest speed, until all four have been studied. Then it is returned to the lowest speed to start the process again. The advancing contact angles can be reproduced up to 1º, but the receding contact angles have larger errors. The 1º error sometimes increases to 5º, and even 10º when the point of entrainment is reached. As will be discussed later, entrainment occurs in the case of receding contact angles and the reported dynamic contact angle is zero. In the receding case only the first set of readings are reported.

In the surface tension mode, the machine measures $\gamma.\cos\lambda$. Glass substrate was used. The solutions wet glass, and Cahn Thermo device was used to measure $\gamma.\cos\lambda$ with

$\lambda = 0^o$ which gives us the surface tension. The advancing equilibrium contact angle on PET was determined using Ramé-Hart contact angle goniometer and the results are listed in Table 3.1.

The polymer polyethylene oxide (PEO) was dissolved in distilled water at concentrations of 1 - 7 g/dl for PEO of molecular weight 3×10^5, as well at 0.5 - 5 g/dl for PEO of molecular weight 4×10^6 same as in the work of de Ryck & Quéré [4], both molecular weight polymers were used here in the rheological and contact angles experiments. These are polymers of very large molecular weights and can tear on too much stirring. They were dissolved in distilled water and left on a shaker for a day after which the solutions were stored sealed for a month. By that time the solutions which looked cloudy turned homogeneous. The densities were calculated assuming the additivity of volume; however, the solutions were so dilute that the specific gravities were about the same as the solvent.

Table 3.1. Macroscopic parameters for PEO solution spreading on the PET substrate

PEO/300K	1gm/dl	2 gm/dl	3 gm/dl	4 gm/dl	5 gm/dl	6 gm/dl
Surface tension γ , mN/m	64.45	65.11	65.60	66.12	66.45	67.12
Adv. equ. contact angle, λ_a	68.50 ±0.86	73.40 ±0.38	70.00 ±1.54	72.60 ±0.64	73.20 ±0.49	72.50 ±0.73
PEO/4M	0.15 gm/dl	0.25 gm/dl	0.5 gm/dl	0.7 gm/dl	1 gm/dl	2 gm/dl
Surface tension γ , mN/m	65.12	66.25	66.80	67.12	67.85	67.89
Adv. equ. contact angle, λ_a	73.30 ±0.41	73.10 ±0.62	71.50 ±0.51	72.80 ±0.45	75.80 ±0.16	74.21 ±0.61

Figure 3.1. shows how the advancing and receding equilibrium contact angles were measured. Standard deviations are shown for the angles. It appears that the advancing equilibrium contact angles as shown in Table 3.1. do not appear to be affected by polymer

concentrations given their standard deviations, and the mean values of 71.6º and 73.5º were used for 300K and 4M polymer respectively. The rheological features were measured using HAAKE Rheometer. The process is standard, but its description lengthy and some results are discussed in the Appendix. The viscosity-shear stress data are fitted to Ellis' model to calculate the zero shear viscosity μ_o as a function of polymer concentration c as shown in the Appendix. Zero shear viscosities are easily determined for the polymer with the lower molecular weight but are more difficult and show more errors, where the molecular weight is high. As a result the $\mu_o - c$ plot for the first has no scatter but the plot for the polymer molecular weight has some.

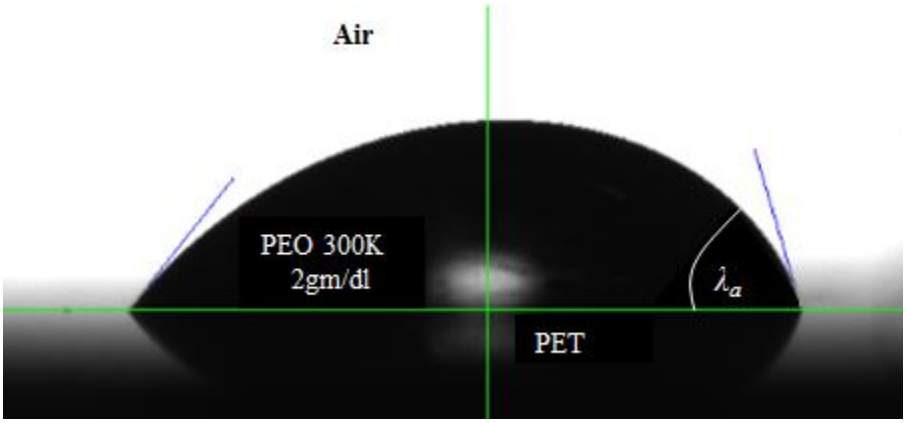

Figure 3.1. A drop of 300K PEO solution on a tilted surface showing advancing and receding equilibrium contact angles.

4. RESULTS AND DISCUSSION

The α versus capillary number results are shown in Figures 4.1. for a polymer with molecular weight of 3 x10^5 and in Figure 4.2. for 4 x 10^6 respectively. The upper values are for the advancing case $\alpha > \lambda$ and the lower values are for the receding case $\alpha < \lambda$, and the advancing equilibrium contact angle values in both cases have been shown on the y-axes. The data cover almost one order of magnitude in polymer concentrations, two to three orders in zero shear viscosity μ_o and two to three orders of magnitude in capillary numbers *Ca*.

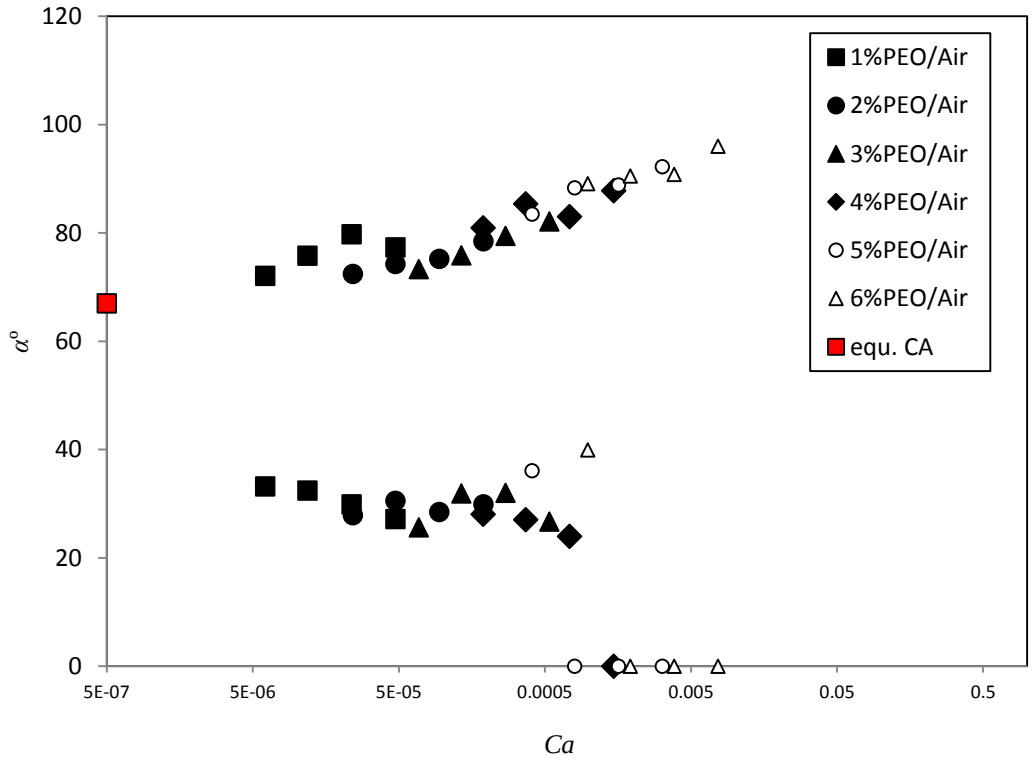

Figure 4.1. Advancing and receding dynamic contact angles versus capillary number for PEO/PET/air system at 300K PEO.

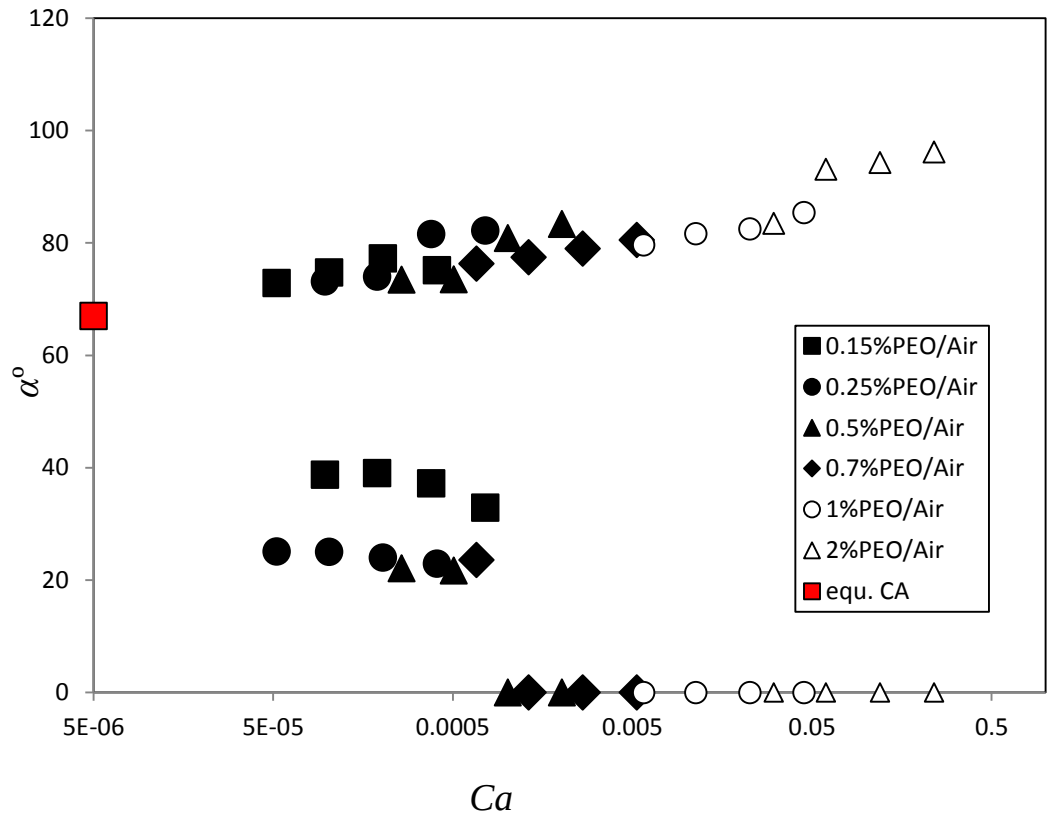

Figure 4.2. Advancing and receding dynamic contact angles versus capillary number for PEO/PET/air system at 4M PEO.

The data have been plotted in logarithmic scale in Figures 4.3. and 4.4., using the results of power law from Eq. (17). The expected fit to straight line in log-log plots is very good. However, a close view of the basic data show that there may be some more effects there, but such signs are too low for us to consider any further. Now, out of six sets of data on each plot, the first three sets show the value of slopes to be essentially the same those measured from the rheological experiments but the remaining three at higher capillary numbers show a smaller dependence of the dynamic contact angle α on the velocity U. We interpret this as due to the effect of elasticity at large values of U as predicted by Eq. (30)

(note that the term *Ca.De* there is independent of viscosity). We cannot say why it results in a power law type of relationship, but many approximations have been made in deriving Eq. (30) and such features could have been lost in them. Our interest lies in the three cases of largest concentrations for both polymers where the elastic effects are the highest. For these cases n is less than 0.5 usually by a small amount except for one case where it is 0.525. That is, in the cases where the elastic effect is expected to show up, the term $(1-2n)$ is positive as required for the above discussion to hold.

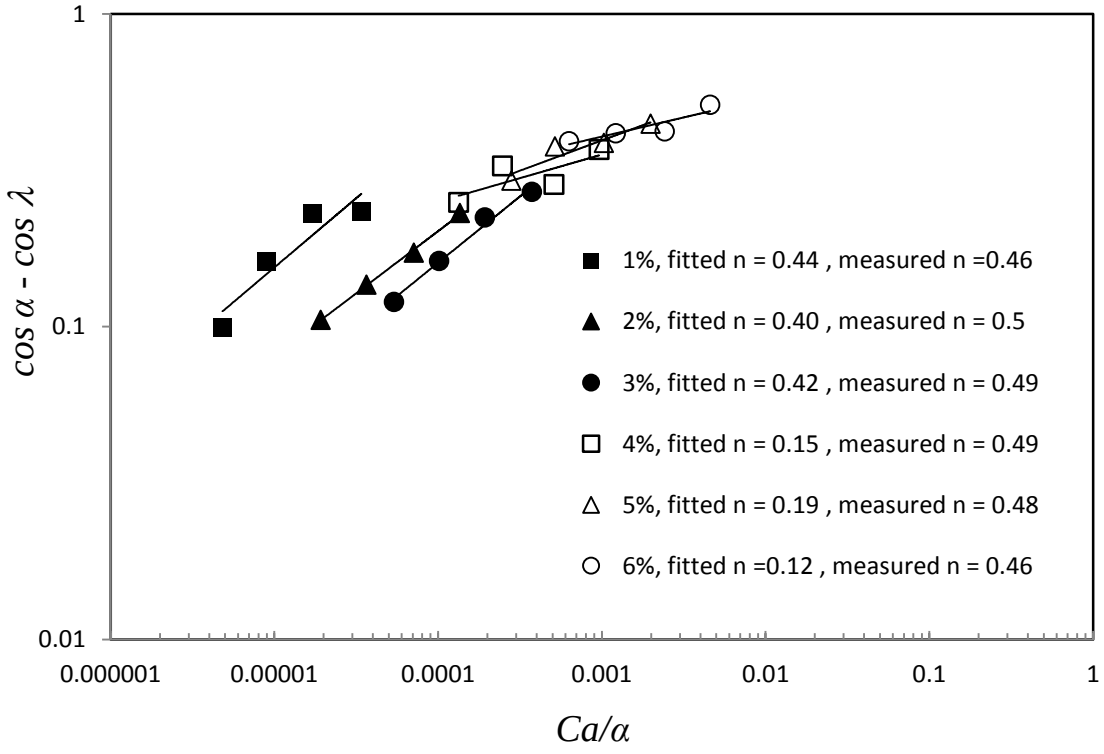

Figure 4.3. Advancing dynamic contact angle data are plotted according to Eq. (17) for power law fluids for 300K PEO. Values of n obtained from the plots corresponding to Eq. (17) and have been shown along with the values obtained from rheological measurements discussed in the Appendix. The polymer concentrations are shown as weight percent.

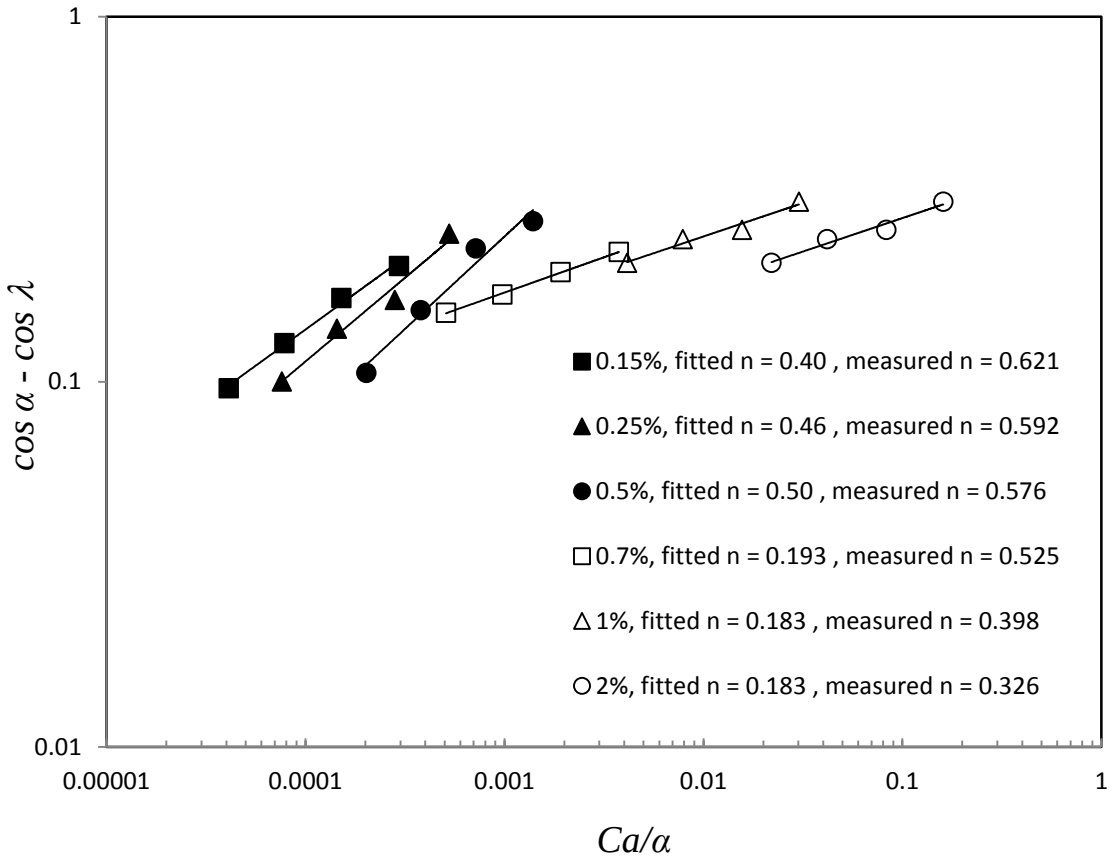

Figure 4.4. Advancing dynamic contact angle data are plotted according to Eq. (17) for power law fluids for 4M PEO. Values of *n* obtained from the plots corresponding to Eq. (17) and have been shown along with the values obtained from rheological measurements discussed in the Appendix. The polymer concentrations are shown as weight percent.

One feature that also needs to be explained is why the present data conform to power law fluid, instead of Newtonian fluid with zero shear viscosity[9]. For answer to this we look at Eq. (24). There is not much difference between h^* and h_o and we will use h_o below. If $h_m \sim \alpha L$ is the largest thickness of the wedge, then if $h_m < h_o$ then we should expect Newtonian behavior. If $h_m > h_o$ then we should expect power law behavior.

However, h_m is difficult to estimate. Consequently, we turn to a less powerful condition that if h_o is small then we should expect power law behavior, but if h_o is large then we expect Newtonian behavior, without much grounds in determining what large or small are. Now, $h_o = 3\mu_o U / \tau_{1/2}$ and requires shear thinning parameters and it also changes with velocity *U*. Other than the present work, only Seevaratnam et al.[8] provide both dynamic contact angles and rheological data that allow us to calculate h_o. All values of h_o below are shown in cms. The above results for 2M xanthan gum in water show large values from 0.02 to 0.2, hence Newtonian behavior is expected and we do see that[9]. On the other hand, present data for 300K PEO show h_o to lie from 3.33×10^{-7} to 6.28×10^{-4}, all very small values suitable for power law as found here. It should be kept in mind that at large values of *U*, elastic effects come into play and the corresponding values of h_o lie outside our discussion. For 4M PEO, the low concentration cases lie from 4.57×10^{-3} to 0.2 and should show power law which they do. At higher concentrations and higher values of *U*, they exceed the limit, but we do not expect these cases to depend on viscosity only as elasticity will play a role. Hence, the milder constraint predicts reasonably when we should see Newtonian and when we should see power law.

Further, Eq. (15) and Figures 4.3 and 4.4, show that the values of *L* can actually be calculated as shown in Figure 4.5. Generally, the values of microlength scales are approximately known, but Figure 4.5. provides the macrolength scale directly for the first time. It is seen that as the concentration of the polymer goes to zero (the liquid becomes Newtonian), *L* settles down to about 1 m. This is what causes the ratio of microlength scale to the macrolength scales to be very small in the experiments [24].

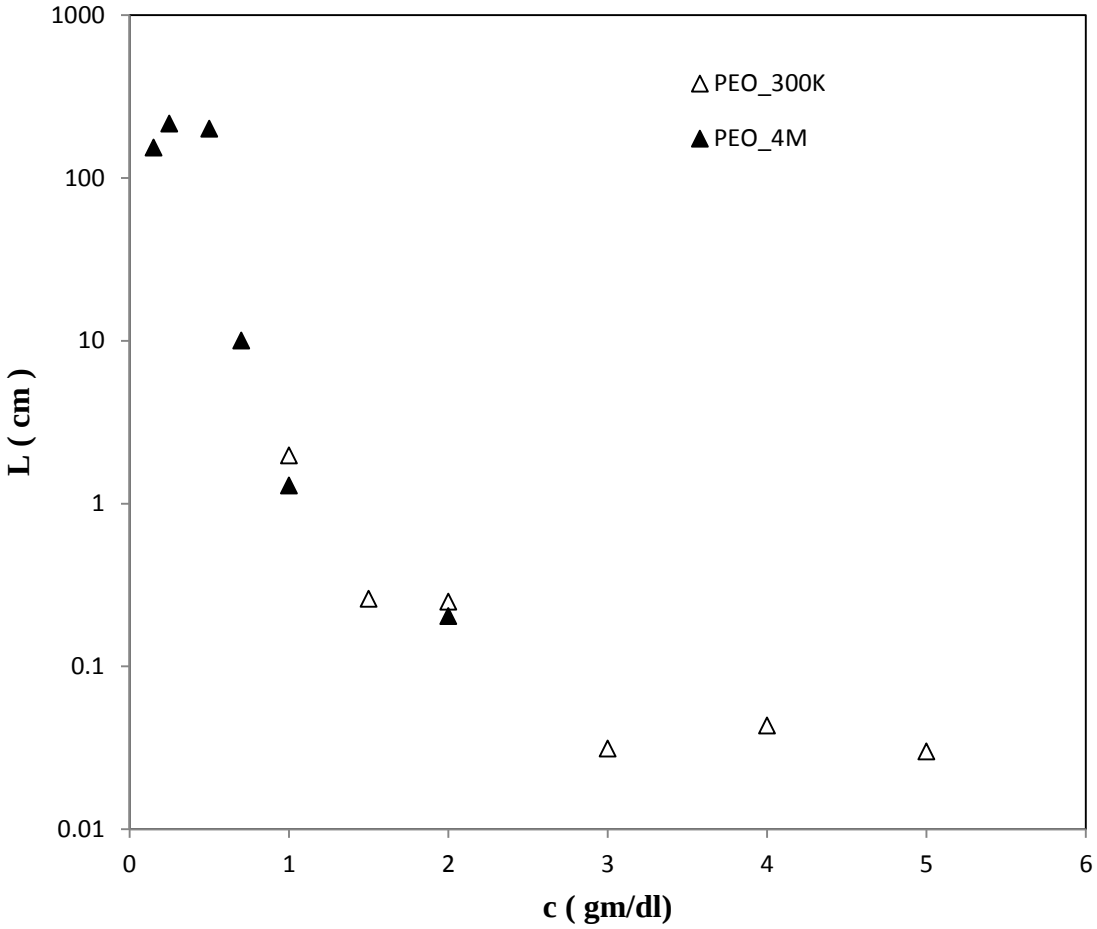

Figure 4.5. The macro length scale according to Eq. (15) versus the polymer concentration of PEO 300K and 4M.

The receding contact angle data in Figures 4.1 and 4.2 are more difficult to quantify. Now, we have shown earlier using photography [24] that zero contact angles imply that entrainment (dip coating). For Figure 4.1, we find a good amount of disarray in the data before the point of entrainment. It can be attributed to the fact that receding cases involve stretching of the fluid and recoil may occur as a consequence of its elasticity. In Figure 4.2 it appears that one more dimensionless group is needed. Since this case has higher elastic effect, Deborah number should play a role. If in Eq. (30), we set $U \rightarrow -U$, we get

$$\cos\alpha - \cos\lambda = \left[\frac{Ca}{3\alpha} - \frac{5}{12}Ca.De\right].\ln\left|\frac{1}{\varepsilon}\right| \tag{31}$$

That is, the effect of elasticity is reversed over the advancing case. Further, if we differentiate Eq. (30) with respect to α and set $dU/d\alpha$ to zero, we get a value for α. This is de Gennes' [25] criterion for entrainment since α versus U in Eq. (30) represents a fold. The above critical value of α determines the nose of the fold beyond which there is no solution. This critical value of α is given by

$$\left(\cos\alpha - \alpha.\sin\alpha - \cos\lambda\right) = \frac{5}{12}Ca.De.\ln\left|\frac{1}{\varepsilon}\right| \tag{32}$$

It says that when *De* is zero, the critical value of α is about $\lambda/\sqrt{3}$, but is dependent on the elastic effect when *De* is not zero.

Finally we note that for receding contact angles, the cases with three lowest concentrations of polymer, fall on the same curve as seen in Figure 4.1. The ones with higher concentrations all entrain. In Figure 4.2 with higher molecular weight polymer, the three at lowest concentrations show increasing departures from λ with increasing polymer concentrations. At higher polymer concentrations entrainment is seen.

5. CONCLUSION

We have shown here that the dynamic contact angles of polymer solutions are affected by shear thinning and elasticity. In case of elasticity, the first normal stress difference has to be high to observe an effect. Our data adhere faithfully to a power law/shear thinning model. We are also able to show that there are conditions under which shear thinning would not have an effect and the viscous effect is fully described by the zero shear viscosity, as shown in Eq. (24). In effect, we have come up with adequate tools to classify "non-Newtonian" behavior for the first time, although more is certainly required.

APPENDIX

In the mode where the cone of the cone and plate rheometer, rotates at constant angular velocity, the viscosity and corresponding shear rates are reported by the machine. These are shown in Figures A1 and A2. The data are fitted to Ellis' model Eq. (2) using vsicosity-shear stress data that are also reported. Zero shear viscosities are seen in Figure A1 and only shoulders are seen in Figure A2. The zero shear viscosities are shown in Figures A3 and A4. In the oscillatory mode, a dissipation (viscous) G'' and storage (elastic) G' are measured as a function of frequency ω. The dissipation leads to viscosity which is not reported here and storage leads to $\Psi_1 = 2G'/\omega^2$ which have been plotted in Figures A5 and A6. Finally in Table A2, we have reported all the data for Ellis' model and data for xanthan 2M solution used by Seevaratnam et al.[8]

Table A1. Ellis' model data

PEO/300K	1gm/dl	2 gm/dl	3 gm/dl	4 gm/dl	5 gm/dl	6 gm/dl
q	2.17	2	2.04	2.04	2.08	2.17
μ_o, Pa.s	0.0095	0.0375	0.1062	0.2924	0.6322	1.5205
$\tau_{1/2}$, Pa	119.587	124.677	119.285	121.773	130.361	138.211
PEO/4M	0.15 gm/dl	0.25 gm/dl	0.5 gm/dl	0.7 gm/dl	1 gm/dl	2 gm/dl
q	1.61	1.69	1.74	1.90	2.51	3.06
μ_o, Pa.s	0.081	0.15	0.402	1.046	8.913	47.347
$\tau_{1/2}$, Pa	0.107	0.129	0.141	0.193	1.349	5.867

xanthan/2M	0.15 gm/dl	0.25 gm/dl
q	2.5	2.94
μ_o, Pa.s	1.43	7.16
$\tau_{1/2}$, Pa	0.215	0.358

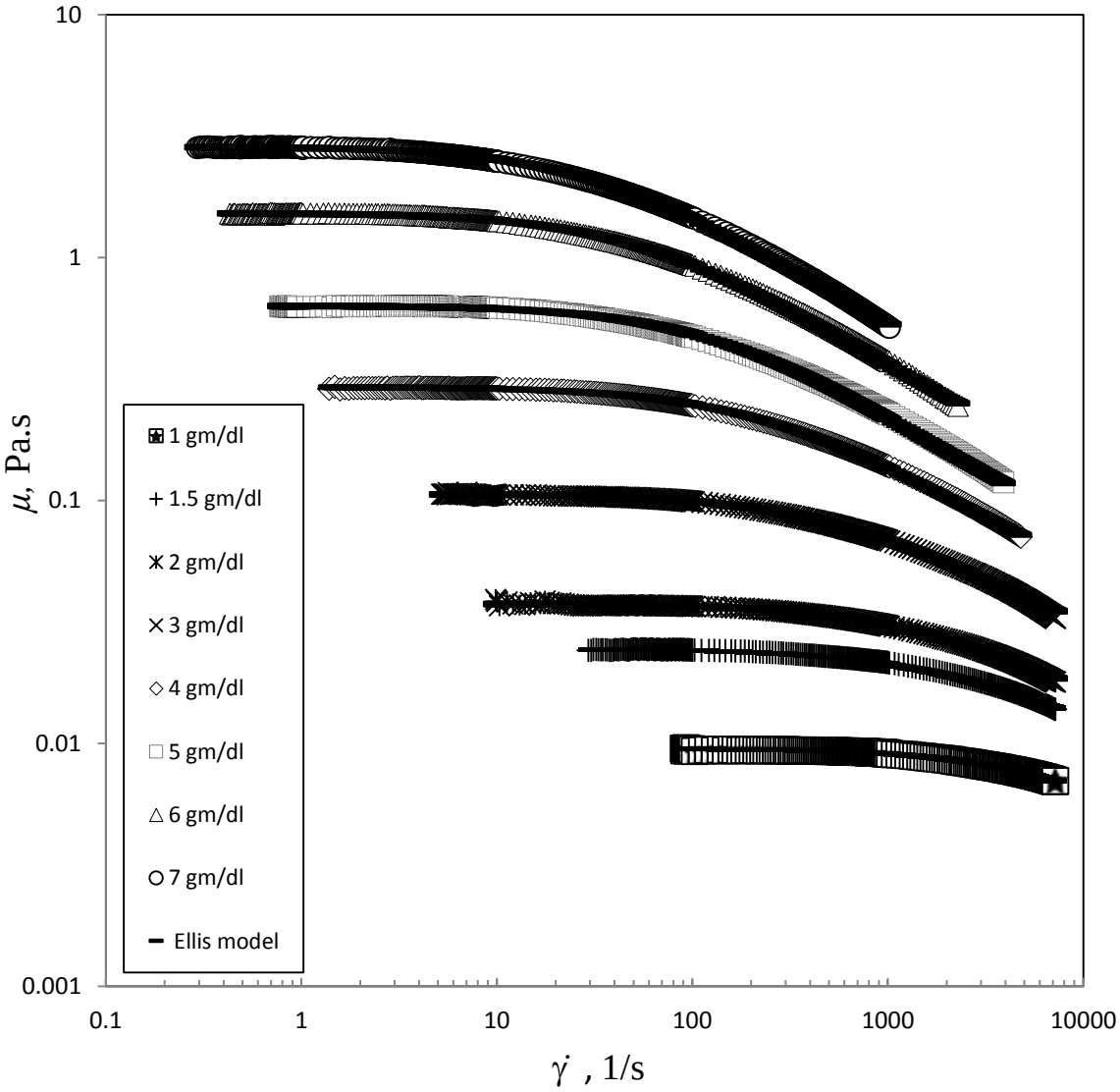

Figure A1. The viscosity and shear rate data are shown for 300K PEO solutions. Also shown are fitted curves of Ellis model

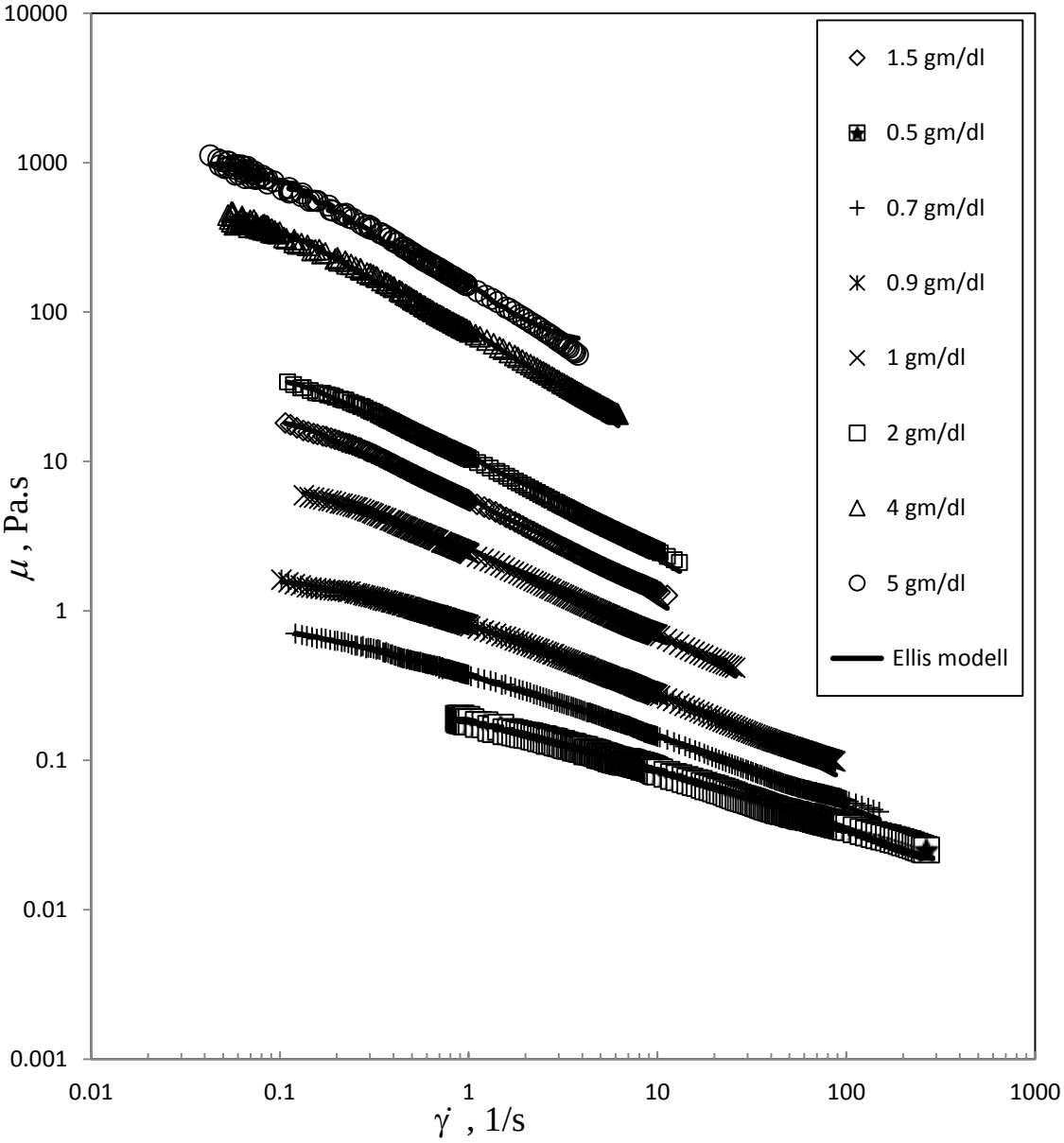

Figure A2. The viscosity and shear rate data are shown for 4M PEO solutions. Also shown are fitted curves of Ellis model.

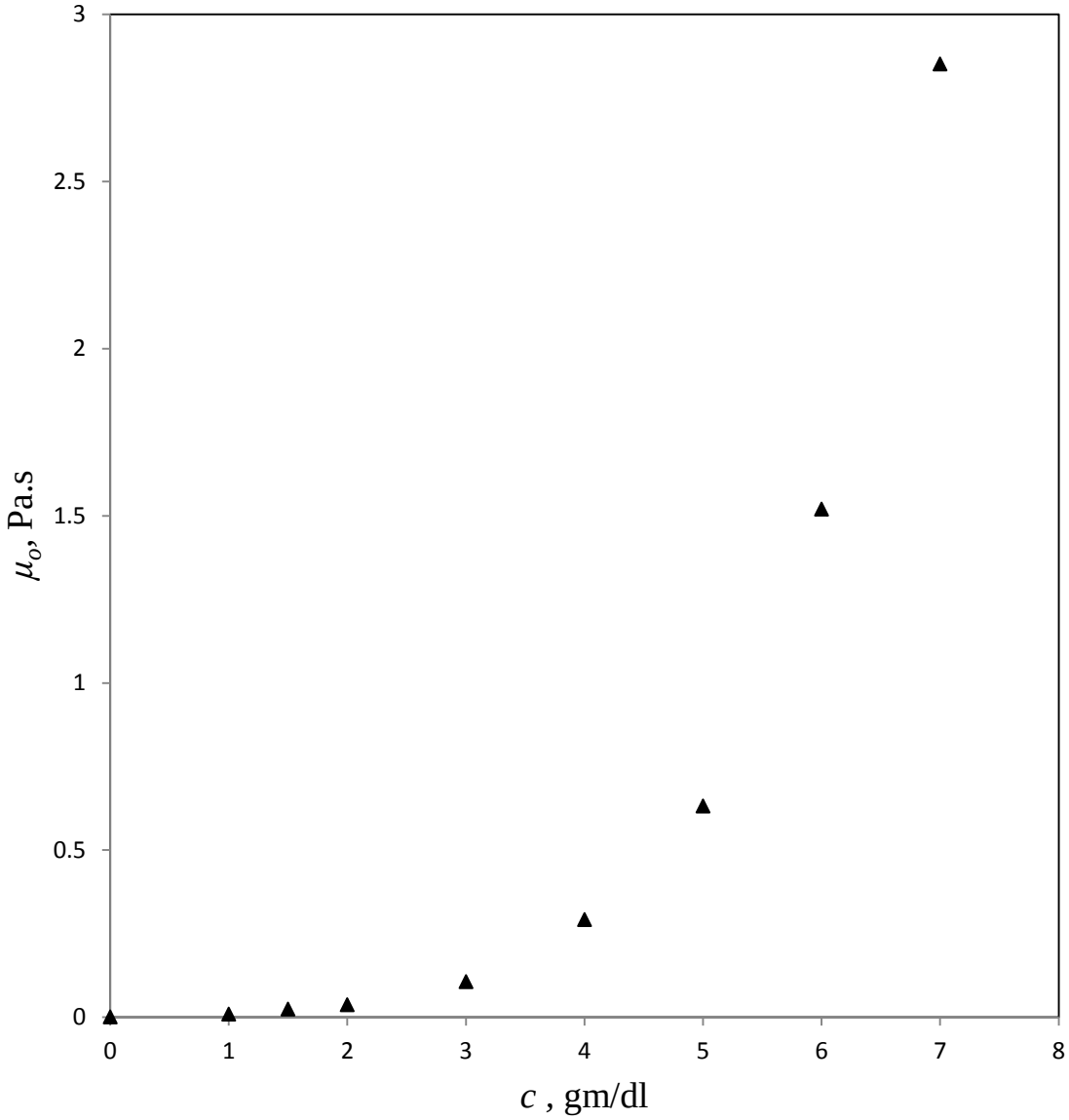

Figure A3: Zero shear viscosities calculated by using Ellis model are shown for 300K PEO solutions versus polymer concentrations.

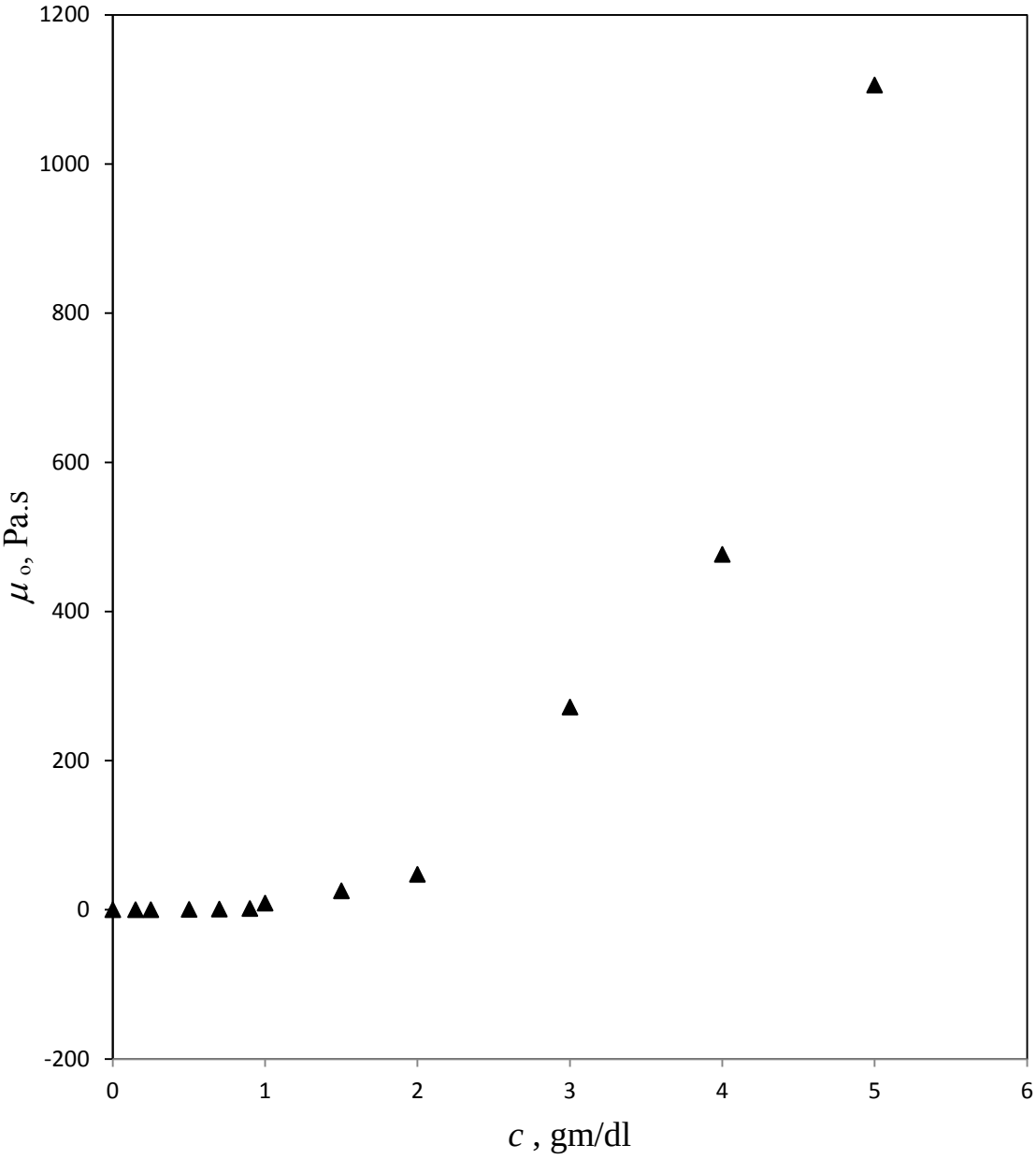

Figure A4: Zero shear viscosities calculated by using Ellis model are shown for 4M PEO solutions versus polymer concentrations.

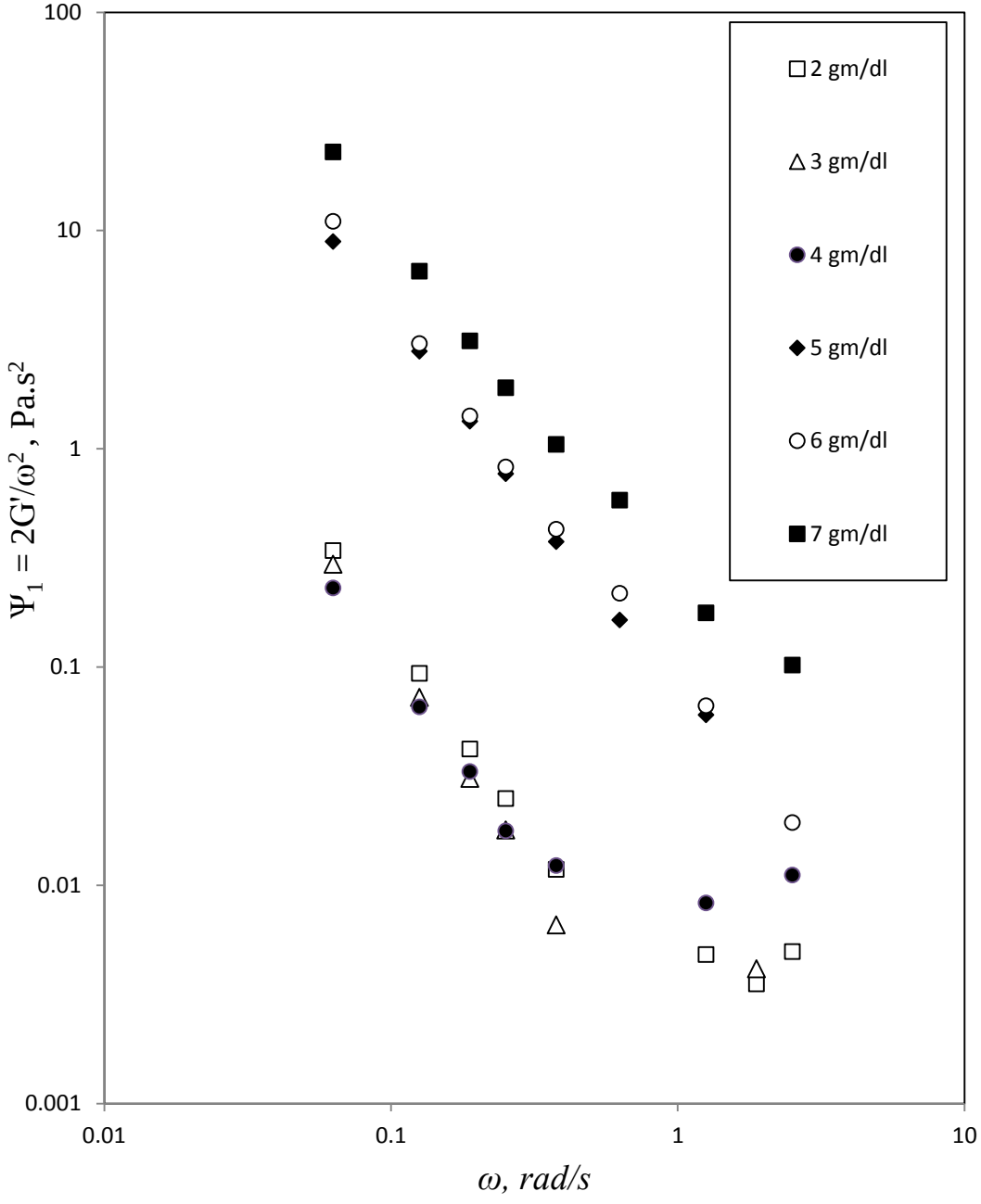

Figure A5. First normal stress coefficient Ψ_1 as a function of ω for PEO 300K

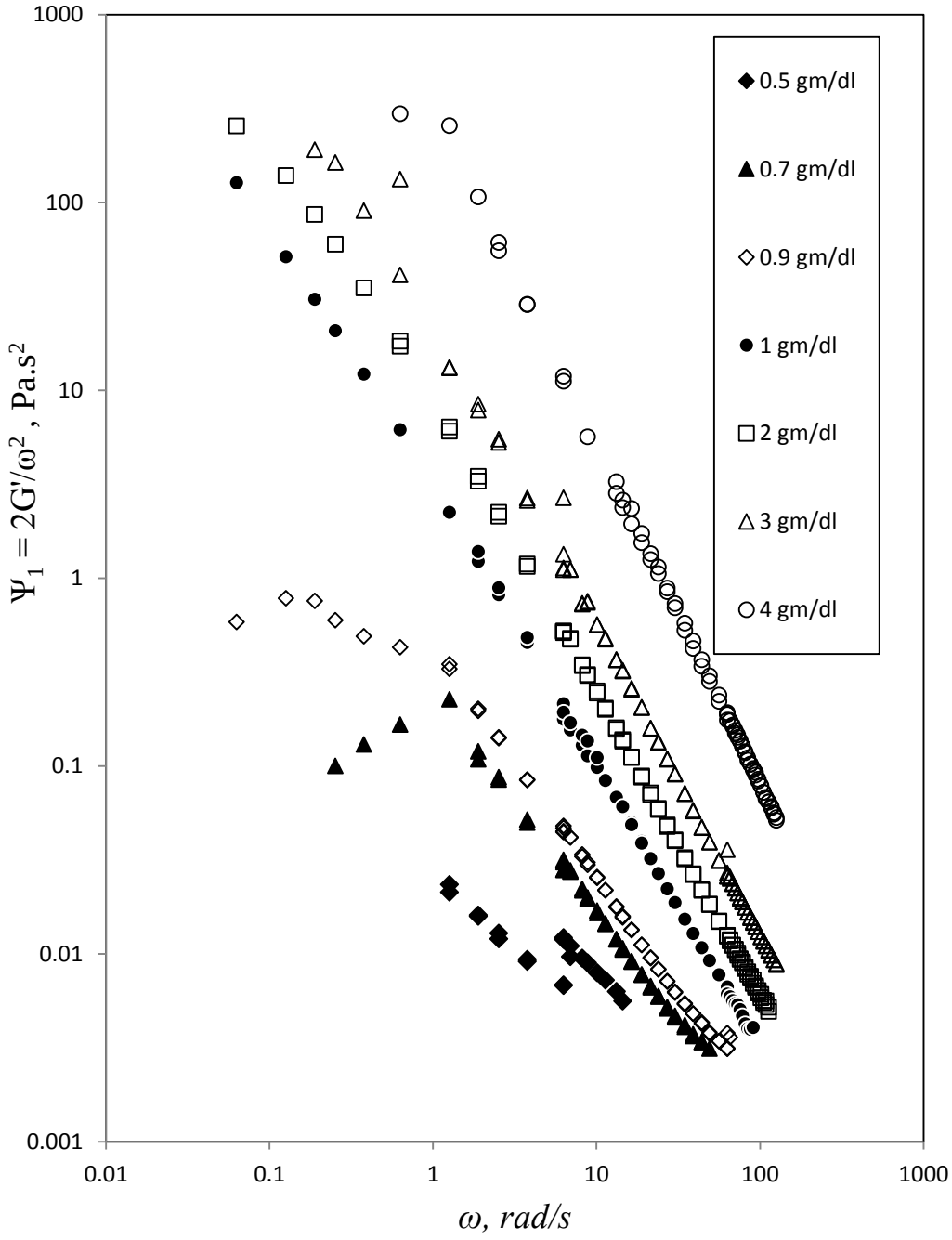

Figure A6. First normal stress coefficient Ψ_1 as a function of ω for PEO 4M

REFERENCES

1. Miller C, Neogi P. *Interfacial Phenomena: Equilibrium and Dynamic Effects*. New York: Marcel Dekker; 2007

2. G.L. Stegemeier. "*Mechanisms of entrapment and mobilization of oil in porous media*." In: Shah DO, Schechter RS, editors. *Improved Oil Recovery by Surfactant and Polymer Flooding* . Academic Press Inc., New York; 1977 . p. 55–91.

3. Bird RB, Armstrong RC, Hassager O. Dynamics of Polymeric Liquids. Volume 1 : Fluid Mechanics. New York: John Wiley & Sons; 1987.

4. De Ryck A, Quéré D. Fluid Coating from a Polymer Solution. *Langmuir*. 1998;14(7) :1911–1914.

5. Nieh S-Y, Ybarra RM, Neogi P. Wetting kinetics of polymer solutions. Experimental observations. *Macromolecules*. 1996;29(1):320–325.

6. de Gennes PG. The dynamics of a spreading droplet. *C R Acad Sci,Ser II Mec, Phys, Chim, Sci Terre Univers*. 1984;298(4):111–5.

7. Neogi P, Ybarra RM. The absence of a rheological effect on the spreading of small drops. *J Chem Phys.* 2001;115(17):7811.

8. Seevaratnam GK, Suo Y, Ramé E, Walker LM, Garoff S. Dynamic wetting of shear thinning fluids. *Phys Fluids*. 2007;19(1):012103/1–9.

9. Neogi P. Dynamic contact angles of shear thinning fluids. *AIChE J*. 2010;56(12):3284–3285.

10. Barone JR. Evaluation of polymer rheology from drop spreading experiments. *Chem Eng Sci*. 2005;60(10):2579–84.

11. Rafaï S, Bonn D, Boudaoud A. Spreading of non-Newtonian fluids on hydrophilic surfaces. *J Fluid Mech.* 2004;513:77–85.

12. Rafaï S, Bonn D. Spreading of non-Newtonian fluids and surfactant solutions on solid surfaces. *Phys A Stat Mech its Appl.* 2005;358:58–67.

13. Wei Y, Rame E, Walker LM, Garoff S. Dynamic wetting with viscous Newtonian and non-Newtonian fluids. *J Phys Condens Matter*. 2009;21(46):464126.

14. Wei Y, Seevaratnam GK, Garoff S, Ramé E, Walker LM. Dynamic wetting of Boger fluids. *J Colloid Interface Sci*. 2007;313(1):274–80.

15. Carré A, Eustache F. Spreading kinetics of shear-thinning fluids in wetting and dewetting modes. *Langmuir*. 2000;16(6):2936–41.

16. Ybarra RM, Neogi P, MacElroy JMD. Osmotic stresses and wetting by polymer solutions. *Ind Eng Chem Res* . 1998 Feb;37(2):427–34.

17. Wasan DT, Nikolov AD. Spreading of nanofluids on solids. *Nature*. 2003;423(6936):156–159.

18. Ghosh M, Fan F, Stebe KJ. Spontaneous pattern formation by dip coating of colloidal suspensions on homogeneous surfaces. *Langmuir*. 2007;23(4):2180–3.

19. Kistler SF. *Hydrodynamics of Wetting*. In: Berg JC, editor. *Wettability*. New York: Marcel Dekker, Inc.; 1993. p. 311–429.

20. Brochard-Wyart F, Gennes P de. Dynamics of partial wetting. *Adv Colloid Interface Sci.* 1992;39(6):1–11.

21. Dussan V. EB. On the spreading of liquids on solid surfaces: Static and synamic contact cines. Annu Rev Fluid Mech. 1979;11:371–400.

22. de Gennes PG. Wetting: statics and dynamics. *Rev Mod Phys.* 1985;57(3).

23. Ashmore J, Shen AQ, Kavehpour HP, Stone HA, McKinley GH. Coating flows of non-Newtonian fluids: Weakly and strongly elastic limits. *J Eng Math*. 2008;60(1):17–41.

24. Al-Shareef A, Neogi P, Bai B. Force based dynamic contact angles and wetting kinetics on a Wilhelmy plate. *Chem Eng Sci*. 2013;99:113–7.

25. de Gennes PG. Deposition of Langmuir-Blofgett layers. *Colloid Polym Sci.* 1986;264(5):463–5.

III. DYNAMIC CONTACT ANGLES IN LIQUID-LIQUID-SOLID SYSTEMS

Amer Al-Shareef [a], P. Neogi[*a], Baojun Bai[b]

[a]*Department of Chemical and Biochemical Engineering*
[b] *Department of Geological Science and Engineering*
Missouri University of Science and Technology
Rolla, Missouri 65409-1203

ABSTRACT

Correlation of the dynamic contact angles as a function of the capillary number in liquid-liquid-solid systems is important in a number of applications. For instance, it is one of the ways used to predict water penetration into a porous medium. The Cahn-Thermo device is used to measure the excess force needed to plunge a plate vertically into a liquid-liquid interface or pull it out. This force is used to calculate the dynamic contact angle. We have used polydimethylsiloxane (PDMS) with different viscosities for the upper phase and water for the lower phase. An algebraic expression that predicts the dynamic contact angles has been derived using the concept that the total viscous dissipation is equal to the surface work in the contact line region. This theory, together with another hydrodynamic theory, was compared to the experiments on the advancing contact angles. The advancing contact lines agree with the theory, and one adjustable parameter that is recovered is found to depend inversely on the viscosity ratio. The receding contact angles showed significant scatter. A closer photographic examination showed the system to be unstable.

NOMENCLATURE

Symbol	Description
A	displaced fluid (silicone oil).
B	displacing fluid (water).
Ca	capillary number.
Ca_B	capillary number based on the viscosity of displacing fluid B.
h	the film thickness, mm
R	viscosity ratio.
U	the velocity of the substrate, μm/sec.
v_r	the velocity component in r-direction, μm/sec.
v_θ	the velocity component in θ-direction, μm/sec.
x	the vertical direction, mm
α	dynamic contact angle, (degree)
γ	surface tension, (mN/m)
γ_{AB}	interfacial tension of silicone oil / water, (mN/m)
γ_{LV}	liquid-vapor surface tension, (mN/m)
γ_{SL}	solid-liquid surface tension, (mN/m)
γ_{SV}	solid-vapor surface tension, (mN/m)
θ	the contact angle, degree
μ	viscosity, cp.
μ_A	viscosity of the displaced fluid, cp.
μ_A	viscosity of the displacing fluid, cp.
π	constant (3.1415)
λ	equilibrium contact angle (degree)

$\lambda a°$	advancing equilibrium contact angle, (degree)
$\lambda r°$	receding equilibrium contact angle, (degree)
ρ	the density of the liquid, kg/m3
ε	singularity, the ratio of micro length scale to the macro length scale.
π_e	the spreading pressure.
ω	molecular kinetics theory constant.
Ω	molecular kinetics theory constant.

1. INTRODUCTION

When a drop or a wedge lies on a solid surface, the line common to the three phases is the three phase contact line, and the angle that the liquid makes with the solid is the contact angle. At equilibrium this value λ is a thermodynamic quantity which is given by the Young-Dupré equation

$$\gamma_{LV} \cos\lambda = \gamma_{SV} - \gamma_{SL} \tag{1}$$

where γ is the surface tension at the liquid-vapor (LV), solid-vapor (SV) and solid-liquid (SL) interfaces. When the surface of the solid ahead of the contact line has an adsorbed layer, γ_{SV} is replaced with $\gamma_{SV} - \pi_e$ where π_e is the spreading pressure. When there is a thin film instead of a layer, a more complicated expression involving disjoining pressure is used instead of π_e (Brochard-Wyart et al., 1991) Thus, the basic format of Young-Dupré equation shows no change although the values of λ will. For wetting liquids $\lambda = 0$ and in many experimental setups equilibrium is not reached. We are interested in non-wetting liquids for reasons discussed below and the differences with wetting liquids are stated in brief where relevant. It is also possible to replace the ambient vapor with an immiscible liquid without change in above. The solid surfaces can be rough at small length scales. Using geometrical arguments Lin et al. (1996) showed that on a rough surface λ carried an error of δ, where δ is the ratio between the length scale of the amplitude to the wavelength of the roughness. Consequently, it is the jagged roughness with high δ that has a large impact on the measured value of λ (Hitchcock et al., 1981) not so much the others.

Under dynamic conditions, the dynamic contact angle α is measured, which is different from λ. According to one theory, the dynamic contact angle represents the breakdown of Eq. (1) (Blake, 1993). However, according to others (Bascom et al., 1964; Radigan et al., 1974) α is an artifact and with better resolution the contact angle is seen to be λ, the equilibrium value. Nevertheless, the reported values of α obtained photographically appeared to be robust and correlate with the capillary number $Ca_B = \mu_B.U/\gamma_{AB}$ where Ca_B is the value based on the lower liquid and μ_B is the viscosity there. We are interested here in liquid-liquid systems, where the lower liquid (B) is water and the upper liquid is oil (A). This setup is found in oil recovery (Morrow, 1990) where water, the displacing liquid, is used for calculating the capillary number as well as in measuring α. The arrangements are shown in Figure 1.1, where in most cases the upper fluid is air. Both advancing and receding cases are studied, and both ranges are cutoff by entrainment. In general, it is important to know the relationship of α as a function of Ca_B, the capillary number of the lower liquid.

Most data have air as the ambient liquid, where the viscosity ratio $R = \mu_A / \mu_B$ is approximately zero. Experimental data on liquid-liquid systems are of interest here and have been given by Foister (1990) and Lin et al. (1998) for a drop spreading on a solid surface under a liquid. These are cases of spontaneous spreading. Data for forced spreading have been reported by Fermigier and Jenffer (1991) for one liquid displacing another in a capillary tube. Gutoff and Kendrick (1982) present some data for liquid-liquid systems using a plate device. All data are for advancing contact lines. The exception is the work on drops by Basu et al.(1996) on receding contact angles but at $R \approx 0$.

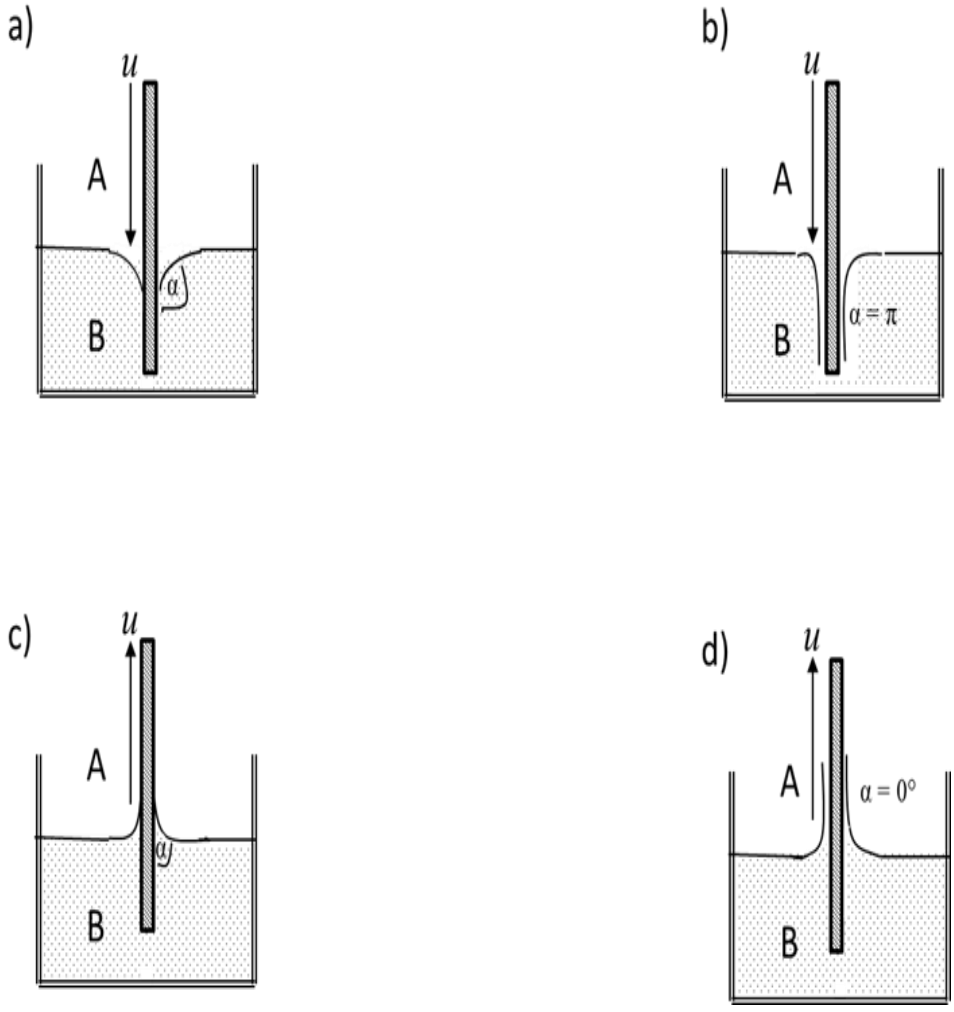

Figure 1.1. (a) The advancing dynamic contact angle at a moderate speed (b) gas entrainment at large values of the advancing speed (d) the nature of the receding dynamic contact angle and (e) liquid entrained on the plate at high velocities during the receding process. A and B are the locations of the phases.

Besides measurements of α versus Ca_B, investigators have also reported instability of the contact lines. Lin et al. (1998) found the contact lines to be scalloped in a liquid-liquid system. A different kind of profile was observed for the receding contact line by Maleki et al. (2007) under air. The conventional profile and the one observed by them

which shows a bead near the contact line are shown in Figure 1.2. They observed that the bead rolled down after a short time. The formation of a bead with a narrow neck is predicted by theory (Duffy and Wilson, 1997). However, investigators have suggested that the region of large curvature at the neck makes it unstable (Neogi, 2010b). The bead will break and roll down.

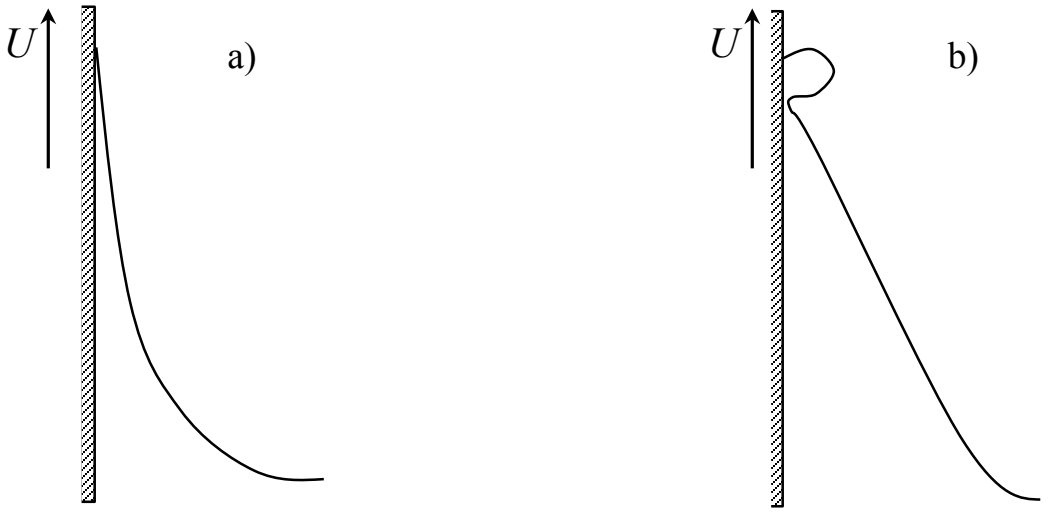

Figure 1.2. a) The usual shape of a meniscus and, b) that when a bead is formed, are shown. The bead is seen only in the receding contact lines.

We have left photography based measurements. The Cahn-Thermo device is a Wilhelmy plate device shown in Figure 1.1, which measures an unbalanced force $\gamma_{AB}\cos\alpha$ in the vertical direction and calculates α when the values of other parameters

are given. There is no guarantee that the values of α measured this way will agree with the values obtained photographically; as is shown in the bead configuration in Figure 1.2. However, most often they agree and it is suggested that even in beads, α measured this way is the slope of the profile away from the bead. Thus, the uncertainties of what the region in the immediate vicinity of the contact line looks like are avoided. However, new issues arise regarding how to explain these measurements theoretically. Now, instead of force balance, de Gennes (1984) made the use of energy balance. He showed that the viscous dissipation in the wedge could be equated to the surface work done. He obtained an expression for α versus Ca_B which agreed with the data obtained from the profiles, at least for some systems. Neogi (2010a) showed that for those conditions the results of force balance and energy methods agree, which establishes the importance of the Cahn-Thermo measurements. Brochard-Wyart and de Gennes (1994) have extended the above by using the fluid mechanical solution by Huh and Scriven (1971). In our previous work, an algebraic expression was derived in a closed form for air-liquid systems; that is, $R \approx 0$ (Al-Shareef et al., 2013) which will be referred to as the de Gennes-Huh-Scriven solution (dHS). It showed excellent agreement with the advancing and receding dynamic contact angle data for air - silicone oil system for both advancing and receding contact lines.

To understand the displacement of one liquid by another in a porous medium at the micro-level, displacement in a single pore or a doublet is often studied. It requires the knowledge of surface tension and contact angles, where the latter is taken to be the equilibrium contact angle although dynamic contact angles should be used. Below we have presented force based dynamic contact angle data. Being force based, they are exactly suitable for above calculations which arise from force balances. We also examine existing

theories to find correlations. In that, we present the modified de Gennes-Huh-Scriven (mdHS) solution for a liquid-liquid system as well as that of Cox (1986) and Blake (1993).

An important feature in all hydrodynamic theories is that the shear stress is found to be infinite at the contact line. As a result a slip boundary condition is necessary which is characterized by the slip length. The dimensionless slip length ε is small such that the effects of slip are not felt unless the local thickness of the liquid layer h becomes comparable to ε. Neogi (2006) has reviewed the extent and nature of roughness on electrochemical and chemical vapor deposited surfaces. Although very smooth crystalline surfaces can be made, it is the surfaces with submicron roughness that are commonly available and need to be addressed first. Neogi and Miller (1983) took this up as a central issue and modeled the surface of the solid as the surface of porous media of permeability $k \sim \varepsilon$. If $\delta \sim \varepsilon$, then as stated earlier the contact angles do not change and slip velocity is given by Darcy's law. Profiles and spreading rates were obtained for both wetting and non-wetting liquids. They compared their results for the rate of spreading of small drops to the available data on wetting liquids to calculate the surface rough as 1-3 μm consistent with information available there. Thus the model deals with what can be considered to be the dynamics of bulk liquid which is usually followed in the experiments. The thin precursor film containing the contact line is lost in the porous surface and as it moves ahead faster than the bulk (Bascom et al., 1964) it does not put a back pressure on the bulk and the dynamics of the two can be uncoupled. Further, the results of spreading kinetics obtained by Neogi and Miller (1983) are no different from the others above where the slip is defined differently. The slip condition defines the mobility of the contact line. Thus on

a smooth surface the next slip mechanism in line steps in as observed by Lin et al. (1996) on spontaneous spreading of small drops on freshly cleaved mica.

Experiments and comparison with theory are given below, and Table 1.1. summarizes where our work belongs.

Table 1.1. Classification of the previous and present works based on the viscosity ratio for advancing and receding cases.

Case type	$R \approx 0$	$R \sim 1$	$R \to \infty$
Advancing	many	Foister (1990), capillary tube Fermigier and Jenffer (1991), capillary tube Gutoff and Kendrick (1982) , flat plate	Present work
Receding	none	none	Present work

2. MODELS

In the first model from de Gennes (1984) an energy balance is made. Huh and Scriven (1971) obtained the stream functions for phase A and phase B, from which the velocities v_r and v_θ can be calculated in each phase. The viscous dissipation (Bird et al., 2007) can be obtained and integrated over the full volume of each phase. Equating this to the surface work leads to the result.

$$\left(cos\lambda\text{-}cos\alpha\right) = 4.Ca_B.ln\left|\frac{1}{\varepsilon}\right|.\left\{c_B^2\left[\frac{\alpha}{2}+\frac{sin2\alpha}{4}\right]\text{-}c_B d_B\left[\frac{1\text{-}cos2\alpha}{2}\right]+d_B^2\left[\frac{\alpha}{2}\text{-}\frac{sin2\alpha}{4}\right]+R\left(\begin{array}{l} c_A^2\left[\frac{\pi}{2}\text{-}\frac{\alpha}{2}\text{-}\frac{sin2\alpha}{4}\right] \\ \text{-}c_A d_A\left[\frac{cos2\alpha\text{-}1}{2}\right]+d_A^2\left[\frac{\pi}{2}\text{-}\frac{\alpha}{2}+\frac{sin2\alpha}{4}\right]\end{array}\right)\right\} \quad (2)$$

where ε is the ratio of micro length scale to the macro length scale. The constants are the same as in Huh and Scriven (1971). The main problem with the solution of Huh and Scriven is that the normal stress boundary condition is not satisfied at the liquid-liquid interface. In addition, the de Gennes development assumes that the interface is given by an equation of a straight line.

$$c_B = \frac{sin^2\alpha\left[sin^2\alpha-\delta^2+R\left(\delta\alpha-sin^2\alpha\right)\right]}{D} \quad (3)$$

$$d_B = \frac{\sin\alpha\cos\alpha\left[sin^2\alpha-\delta^2+R\left(\delta\alpha-sin^2\alpha\right)-R\pi\tan\alpha\right]}{D} \quad (4)$$

$$c_A = \frac{sin^2\alpha\left[sin^2\alpha-\delta\alpha+R\left(\alpha^2-sin^2\alpha\right)\right]}{D} \quad (5)$$

$$d_A = \frac{\sin\alpha\cos\alpha\left[sin^2\alpha-\delta\alpha+R\left(\alpha^2-sin^2\alpha\right)-\pi\tan\alpha\right]}{D} \quad (6)$$

$$D=\left(\sin\alpha\cos\alpha-\alpha\right)\left(\delta^2-\sin^2\alpha\right)+R\left(\delta-\sin\alpha\cos\alpha\right)\left(\alpha^2-\sin^2\alpha\right) \tag{7}$$

$$\delta=\pi-\alpha \tag{8}$$

Although this method does not satisfy force balances adequately, the results have been shown to compare well with the experiments (Al-Shareef et al., 2013; Neogi, 2010a). Further, Basu et al. (1996) have used this method to quantify their experimental results. de Gennes (1984) used a cutoff instead of slip, but the results (where they can be compared) are the same.

Cox's results are

$$g(\alpha)-g(\lambda)=Ca_B.\ln\left|\frac{1}{\varepsilon}\right| \tag{9}$$

$$g(\alpha,R)=\int_0^{\alpha}\frac{d\theta}{f(\theta,R)} \tag{10}$$

$$f(\theta,R)=\frac{2\sin\theta\left[R^2\left(\theta^2-\sin^2\theta\right)+2R\left\{\theta(\pi-\theta)+\sin^2\theta\right\}+\left\{(\pi-\theta)^2-\sin^2\theta\right\}\right]}{R\left(\theta^2-\sin^2\theta\right)\left\{(\pi-\theta)+\sin\theta\cos\theta\right\}+\left\{(\pi-\theta)^2-\sin^2\theta\right\}(\theta-\sin\theta\cos\theta)} \tag{11}$$

Cox's solution assumes that $\left|\cos\alpha-\cos\lambda\right|$ are small and a smaller term of the order of *Ca* has been ignored in above. Besides the continuum models, Blake (1993) has proposed a theory of wetting kinetics using a molecular model which takes the form

$$\gamma_{AB}(\cos\lambda-\cos\alpha)=\Omega\sinh^{-1}[\omega\mu_A Ca_B] \tag{12}$$

where ω and Ω are constants. Consequently, we have in above an energy balance approach in mdHS model, a profile based approach and a molecular model to analyze the data presented next.

3. EXPERIMENTAL

3.1. DIP COATING OF COVER GLASS WITH PVC

The glass cover slips 1" x 1" were cleaned first in ethanol for 10 minutes and then in distilled water for 30 minutes. They were dried in an oven at 40ºC for an hour. Separately we dissolved polyvinyl chloride (PVC) in the solvent tetrahydrofuran (THF), and solutions were prepared with different concentrations of PVC: 0.25gm/dl, 0.5gm/dl, 1gm/dl, and 5gm/dl. We then deposited the PVC on the cover glass slips by dip coating at slow speeds. The dip coating step had been the procedure used earlier by Al-Shareef et al. (2013) for coating glass with a fluoropolymer. The samples were then kept in the oven at 40°C for 30 minutes till dry and examined under microscope at 40X as shown in Figure 3.1. Only 3c was used which in our estimate has roughness of about ~ 0.5 μm in height. The second substrate was PET (polyethylene terephthalate) slips used as supplied. Manufactures quote a tolerance in the thickness of PET sheets ~ ± 1.25 μm. However, the thickness varies on the surface over a large length scales and no bumps can be see under the microscope. Some sparse sets of scratches could be seen.

For all measurements involving two liquids, it is necessary to rule out mass transfer even though the silicone oils very strongly repel water. The two liquids were first emulsified using a homogenizer, then centrifuged and allowed to settle overnight following an earlier procedure (Lin et al., 1998).

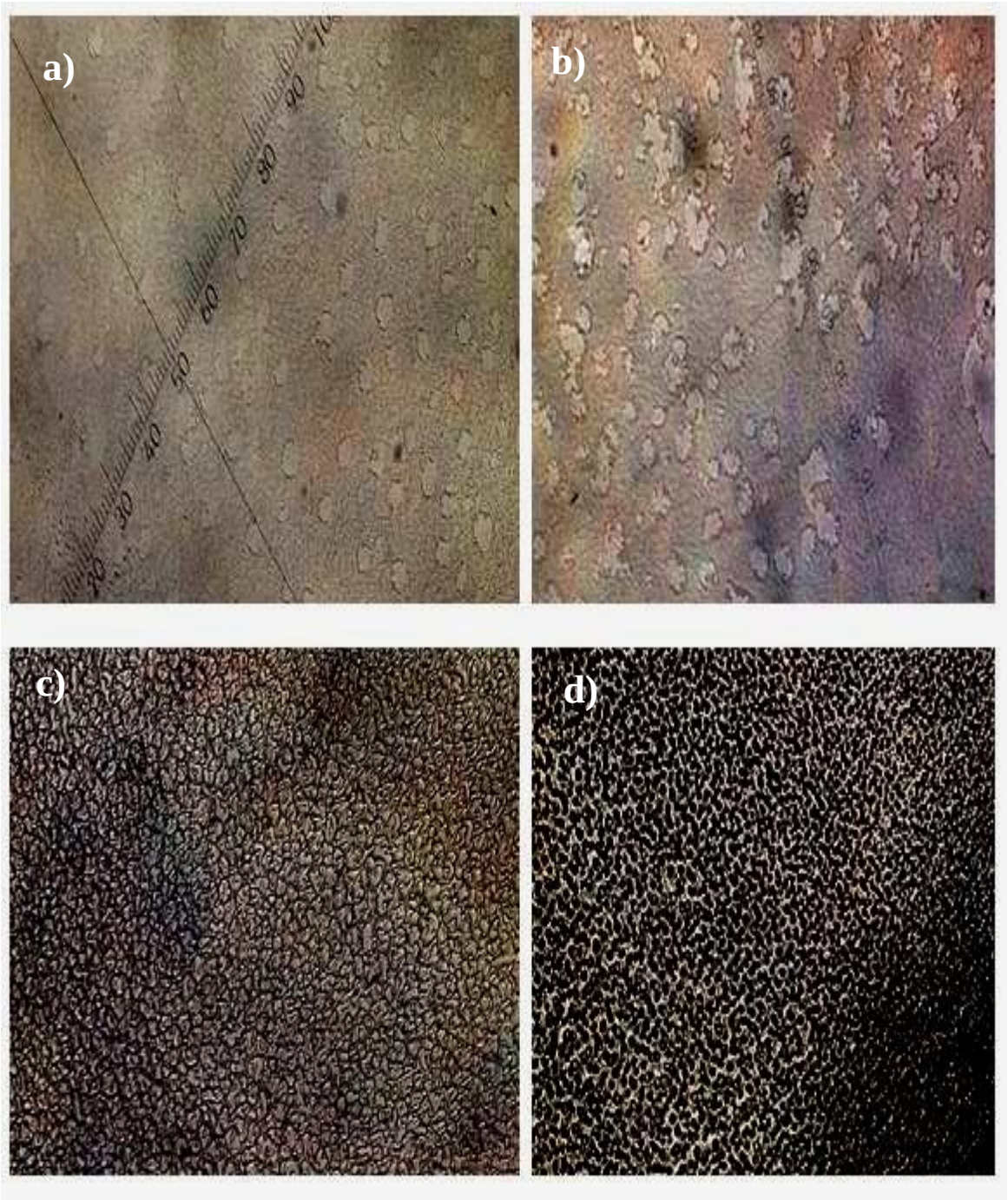

Figure 3.1. PVC was deposited on the cleaned glass surface at different concentrations of a) 0.25, b) 0.5, c) 1 and d) 5 wt% in tertrahydrofuran (THF). Microscopy images 40x are shown. The case c) was picked both because of somewhat homogeneous appearance and as the equilibrium contact angles showed reproducibility.

3.2. EQUILIBRIUM ADVANCING AND RECEDING CONTACT ANGLE MEASUREMENTS

We have measured the equilibrium contact angles through water using a Ramé-Hart contact angle goniometer. A drop of water was layered under air and the chamber was flooded with oil. The drop volumes were larger than 10 μl which is the limit below which gravity is negligible. The advancing and receding contact angles were measured by tilting the sample as shown in Figure 3.2. as observed in a contact angle goniometer. The angle of tilt could go up to about 70º. However, the values of contact angles became independent of the tilt angle much earlier. The values of contact angles are given in Table 1.1. $\lambda \sim 90°$ is useful since the range of α for advancing dynamic contact angle is 180º to λ and for receding case λ to 0º. If λ were zero (wetting) then the receding case would be fully suppressed, but an intermediate value of λ makes certain that neither advancing nor receding ranges are suppressed.

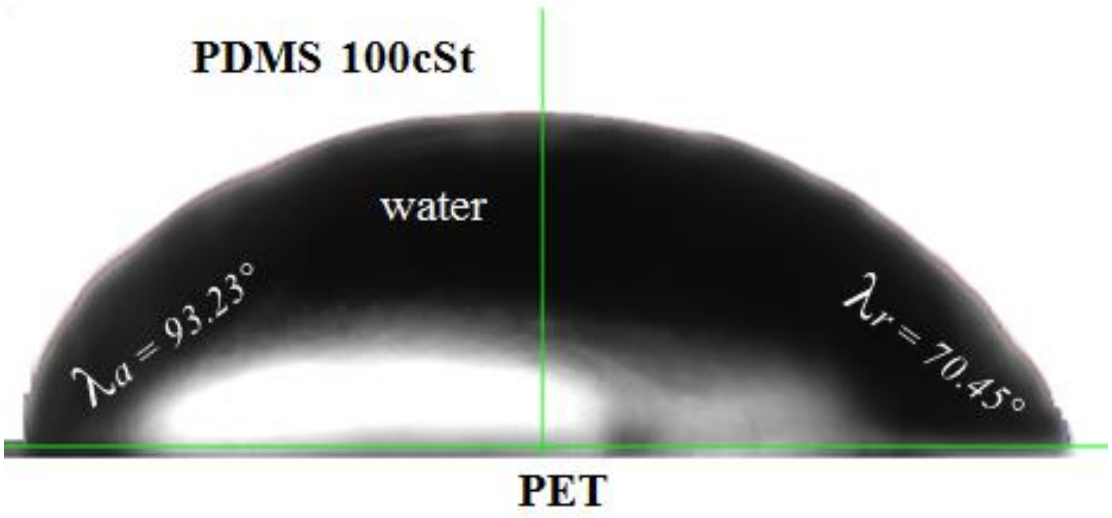

Figure 3.2. View of a water droplet under silicone oil in the goniometer under oil on an incline. Small amount of potassium permanganate has been added to water for contrast

3.3. INTERFACIAL TENSION MEASUREMENTS OF PDMS / WATER SYSTEM

It is possible to measure the interfacial tension using the Wilhelmy plate technique. It is the force on the plate that is measured and used to calculate γ_{AB}. For a non-wetting liquid

$$\gamma_{\text{exp.}} = \gamma_{AB}.\cos\lambda \tag{13}$$

Obviously, λ has to be measured separately. This experiment was carried out on glass where λ = 65.36º (measured using contact angle goniometer and translated to the value of contact angle measured through water). γ_{AB} works out to be 40.77 mN/m. Note that the scope of error with polymer substrate is very high as $\lambda \sim 90º$ in Eq. (13). This compounds the already problematic feature that the two liquids have specific gravities that are quite close. Hence, glass substrate was used. Glass was washed in KOH-isopropyl alcohol for four hours followed by three washes in distilled water (Nieh et al., 1996).

3.4. CAHN-THERMO TECHNIQUE

The force balance method was used to measure the advancing and receding dynamic contact angles. The tensiometer eventually calculates $\gamma_{AB}.\cos\alpha$ when the two densities, the wetted perimeter and γ_{AB}, are supplied. The machine is a balance and the two liquids in a beaker are moved up or down at fixed velocities. For an air-liquid interface, the plate weight in air is set to zero. When the plate moves into the liquid a jump in weight is measured and a base line in the change in weight due to buoyancy is also measured and used to calculate this value accurately. The base line is calculated from the velocity of travel, time taken, the height of travel and the specific gravity of the liquid. This jump is perimeter times $\gamma.\cos\alpha$. For the liquid-liquid system, the plate is initially all submerged in

the upper liquid and the specific gravity of the lower liquid is now replaced in calculations with the specific gravity of the bottom liquid (water) less the specific gravity of the top liquid (oil). The entire above are automated and only the value of α is returned.

The Cahn-Thermo operates at speeds of 42, 82, 164 and 328 μm/s with which the motorized platform moves up or down. These are larger than the velocities encountered in oil recovery work (~ 7 μm/s). One fluid will displace another at the moving contact line and at those velocities. The plate was also made to move from the upper liquid where it was fully immersed at the start, and then fully into the lower liquid. The total travel is 10 mm. The procedure was started by immersing the plate fully in oil, and then it was lowered into water at the lowest speed.

After fully immersing it in water, the travel was reversed until the plate became fully immersed in oil. Both operations were conducted at the lowest velocity. The procedure was started again with the next velocity until the four cycles were completed. This was followed by another cycle at the lowest speed to check if the results were the same as in the first operation. The results for the advancing dynamic contact angles were always within 1º and the data were accepted for that oil – water pair. However, the receding dynamic contact angles looked significantly different and led us to investigate the situation further.

Dow Corning silicone oils of high viscosities, from 100 cSt to a 500 cSt were used as the upper phase and distilled water as the lower phase. The viscosities were measured using Brookfield viscometer.

4. RESULTS AND DISCUSSION

The measured advancing and receding equilibrium (static) contact angles are listed in Table 4.1. The contact angles were measured through water.

Table 4.1. Advancing and receding static contact angles for different viscosity ratio.

Phase A	γ_{AB} mN/m	Water /Oil/Glass		Water /Oil/PET		Water /Oil/PVC	
		$\lambda_a°$	$\lambda_r°$	$\lambda_a°$	$\lambda_r°$	$\lambda_a°$	$\lambda_r°$
100 cSt	40.01	65.36	30.12	93.29	70.45	94.66	78.24
200 cSt	40.12	66.54	34.15	94.63	73.41	94.22	80.49
350 cSt	40.23	66.85	37.17	94.88	74.45	94.36	83.45
500 cSt	40.89	67.45	39.42	94.65	75.89	94.97	84.45

The mean values over three runs are shown. The standard deviations were calculated all were all less than ± 2.14º, which is larger than the variations among cases of oils of different viscosities for all the contact angles. So we use one value for the advancing equilibrium contact angles and that is chosen to be that of 100 cSt oil, 65.36º. The 100 cSt oil moves five times faster than 500 cSt oil and these drops are closer to being equilibrated. Using above contact angle on glass, γ_{AB} was obtained as 40.77 mN/m as mentioned earlier and by using the advancing equilibrium contact angle. It agrees with the result of Marinova et al.(2005) of 41 ± 0.5 mN/m.

Now, the advancing dynamic contact angles are shown along with the fit to the mdHS and Cox's theory in Figures 4.1 and 4.2 respectively. Eq. (2) is restated as

$(\cos\lambda - \cos\alpha) = Ca_B.\ln\left|\frac{1}{\varepsilon}\right|.X(\alpha, R)$ and hence $Y(\alpha, R) = \frac{(\cos\lambda - \cos\alpha)}{X} = Ca_B.\ln\left|\frac{1}{\varepsilon}\right|$. This has allowed us to plot *Y* versus Ca_B in Figures 4.1 and 4.2. Similarly, Eq. (9) is written as $Y(\alpha, R) = g(\alpha) - g(\lambda) = \ln\left|\frac{1}{\varepsilon}\right|.Ca_B$ and plotted as *Y* versus Ca_B.

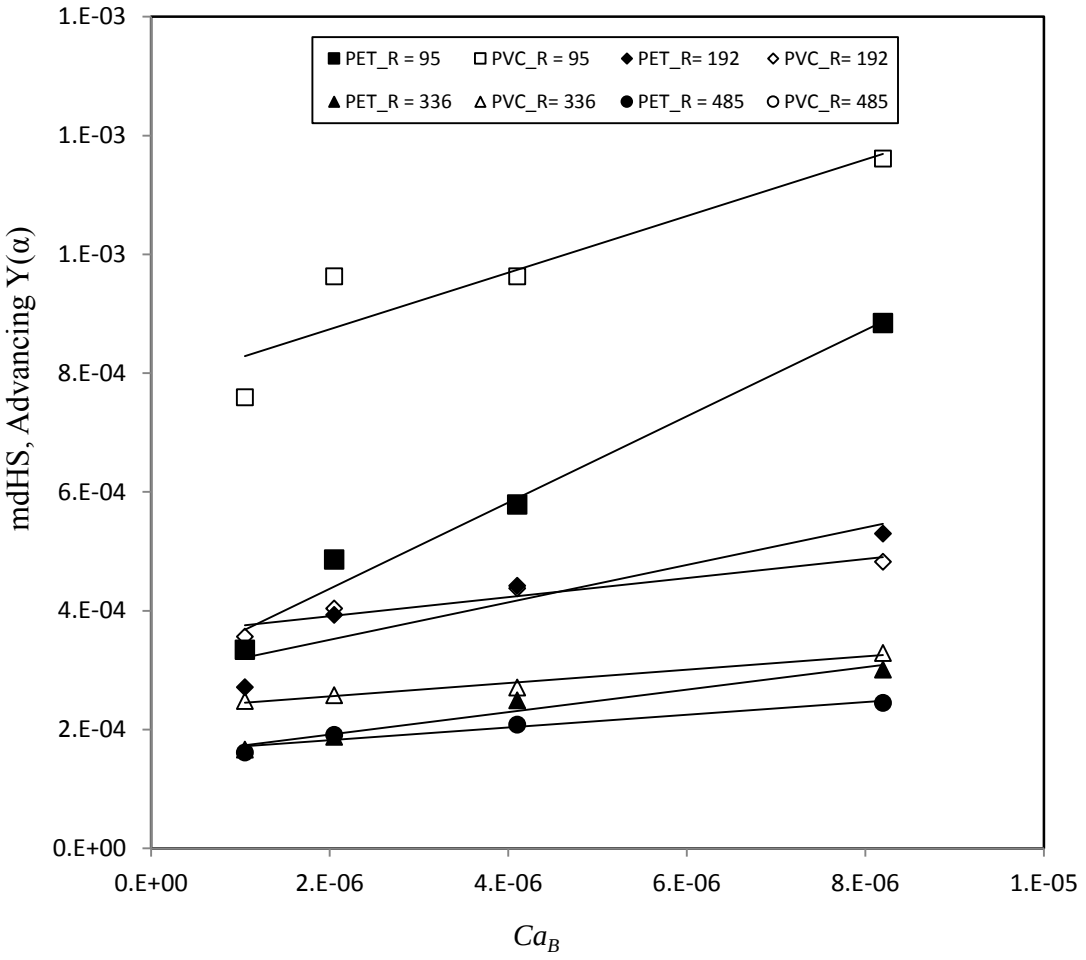

Figure 4.1. *Y* defined in the text for mdHS model has been plotted against Ca_B. The data fit straight lines with slopes of $\ln\left|\frac{1}{\varepsilon}\right|$. The error in measuring α is about 1°.

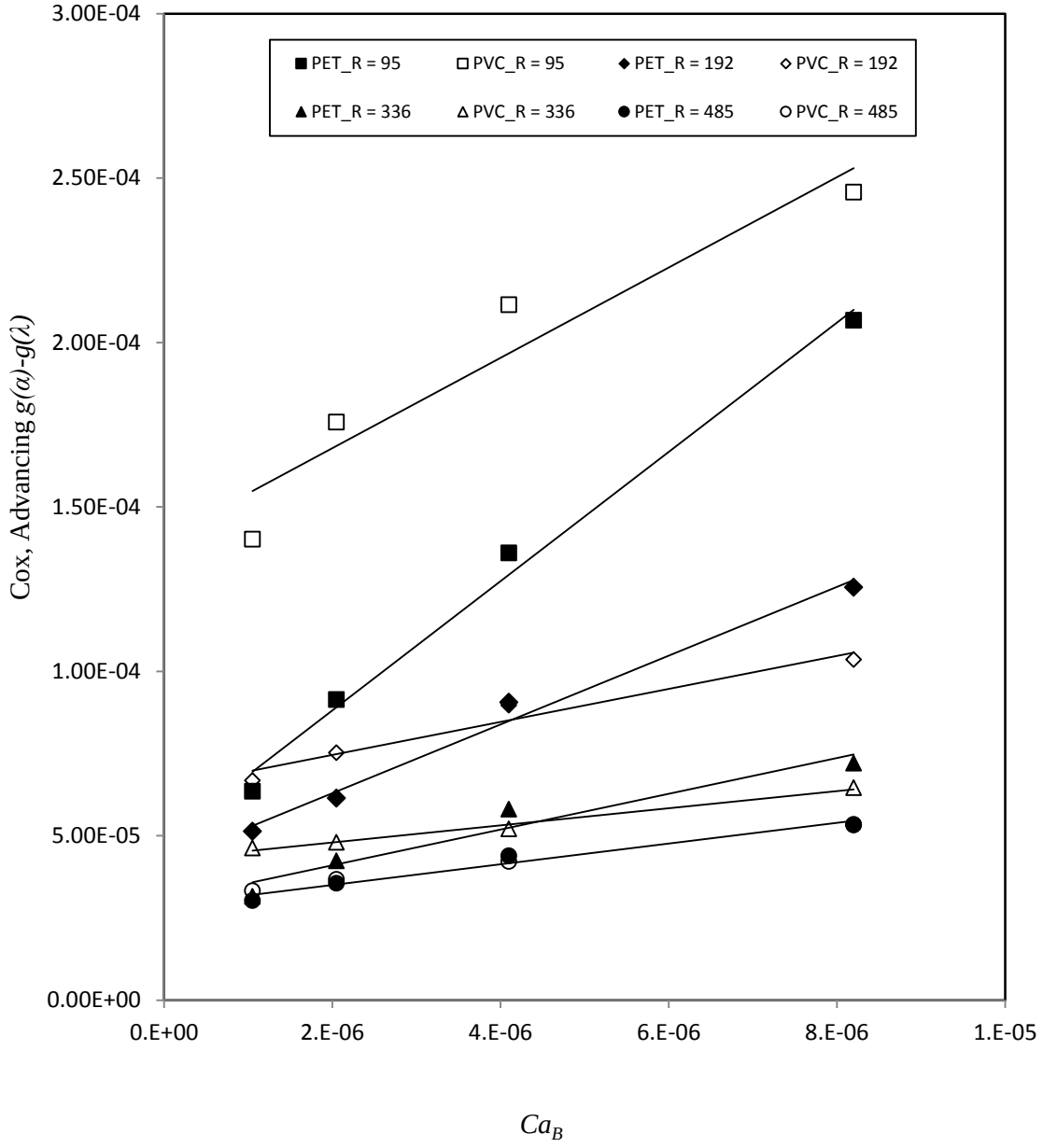

Figure 4.2. *Y* defined in the text for Cox's model has been plotted against Ca_B. The data fit straight lines with slopes of $\ln\left|\frac{1}{\varepsilon}\right|$. The error in measuring α is about 1°.

The reason is that in both cases, the theories suggest that the data when plotted as Y versus Ca_B should fall on straight lines and they do. There is a small but non-zero intercept.

All values of Y should go to zero at zero capillary number and provide zero intercepts showing that there equilibrium contact angle is reached, and the data nearly do so. However, the fit is not as good as the experiments error in measuring α (± 1°).

It is possible that a small term discarded in the theory presented here, may improve the fit when it is included. Now, the slopes which are $\ln\left|\frac{1}{\varepsilon}\right|$ vary a lot. These values are plotted in Figure 4.3, where it appears that they fit to very good approximation $\ln\left|\frac{1}{\varepsilon}\right| \propto R^{-1}$ for both theories. To fit their data to Cox's theory, Fermigier and Jenffer (1991) obtain ~ 55, which falls in the range in Figure 4.3.

Their data were collected from number of experiments conducted in capillary glass tube with different systems of displacement, silicone oil / air and silicone oil / glycerin. The comparison was with Hoffman-Tanner law and theory of Cox. Their experimental data of dynamic contact angles in liquid-liquid system show a significant increase compared to the dynamic contact angles predicted by theory of Cox. The fitting parameter was quite large also.

Similarly, Foister's (1990) numbers are also in this range. Since our data are force based dynamic contact angles, their indirect agreement with the profile based contact angle data suggest that the two sets are at least close.

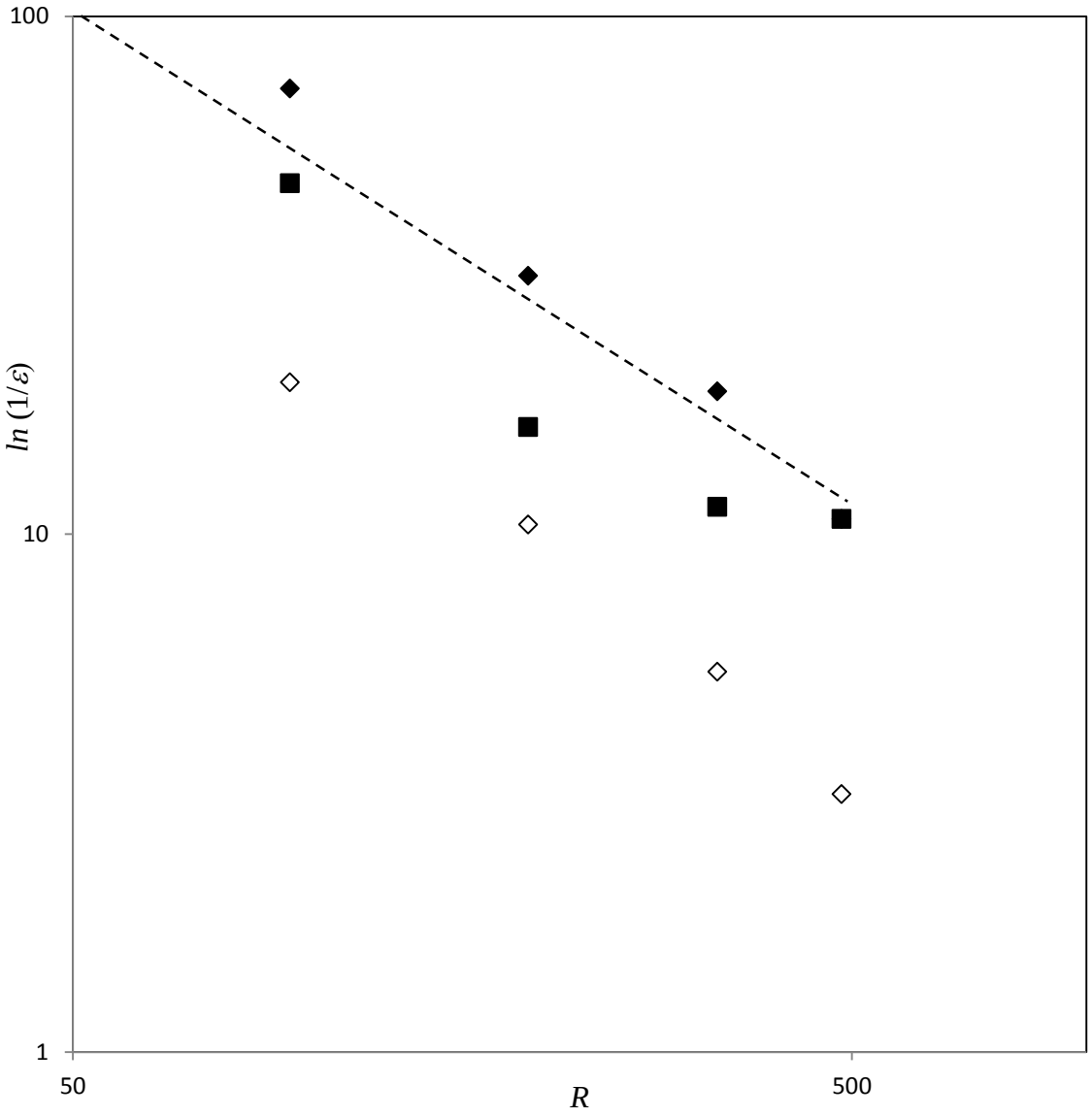

Figure 4.3. The values of $\ln\left|\frac{1}{\varepsilon}\right|$ for the advancing case have been plotted against R in log-log. The black symbols are when mdHS model has been used and white when Cox's model has been used. Further, the diamonds are for the PET substrate and the squares are for the PVC substrate. In all cases $\ln\left|\frac{1}{\varepsilon}\right|$ is a good approximation proportional to R-1. In fact; a line of slope – 1 is obtained by joining the top left corner (50, 100) to (500, 10).

Both force based data and their apparent agreement with profile based data are shown for the first time. Whereas some ideas exist for the microscopic length, the Wilhelmy plate does not provide a macroscopic length scale. If the macroscopic length scale is taken to be in (mm – cm), $\ln\left|\frac{1}{\varepsilon}\right|$ works out to 5 – 9. However, when fitted to the data, a much larger range of 25 - 75 is observed. Although some thinking has gone into what the macro length scale could be for liquids under air (Eggers and Stone, 2004), there is still no conclusion. For the liquid-liquid system the result that $\ln\left|\frac{1}{\varepsilon}\right| \propto R^{-1}$ is striking.

One feature seen here is interesting and of consequence. Over the range of Ca_B used here α does not change much over the equilibrium value λ. Possibly in the liquid-liquid systems, the viscous dissipation when the contact angle changes from λ to α is large and cannot be balanced by surface work unless this change remains small. That is, compared to liquid-air system (Al-Shareef et al., 2013).

The receding contact line data have been plotted in Figures 4.4 and 4.5 differently from those in the advancing case. The fitted values of $\ln\left|\frac{1}{\varepsilon}\right|$ range from 50 to 1000. The logarithm scale in Ca_B compresses a family of theoretical plots into what appears to be a single curve. The bold lines follow mdHS, Eq. (1) and the dashed one in the theory of Cox, Eq. (8). The reason for illustrating the receding contact line data in this form is that in spite of significant effort on our part to bring the data together, the data still show large scatter. (If the advancing dynamic contact angles were plotted this way, then all the data would fall on one another and on the theoretical plot.)

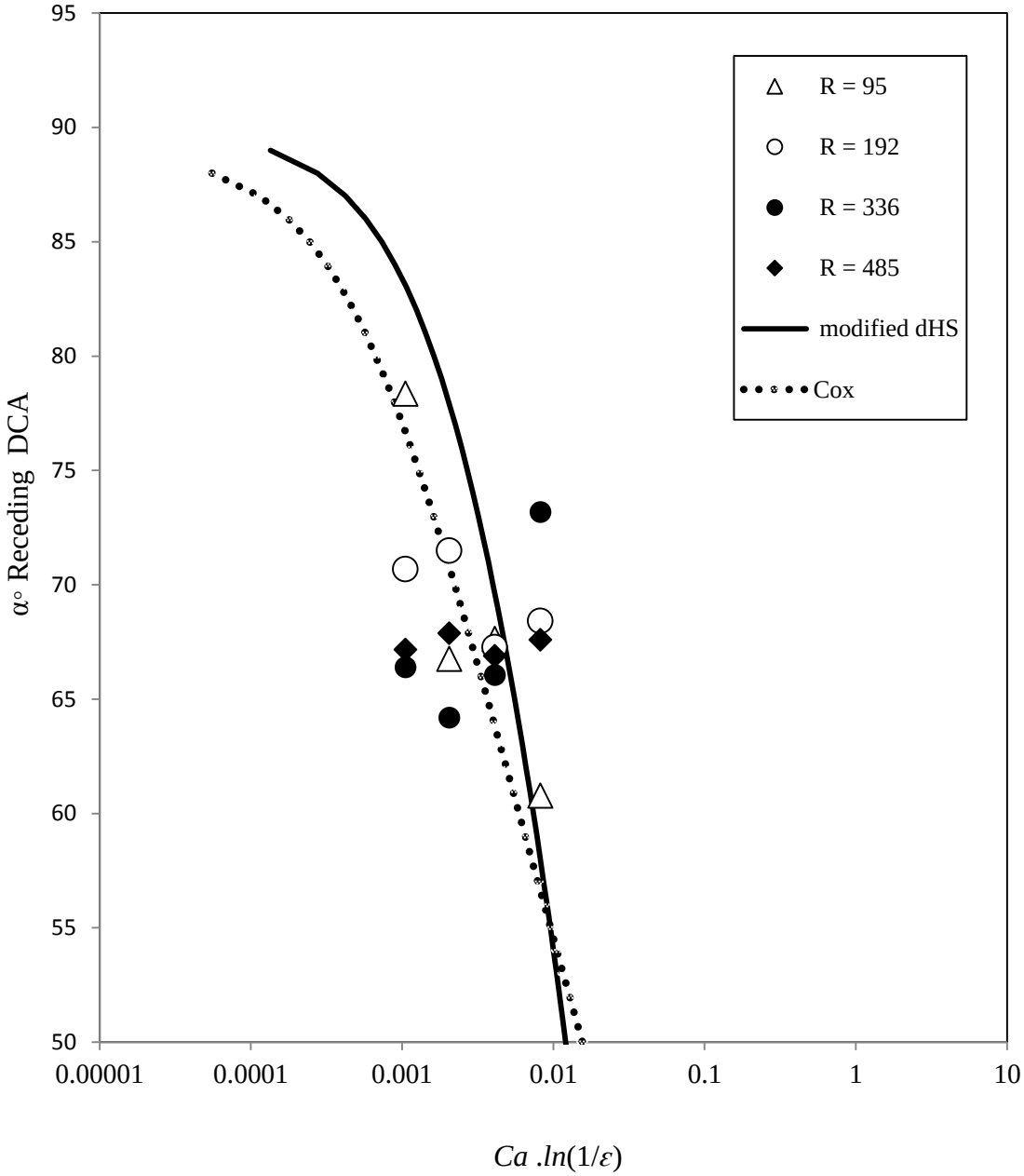

Figure 4.4. Experimental data of receding contact angles versus the capillary number for the PDMS/Water/PET system; the bold line is the fitting with mdHS, Eq. (1), solution at cutoff length $ln(1/\varepsilon) = 1000$,and dotted line is the fitted with Cox's, Eq. (8) at cutoff length $ln(1/\varepsilon) = 1000$. The theoretical curves are independent of R at the large values of R used here

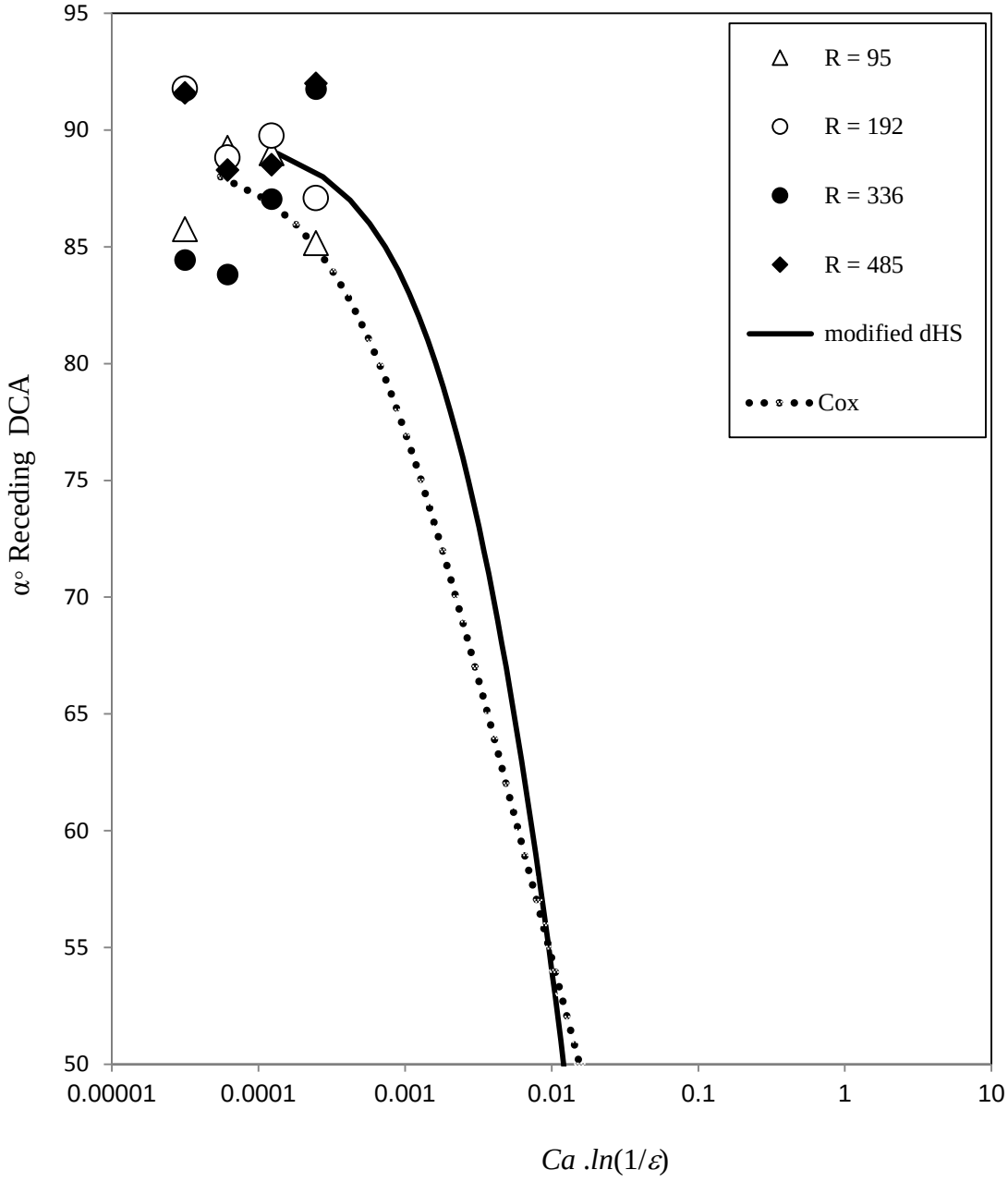

Figure 4.5. Experimental data of receding contact angles versus capillary number for PDMS/Water/PVC system, the bold line is the fitting with mdHS, Eq. (1), solution at cutoff length $ln(1/\varepsilon) = 30$,and dotted line is the fitted with Cox's, Eq. (8) at cutoff length $ln(1/\varepsilon) = 30$. The theoretical curves are independent of R at the large values of R used here.

As a result, we further investigated the receding contact lines using photography. This is shown in Figure 4.6, which shows that in 4.6 (a) the advancing contact lines and the menisci on two sides are similar, smooth and given reasonably by an equation of a straight line. However, beads form at the receding contact line as seen in Figure 4.6 (b). Both (c) and (d) cases are not symmetric; (c) shows that one bead is beginning to collapse, and both (c) and (d) show the presence of waves running perpendicular to the figure. Figure 4.7 has been drawn as an aid in viewing Figure 4.6. The representative dimension here is about 2 mm. Water (B), the lower liquid has been colored with a small amount of potassium permanganate. The curved walls of the beaker and the presence of a small meniscus there give rise to some distortions in the images. It becomes clear that this formation of beads leads to unstable contact lines and hence shows a scatter in the measured values of α.

Neogi (2010a) argued that the contact line in the receding case was a stagnation region where the stream lines turn around, and hence, the pressure there is high and a bump or bead appears. A typical fluid mechanical model for the meniscus in Figure 1.2 uses lubrication theory approximation. It leads to the equation (Duffy and Wilson, 1997; Neogi, 2010b)

$$h^2 \frac{d^3 h}{dx^3} = \frac{3\mu U}{\gamma} \tag{14}$$

Here, h is the film thickness and x is the vertical direction. The system is liquid under air, R = 0, and the solution shows bead formation. This profile was matched with the equilibrium profile that is formed as a balance between gravity and capillarity. The bead shows a very narrow neck and (Neogi, 2010a) argued on the basis on previous work (Neogi,

2001) that the region of large curvature was unstable, will break and the bead will roll off as seen in the experiments of Maleki et al.(2007).

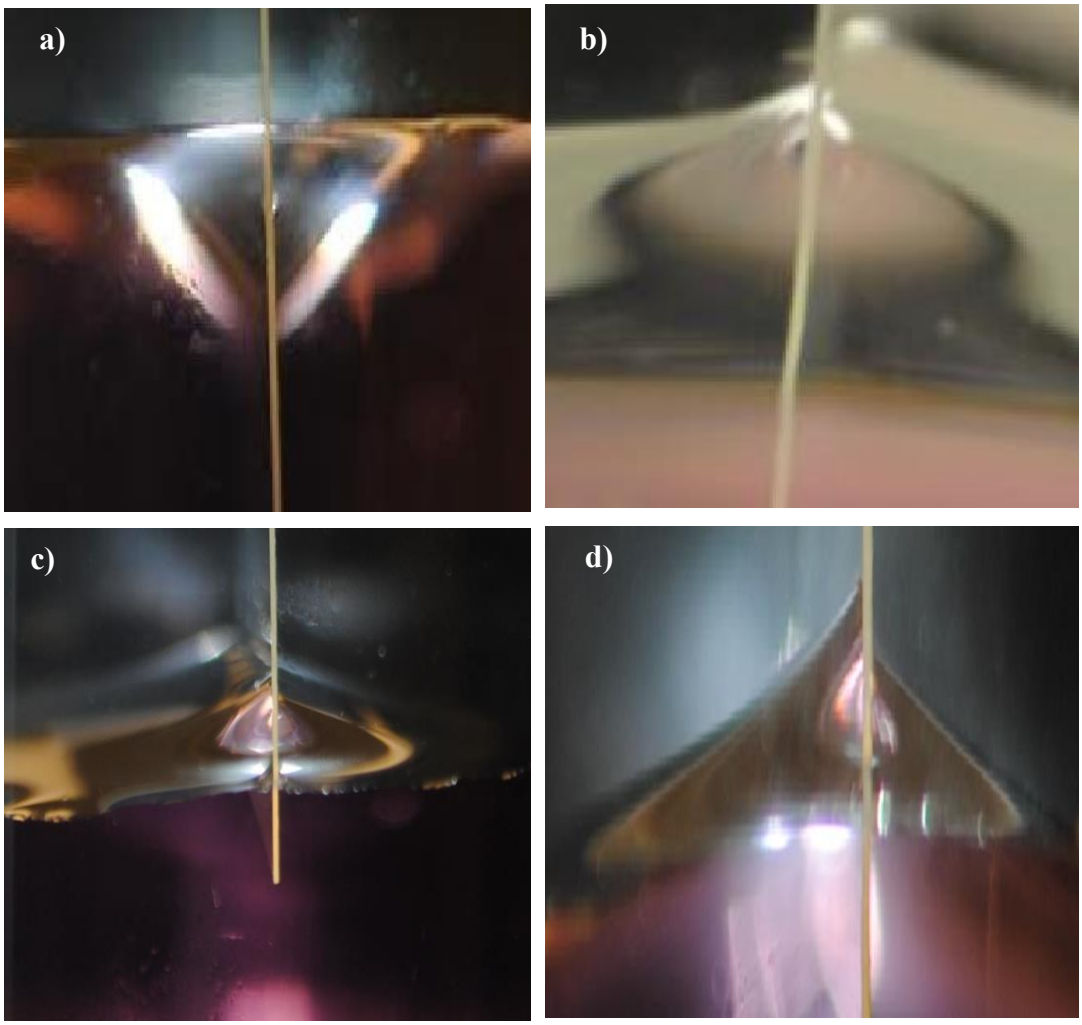

Figure 4.6. a) The menisci on the two sides for the advancing case are almost linear and almost symmetric. b) The menisci for the receding case show clearly the formation of beads. c) The bead on the left appears to have collapsed and concentric patterns show waves in the direction perpendicular to the plane of the figure and. d) The same view emphasizing the waves and the lack of left and right symmetry of deformable bead. The scale of the objects is in few millimeters and water, the lower liquid, has been colored with potassium permanganate.

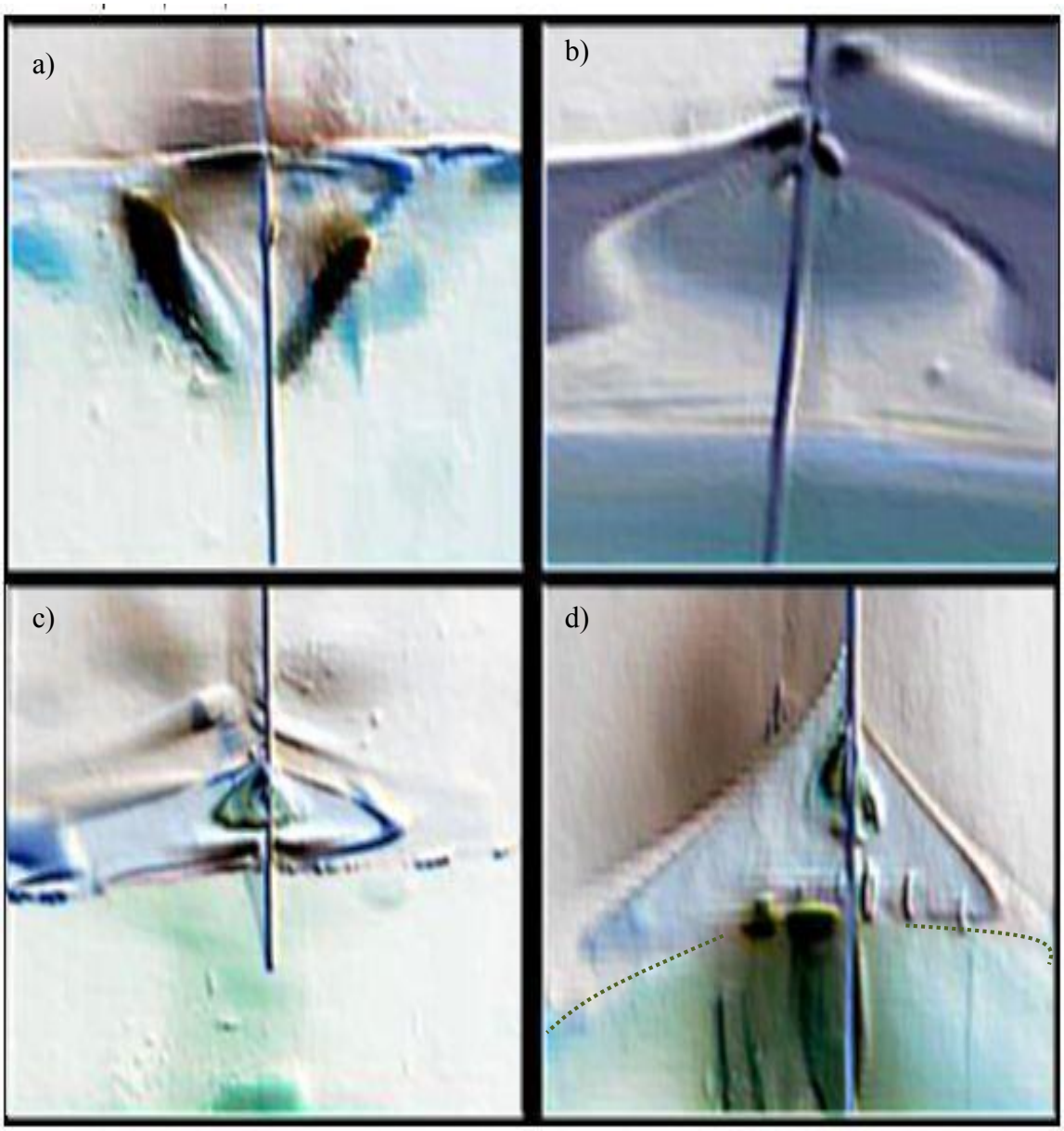

Figure 4.7. The contours of Figure 4.6 after image processing to remove the shadows and glare.

That gravity may not be the reason for the break is suggested by the scale of the region ~ 2mm. The disturbances of the wavelengths that are affected by gravity are long. Nevertheless, their rolling down after the break is due to gravity.

In a liquid-liquid system, when the upper liquid (A) is a very viscous liquid, that is, *R* is very large (here, *R* lies at 100 and above), then the zero tangential stress boundary condition at the interface will be changed to zero tangential velocity boundary condition. The only change is that the factor 3 in Eq. (14) is changed to 6. In that case all features discussed for liquid-air system will remain. That is, bead will form, break and roll down (although very slowly because of the large buoyancy effect). It is interesting that in most theoretical developments including Cox's, the capillary number $\mu U/\gamma$ is assumed to be small, or terms of methods of matched asymptotic expansions ~$o(1)$, actually $O([\ln 1/\varepsilon]^{-1})$. However, the bead formation is seen only when it is ~ $O(1)$. The full solution for the meniscus needs gravity and although the capillary numbers in Figures 4.4 and 4.5 appear to be small, this is not the case (Neogi, 2010a) .

Blake's theory (1993) in Eq. (12) suggests that all data for the advancing contact angles would fall on a single curve if $\gamma_{AB}(\cos\lambda - \cos\alpha)$ were plotted against $\mu_A Ca_B$. They do not. The scatter is significant and the model was not investigated any further.

5. CONCLUSION

The force based contact angles have been reported here. The system is that of a liquid displacing another liquid where the displacement velocities and the viscosity ratios correspond to those in crude oil recovery. We found the fitting parameter, logarithmic of the ratio of microscopic to the macroscopic length scale using the mdHS (modified de Gennes Huh Scriven) model as calculated by us and another by Cox (1986). Both cases led to the observation that the logarithm is inversely proportional to the viscosity ratio. In this range both mdHS (modified de Gennes Huh Scriven) model and Cox's model are adequate for predicting the values of contact angles for the advancing case. In the receding case there is instability near the contact line because of which good data could not be obtained.

REFERENCES

Al-Shareef A, Neogi P, Bai B (2013) Force based dynamic contact angles and wetting kinetics on a Wilhelmy plate. *Chem Eng Sci* 99:113–117. doi: 10.1016/j.ces.2013.05.052

Bascom W, Cottington R, Singleterry C (1964) Dynamic surface phenomena in the spontaneous spreading of oils on solids. In: Gould R (ed) Contact Angle, *Wettability, and Adhesion. American Chemical Society*, Washington, D. C., pp 355–380

Basu S, Kandakumar K, Masliyah HJ (1996) A study of oil displacement on model surfaces. *J Colloid Interface Sci* 182:82–94. doi: 10.1006/jcis.1996.0439

Bird R, Stewart W, Lightfoot E (2007) *Transport Phenomena*, 2nd edn. John Wiley & Sons, New York

Blake TD (1993) Dynamic contact angles and wetting kinetics. In: Berg JC (ed) *Wettability*. Marcel Dekker, Inc., New York, pp 251–309

Brochard-Wyart F, Gennes P de (1994) Spreading of a drop between a solid and a viscous polymer. *Langmuir* 10:2440–2443.

Brochard-Wyart F, Meglio J, Quere D, Gennes P (1991) Spreading of nonvolatile liquids in a continuum picture. *Langmuir* 12**:**335–338. doi: 10.1021/la00050a023

Cox RG (1986) The dynamics of the spreading of liquids on a solid surface. Part 1. Viscous flow. *J Fluid Mech* 168:169–194. doi: 10.1017/S0022112086000332

de Gennes PG (1984) The dynamics of a spreading droplet. *C R Acad Sci,Ser II Mec, Phys, Chim, Sci Terre Univers* 298:111–115.

Duffy BR, Wilson SK (1997) A third-order differential equation arising in thin-film flows and relevant to Tanner's Law. *Appl Math Lett* 10:63–68. doi: 10.1016/S0893-9659(97)00036-0

Eggers,J., Stone, H.A.,2004. Characteristic lenghts at moving contact lines for a perfectly wetting fluid: the interface of speed on the dynamic contact angle. *J.Fluid Mech.* 505,309-321.

Fermigier M, Jenffer P (1991) An experimental investigation of the dynamic contact angle in liquid-liquid systems. *J Colloid Interface Sci* 146:226–241.

Foister R (1990) The kinetics of displacement wetting in liquid/liquid/solid systems. *J Colloid Interface Sci* 136:266–282.

Gutoff EB, Kendrick CE (1982) Dynamic contact angles. *AIChE J* 28:459–466.

Hitchcock SJ, Carroll NT, Nicholas MG (1981) Some effects of substrate roughness on wettability. *J Mater Sci* 16:714–732. doi: 10.1007/BF00552210

Huh C, Scriven L (1971) Hydrodynamic model of steady movement of a solid/liquid/fluid contact line. *J Colloid Interface Sci* 35:85–101.

Joanny J-F, Andelman D (1987) Steady-state motion of a liquid/liquid/solid contact line. *J Colloid Interface Sci* 119:451–458. doi: 10.1016/0021-9797(87)90290-6

Lin C, Neogi P, Ybarra R (1998) Wetting kinetics of a drop on a horizontal solid surface under a viscous ambient liquid. *Ind Eng Chem Res* 5885:66–70.

Lin C, Ybarra R, Neogi P (1996) Three-and two-dimensional effects in wetting kinetics. *Adv Colloid Interface Sci* 67:185–204.

Maleki M, Reyssat E, Quéré D, Golestanian R (2007) On the landau-levich transition. *Langmuir* 23:10116–10122.

Marinova K, Christova D, Tcholakova S (2005) Hydrophobization of glass surface by adsorption of poly (dimethylsiloxane). *Langmuir* 21:11729–11737.

Morrow N (1990) *Interfacial Phenomena in Petroleum Recovery*. Marcel Dekker Inc., New York

Neogi P (2010a) Bead formation near the contact line in forced spreading. *Chem Eng Sci* 65:4572–4578. doi: 10.1016/j.ces.2010.04.040

Neogi, P., Miller,C.A.,1983. Spreading kinetics of a drop on a rough solid surface. *J. Colloid & Interface Sci.* 92:338–349.

Neogi P (2010b) Large dynamic contact angles. *Chem Eng Sci* 65:708–712. doi: 10.1016/j.ces.2009.09.024

Nieh S-Y, Ybarra RM, Neogi P (1996) Wetting kinetics of polymer solutions. Experimental observations. *Macromolecules* 29:320–325. doi: 10.1021/ma950424r

Radigan W, Ghiradella H, Frisch H, et al (1974) Kinetics of spreading of glass on fernico metal. *J Colloid Interface Sci* 49:241–248.

IV. DYNAMIC CONTACT ANGLES IN OIL-AQUEOUS POLYMER SOLUTIONS

Amer Al-Shareef [a], P. Neogi[*a], Baojun Bai[b]

[a]*Department of Chemical and Biochemical Engineering*
[b] *Department of Geological Science and Engineering*
Missouri University of Science and Technology
Rolla, Missouri 65409-1203

ABSTRACT

Polymer flooding is an important process in oil recovery. The displacement front is unstable when low viscosity brine displaces the crude oil in the reservoir. Polymer is added to the brine to increase its viscosity which stabilizes the displacement process. To investigate the displacement process at a micro-level, we have investigated the dynamic contact angles in silicone oil-polymer (polyethylene oxide) solution. Dynamic contact angle is the apparent contact angle at the three phase contact line which governs the capillary pressure, which is important in the displacement process. The data show no obvious signs of either shear thinning or elastic behavior; although for some systems with highest elastic effects some unexplained effects are seen. Overall, dynamic contact angles are explained well using existing models for two Newtonian fluids, when the zero shear viscosity is used for the polymer solution.

1. INTRODUCTION

Polymer flooding has been one of older enhanced oil recovery processes and perhaps the most successful one [1–5]. The key feature is that the displacement of oil by brine has an unfavorable mobility ratio, explained in a simple way as the high ratio between the viscosity of oil to the viscosity of brine. As a result the displacement front in the oil field, which is a porous medium, becomes unstable. If a thickener such as a polymer is added to the brine then the mobility ratio becomes less than one (favorable) and the displacement becomes stable. The question also arises as to what happens at the micro level[6] other than polymer adsorption and exclusion from very fine pores.

At micro level the interfacial tension plays an important role. When a drop lies on a solid surface, Young-Dupré equation is given by

$$\gamma_{LV}.\cos\lambda = \gamma_{SV} - \gamma_{SL} \tag{1}$$

where γ is the surface tension and S, L and V are solid, liquid and vapor phases, and λ is the equilibrium contact angle which is the angle the drop makes with stationary solid surface at the contact line. The schematic view is shown in Figure 1.1. The vapor phase can be replaced by a second immiscible liquid.

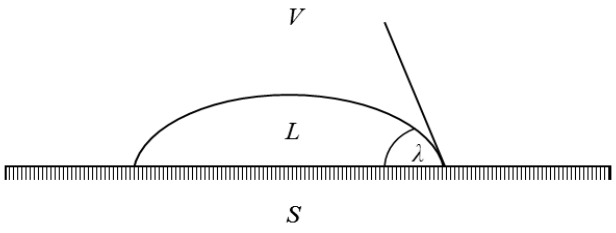

Figure 1.1. A drop of liquid is shown on a plate with a horizontal upper surface. Three phases, solid (S), liquid (L) and vapor (V) are shown where the vapor phase can be replaced with an immiscible liquid. The contact line is at O and the equilibrium contact angle is λ.

In addition, under dynamic conditions (such as the substrate moving tangentially at a velocity *U*), λ is replaced by α, the dynamic contact angle. However, under dynamic conditions λ should be replaced by α, the dynamic contact angle. Like λ, which has an advancing equilibrium contact angle and a receding equilibrium contact angle, α too has advancing dynamic contact angles and receding dynamic contact angles. For the advancing case, $\alpha > \lambda$, and for the receding case $\alpha < \lambda$. The values of substrate velocities *U* are capped by entrainment. The arrangement is shown in Figure 1.2. Above discussion assumes that the ambient fluid is air. However, air can be replaced with a second immiscible liquid and the present discussion will hold.

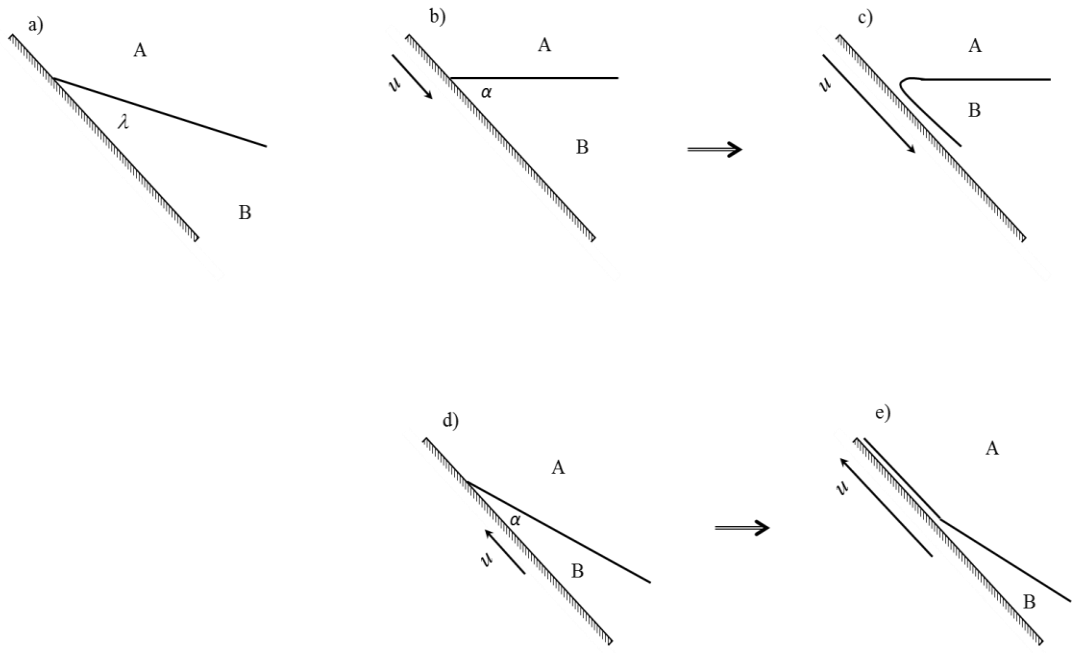

Figure 1.2. The arrangement for dynamic contact angle (α) is shown. Liquid A is crude/silicone oil and liquid B is water/brine/aqueous polymer solution. The contact angle is measured through the aqueous phase and α is the advancing contact angle. Receding contact angle is observed when the direction of plate velocity *U* is reversed. The liquid entrainment also takes place at large speed of the plate.

In general, capillary imbibition in a porous medium[7] has surface forces in form of $\gamma.\cos\lambda$ where under dynamic conditions λ should be replaced with α, and such efforts are being made[8,9]. Similarly in a consolidated porous medium, $\gamma.\cos\lambda$ term is used to correlate the capillary pressure p_c [10] whereas α should be used.

Recent work by the present investigators[11] using water and silicone oils, showed that over ranges of interest α did not change significantly from λ. Instead of brine, water was used as no effect was found on adding 1wt % NaCl to water. Silicone oils were used instead of crude oil because the ability to observe visually the experiments was important. For instance Keller et al.[12] report only advancing contact angles of crude oil under air. The problem now is if water is replaced with a polymer solution, we no longer have a Newtonian liquid. Previously, it had been suggested that shear thinning and elastic effects do not play a role[13]. Although this is true for the most part, exceptions appear now and then[14–16]. In addition to possible effects of non-Newtonian behaviors, presence of polymers affects the equilibrium contact angles[17,18]. The reasons are that polymer coils cannot squeeze into narrow corners. When they do, the solution becomes non-wetting even though the solvent may be wetting. Such issues also arise when squeezing polymer molecules into fine pores[19], however those are not being considered here.

Below, we present data on dynamic contact angles measured when a flat plate is inserted vertically into a liquid-liquid interface or withdrawn from it. The top liquid is silicone oil with fixed viscosity 100cSt, and the bottom liquid is the polymer solution with various concentrations. The polymer used is polyethylene oxide (PEO) of molecular weights of 300K and 4M at various concentrations. We have chosen PEO because PEO is a linear uncharged polymer and is easy to characterize. We also use polyethylene

terephthalate (PET) sheet as the solid substrate for ease of measurement. Correlations produced in this manner, will not exclude the cases of small or large equilibrium contact angles. We follow our previous work on dynamic wetting by polymer solutions under air quite closely[16] and will refer to it as part I (paper II).

2. EXPERIMENTAL

Polyethylene terephthalate (PET) sheets were cut and used as such (same as in part I (paper II)). They have a tolerance of ± 1.25 μm and under microscope (40X) no bumps or patches were seen on the surface. The polymer polyethylene oxide (PEO) was dissolved in distilled water at 1-5 gm/dl concentrations for PEO of molecular weight 3 $x10^5$ (300K), as well at 0.15 - 2 gm/dl for PEO of molecular weight 4 $x10^6$ (4M) same as in de Ryck and Quéré[20]. As these are polymers of very large molecular weights and can tear on too much stirring, they were dissolved in distilled water and left on a shaker for a day after which the solutions were stored sealed for a month, by that time they turned homogeneous. The solutions prepared are the same ones used in part I (paper II). They were characterized for their rheological properties using Haake rheometer the results of which have also been given there. The difference between part I (paper II) and the present problem is that air as the top fluid has been replaced by polydimethylsiloxane. Thus to the above polymer solutions polydimethylsiloxane oil (PDMS) at 100 cSt was added. To prevent any effect of mass transfer, the immiscible mixtures were hand shaken to form emulsions, and then left on shaker for a day. They were then left to stand where they formed two phases. The systems were then centrifuged to make the separation certain.

Equilibrium advancing contact angles were measured through the aqueous phase in a Ramé-Hart contact angle goniometer. The ambient fluid was PDMS previously equilibrated with the aqueous phase, which was lightly colored by using a small amount of potassium permanganate. The base plate was tilted up to 70º, and the angle at the leading edge is the advancing equilibrium contact angle. It was found that this value steadied very quickly with increasing tilt angles and showed no change beyond tilt angle of ~ 30º.

The advancing and receding dynamic contact angles were measured using Cahn Thermo device. It is a balance to which the PET plate is attached. The beaker contains the two immiscible liquids placed on a motorized stage is moved up or down at 42, 82, 164 and 328 μm/s traversing the interface. The force that is measured is the weight of the plate less buoyancy forces and if the value of perimeter *P* and surface tension are supplied,

$$F = W - HP\rho_L g + P\gamma\cos\alpha \qquad (2)$$

α can be calculated. Eq. (2) applies to air-liquid system. The same holds for liquid-liquid system except that ρ_L is replaced by ρ_L less the density of the upper liquid. The plate can cut through only the liquid-liquid interface, starting with it being fully immersed in one liquid and finishing with it fully immersed in the other liquid over the distance of travel of 1 cm. The procedure that we use is first advancing then receding the plate, both at the lowest velocity. This is followed by the same at the next higher velocity, etc., until the set is complete. The entire set is redone to check reproducibility. Although the advancing dynamic contact angle values are reproducible to ~ 1º, the receding values are unsatisfactory with variations up to 15º.

We repeat here that the lower liquid is the aqueous solution of PEO (B) and the upper liquid is the silicone oil (A). All contact angles reported in the next section are those through the aqueous phase, fluid B in Figure 1.2.

Other than measuring the dynamic contact angles, Cahn Thermo can also be using to measure interfacial tension. It measures $\gamma.\cos\lambda$. If λ is measured separately using a contact angle goniometer, the interfacial tension can be calculated. Because the measured interfacial tensions were low, we also checked our results using du Nuoy ring. In one case only du Nuoy ring could be used. The method is described in Figure 2.1.

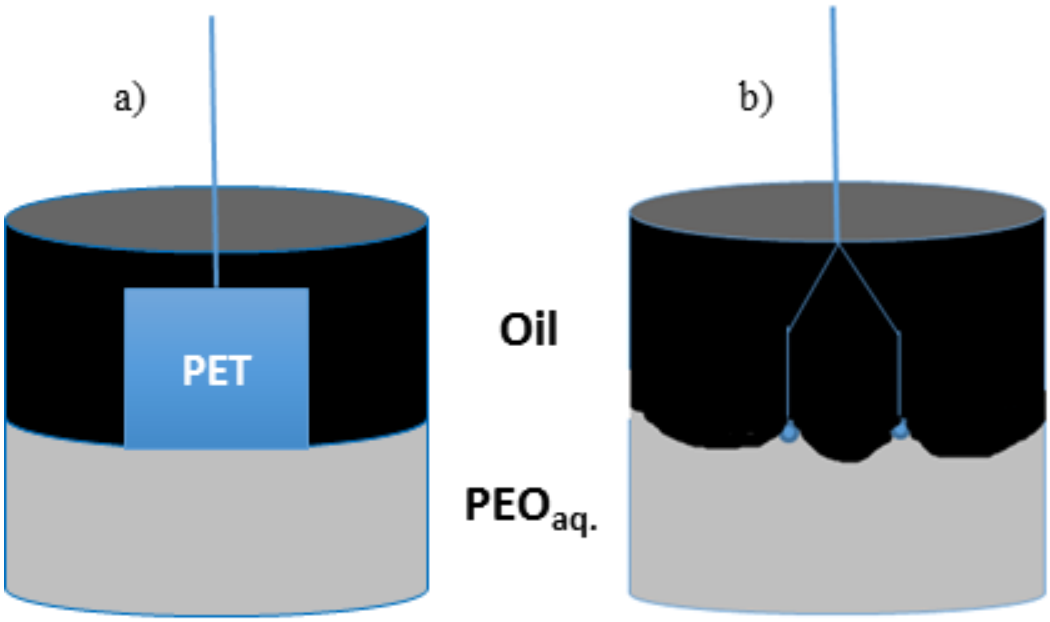

Figure 2.1. Schematic shows IFT techniques: a) Wilhelmy plate, b) duNuoy ring.

3. RESULTS AND DISCUSSION

The advancing equilibrium contact angles measured (through the aqueous phase) are shown in Figure 3.1.

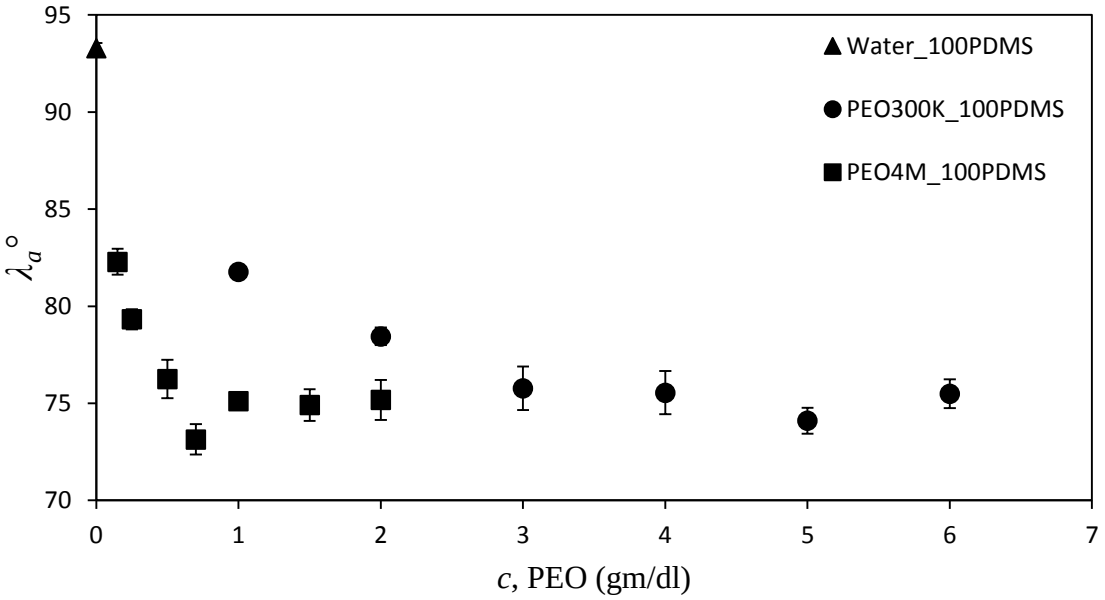

Figure 3.1. Advancing equilibrium contact angles for oil-aqueous PEO solutions are shown. Initially the drop in the value is large followed by levelling off.

The substrate moves towards becoming water wet by more than 15º. We do not know what causes this behavior, but in systems where PEO is replaced by air in part I (paper II), the addition of polymer in water initially also decreases the advancing equilibrium contact angle similarly, but no significant changes are seen with subsequent increase in polymer concentration.

Similarly, the surface tension at oil-water interface as shown in Figures 3.2 and 3.3 for PEO 300K and 4M respectively also reduces substantially on introducing the polymer in water. PEO must adsorb at the oil-water interface for the surface tension to decrease even though oil is very hydrophobic and the polymer very hydrophilic. Both decrease in contact angle (from the water side) and decrease in interfacial tension, would improve oil recovery. It is noteworthy that the surface tension also changes similarly when PEO is replaced by air as observed in part I (paper II).

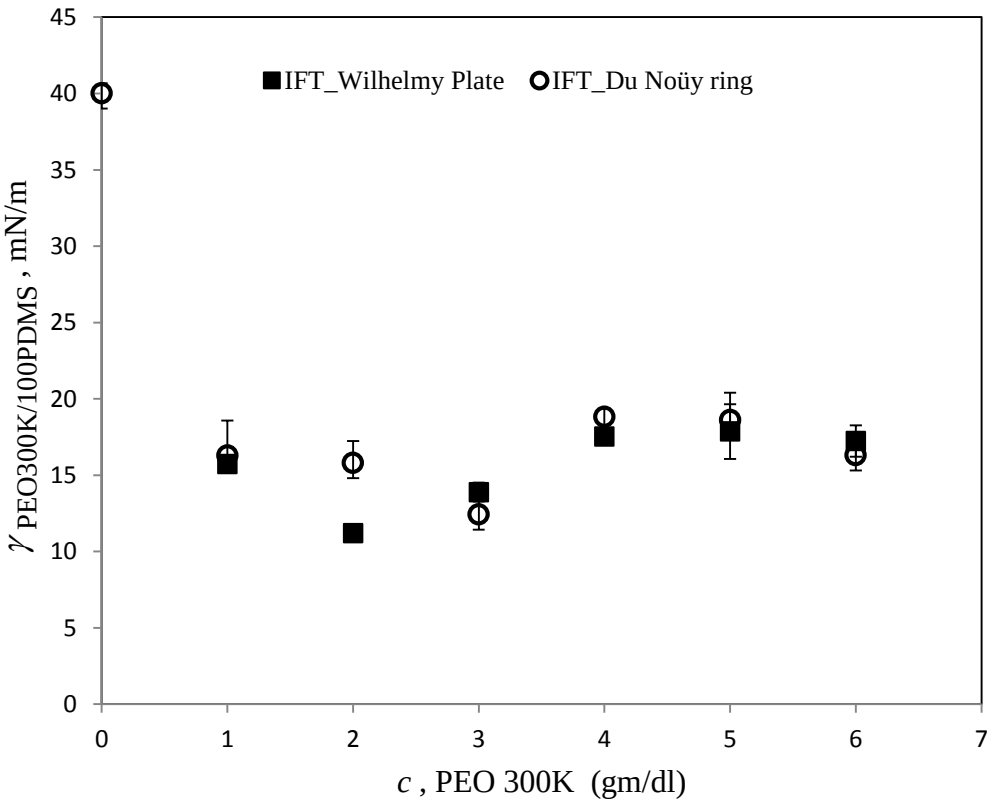

Figure 3.2. Interfacial tension measurements using Wilhelmy plate and Du Nouy ring techniques for oil-aqueous polymer PEO 300K system versus PEO 300K polymer concertation.

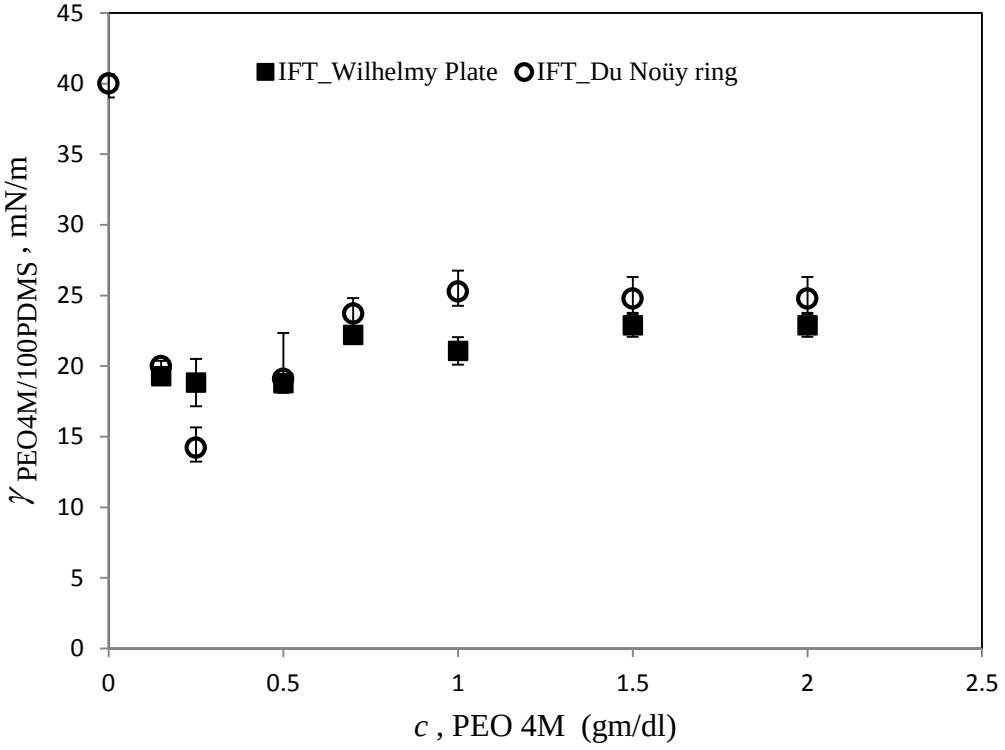

Figure 3.3. Interfacial tension measurements using Wilhelmy plate and Du Nouy ring techniques for oil-aqueous polymer PEO 4M system versus PEO 4M polymer concertation.

The advancing dynamic contact angles have been plotted in Figures 3.4 and 3.5 for PEO of two molecular weights 300K and 4M, in a form suited for comparison with a model called the modified de Gennes[21]-Huh-Scriven[22] model (mdHS) where a function of α is plotted against Ca_B. Here $Ca_B = \frac{\mu_B U}{\gamma_{A/B}}$ is the capillary number of the lower liquid, polymer solution. Its viscosity $\mu_B = \mu_o$ is the zero shear viscosity reported in part I (paper II). The model along with the physical basis are given in the Appendix[16]. The important feature in the plots is that in mdHS model both liquids are Newtonian. There is no sign of shear

thinning or elastic behaviors that have been observed in part I (paper II) for the same polymer solutions under air.

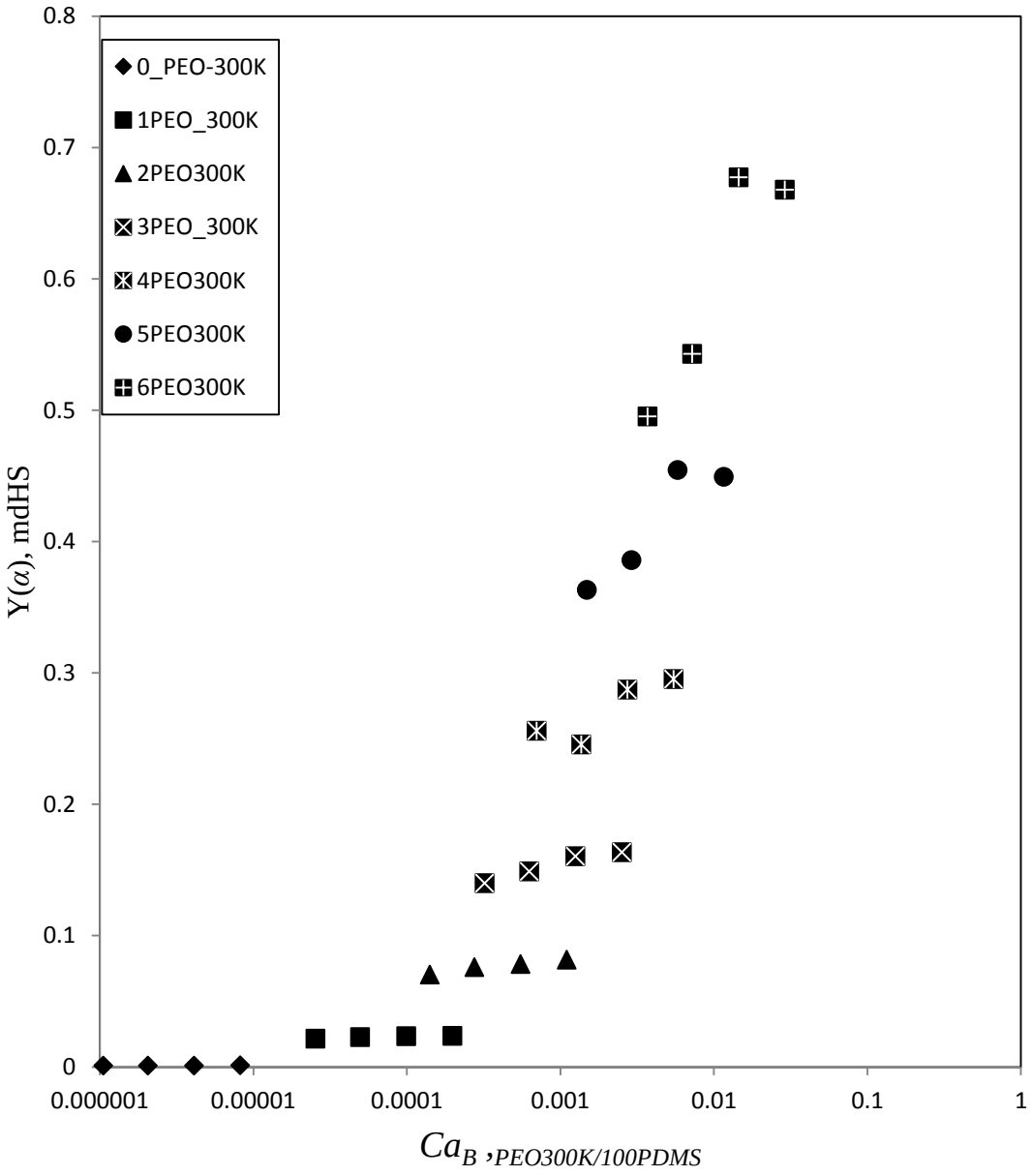

Figure 3.4. The advancing dynamic contact angles have been plotted for PEO 300K in a form suited for comparison with modified de Gennes-Huh-Scriven model (mdHS) where a function of α is plotted versus Ca_B.

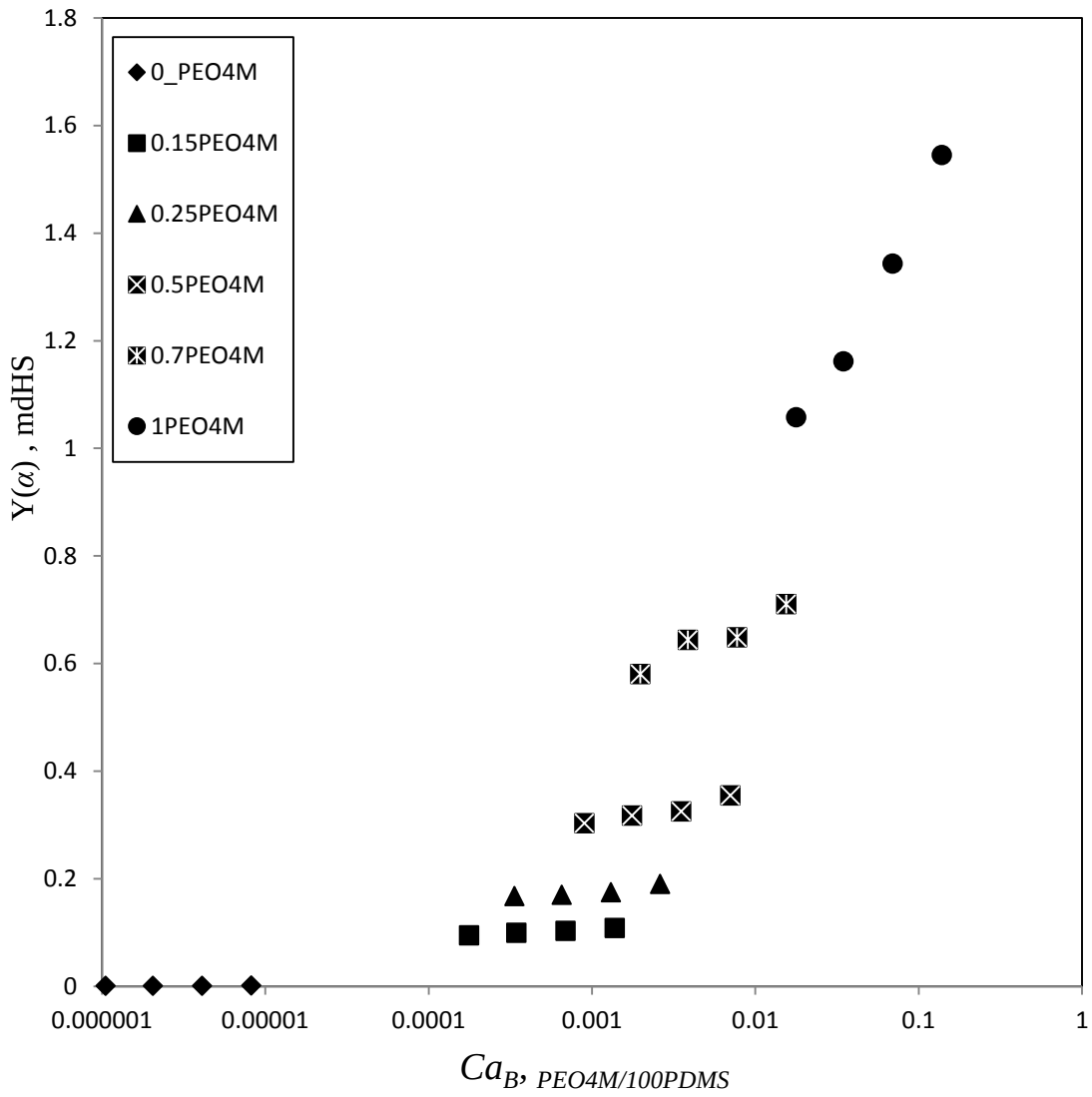

Figure 3.5. The advancing dynamic contact angles have been plotted for PEO 4M in a form suited for comparison with modified de Gennes-Huh-Scriven model (mdHS) where a function of α is plotted versus Ca_B.

The data fit a straight line in the main suggesting that the approximate model is reasonable. The straight lines indicate that intercepts as Ca_B goes to zero are zeros or close, that is equilibrium is attained in that limit. However, some data sets show a peak, and sometimes a smaller peak is observed in part I (paper II). Experimentally we have not

observed anything that explains why that peak happens (such as waves, unstable behavior, etc.), and in any case the model used is too simplified to provide the secondary effects.

In Figures 3.6 and 3.7 the data have been plotted following Cox's[23] results which holds for two Newtonian liquids displacing one another. Cox's[23] results have also been included in the Appendix. The results of fitting are similar to the mdHS case. The major difference lies in the term $\ln\left|\frac{1}{\varepsilon}\right|$.

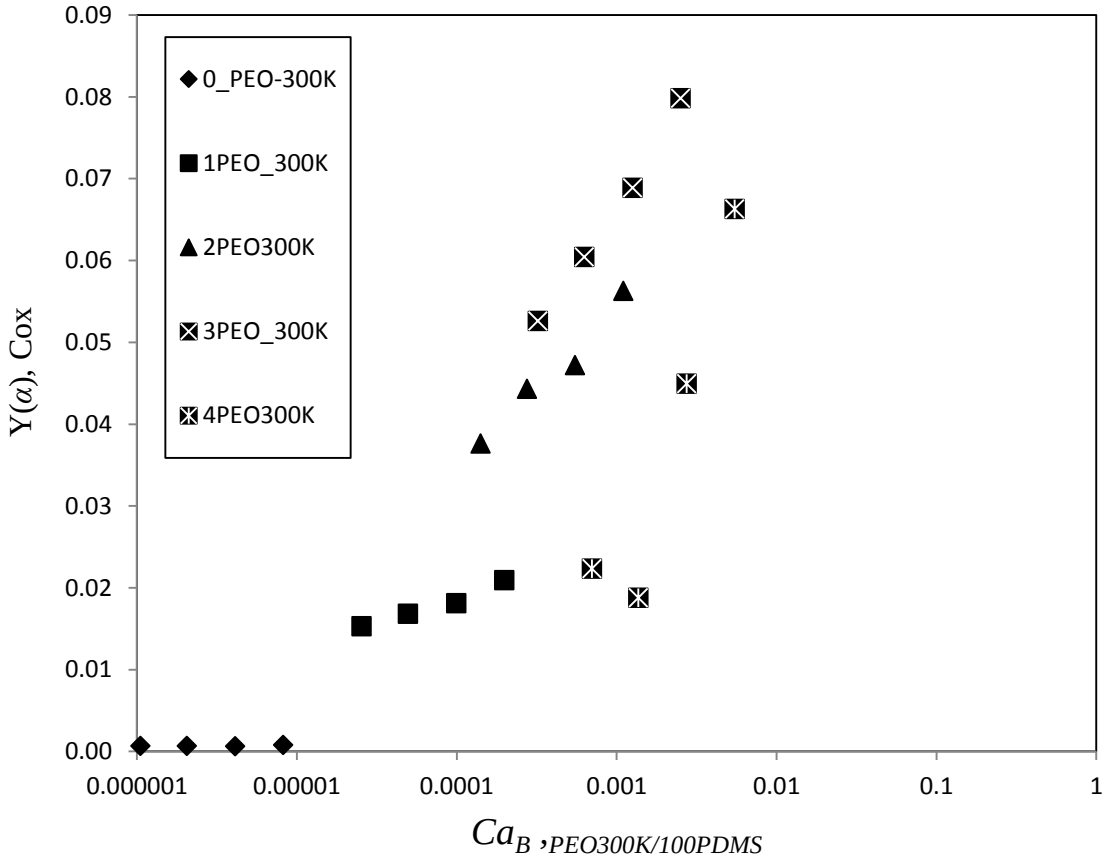

Figure 3.6. The advancing dynamic contact angles have been plotted for PEO 300K in a form suited for comparison with Cox's theory where a function of α is plotted versus Ca_B.

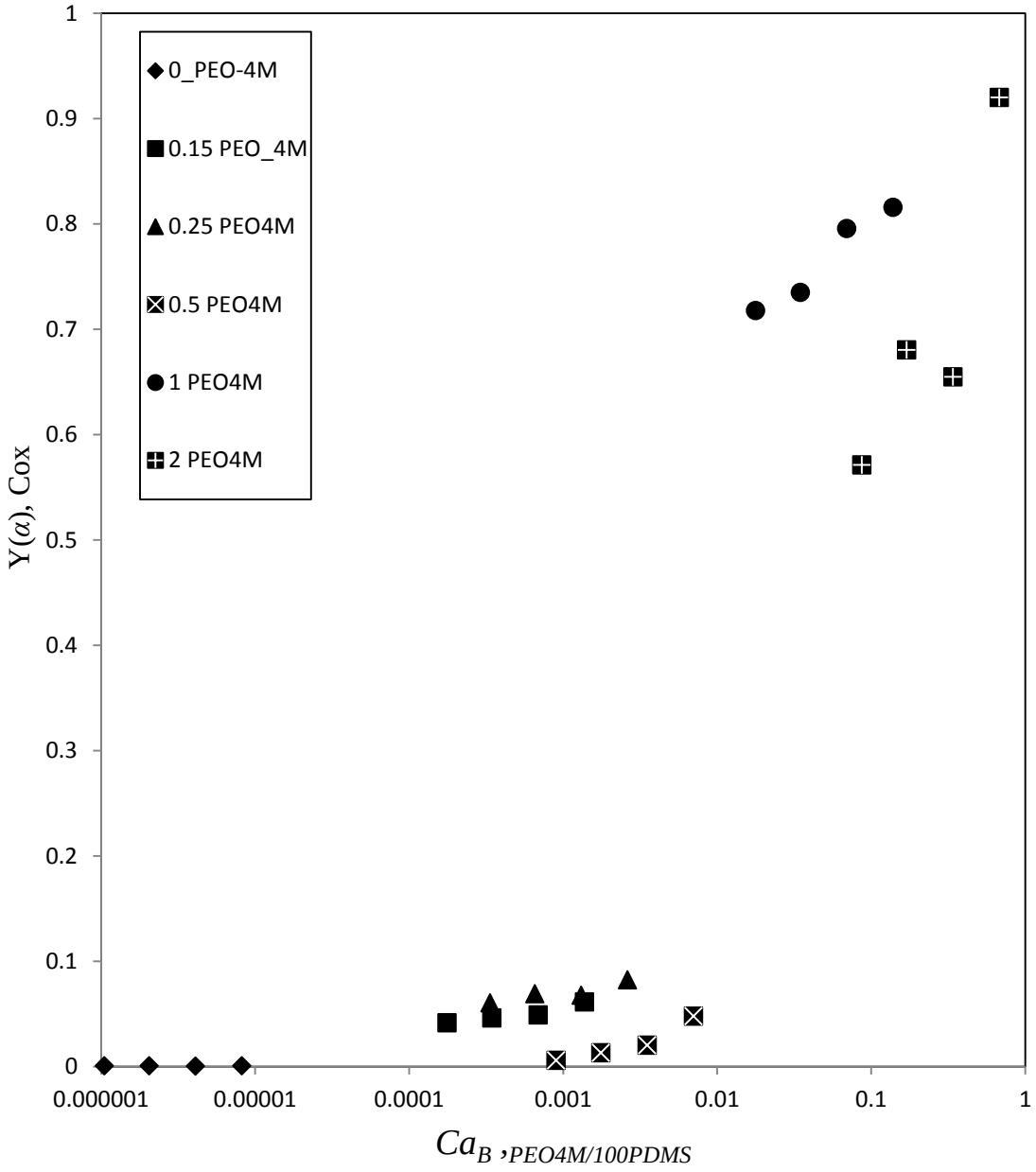

Figure 3.7. The advancing dynamic contact angles have been plotted for PEO 4M in a form suited for comparison with Cox's theory where a function of α is plotted versus Ca_B.

This has been plotted in Figures 3.8 and 3.9 against *R* the viscosity ratio for mdHS, where ε is a small dimensionless cutoff lengths, and Cox's respectively, where ε is a small dimensionless slip length. In both cases a macroscale length scale *L* has been used for non-dimensionalization.

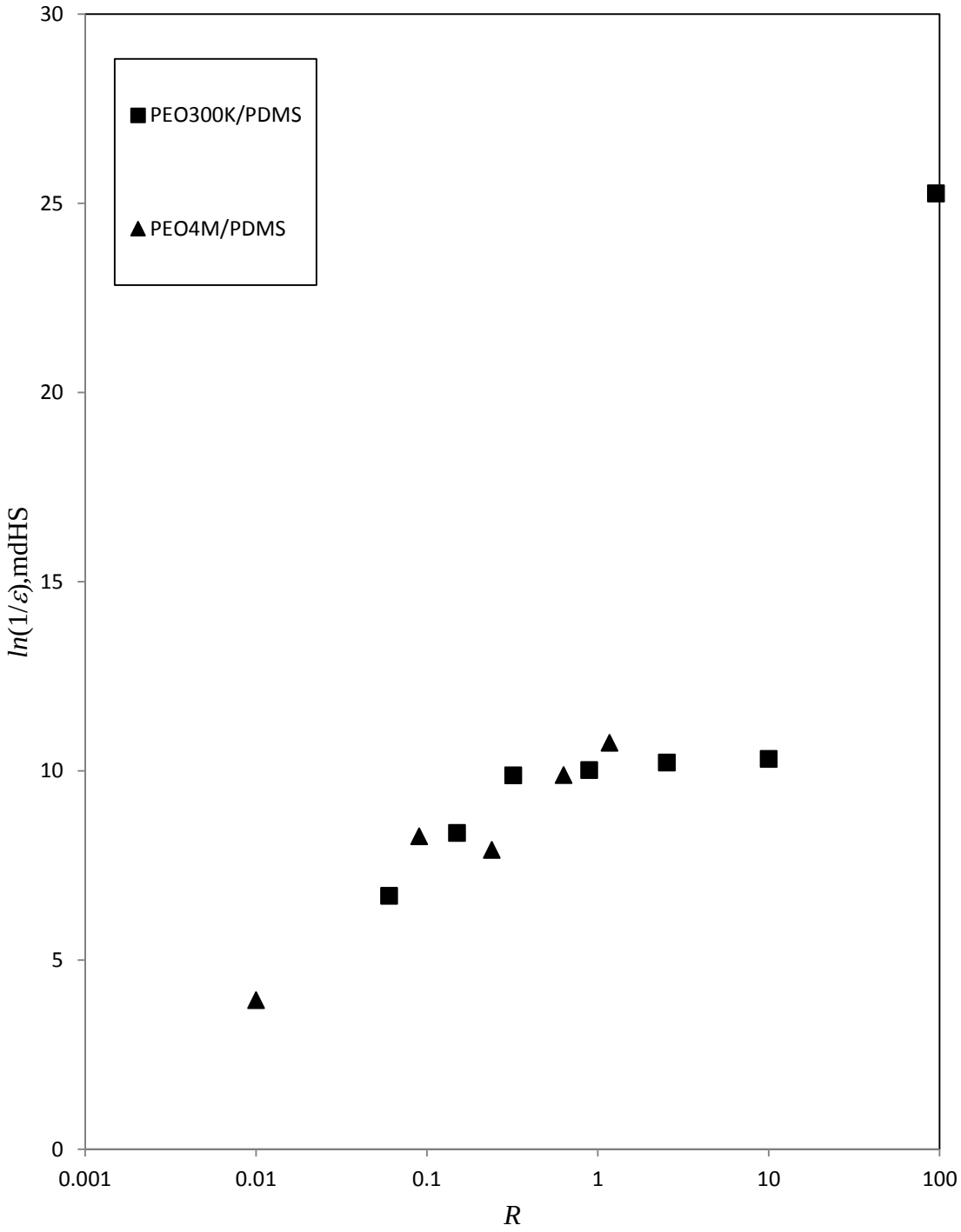

Figure 3.8. The fitting parameter $\ln\left|\frac{1}{\varepsilon}\right|$ calculated by mdHS model has been plotted versus viscosity ratio *R* to the given system.

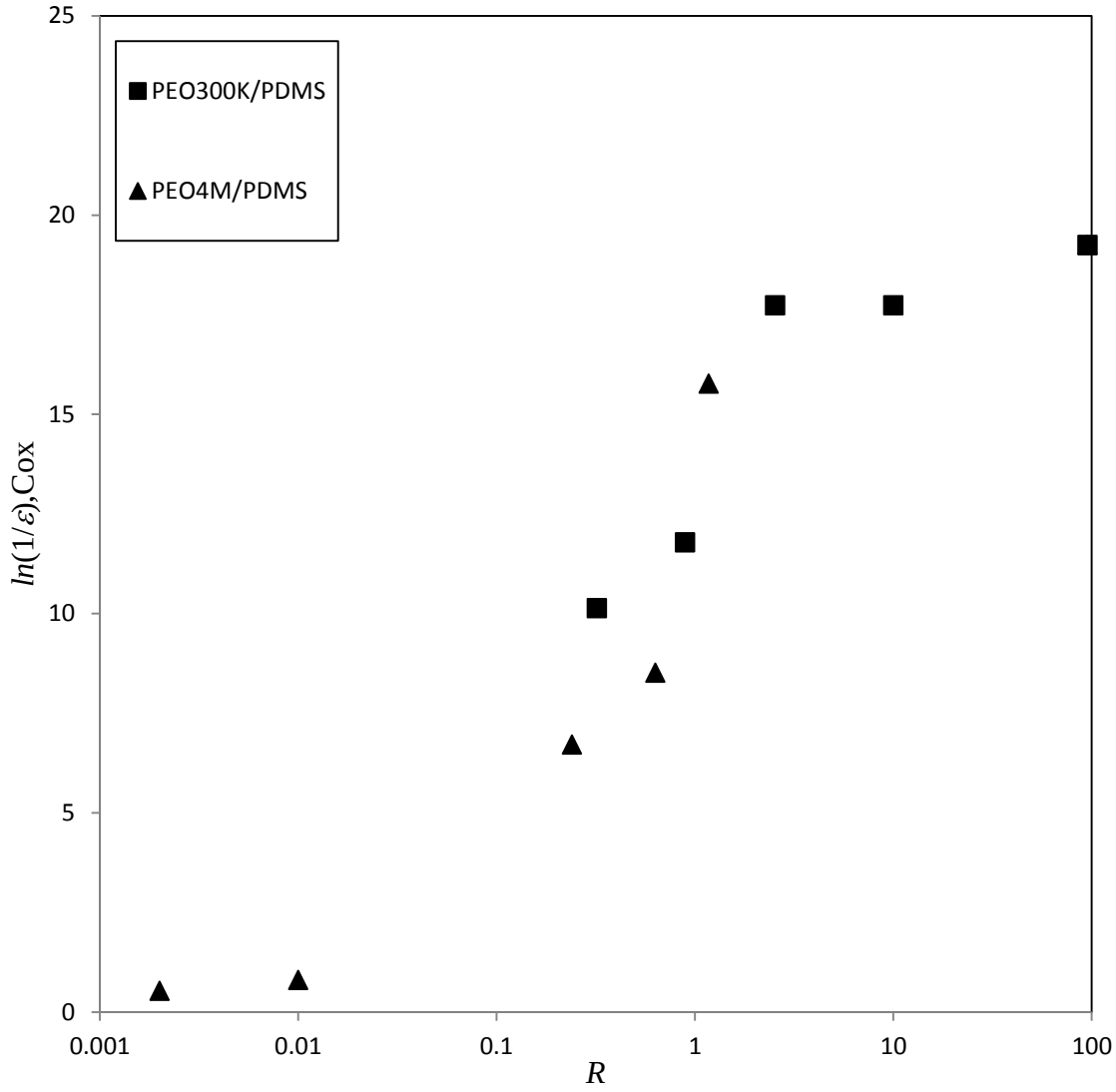

Figure 3.9. The fitting parameter $\ln\left|\frac{1}{\varepsilon}\right|$ calculated by Cox's model has been plotted versus viscosity ratio *R* to the given system.

In part I (paper II), we found that the substrate length, that is, the macrolength *L* decreases with increasing polymer concentrations. If the microlength scale is assumed to depend on surface roughness, then this value is same as in part I and here, as the PET sheets were cut from the same sample. Hence ε increases with increasing polymer concentration

and thus $\ln\left|\frac{1}{\varepsilon}\right|$ decreases with increasing polymer concentration. Since *R* decreases with increasing polymer concentrations, $\ln\left|\frac{1}{\varepsilon}\right|$ should increase with *R* as seen in Figures 3.8 and 3.9.

In the part I (paper II), data of polymer solution under air were very strongly influenced by the shear thinning nature of the liquid. However, many other data for shear thinning fluids show only Newtonian behavior with a viscosity that is the zero shear viscosity for the liquid. A criterion was proposed when the liquid would show shear thinning or Newtonian behavior. However, the criterion was difficult to use and a weaker criterion based on same principles and the parameters describing the shear thinning was used successfully. It showed that indeed the weaker criterion worked to separate the two cases where the parameters were reported. To extend such analysis to liquid-liquid systems is practically impossible because the flow in the ambient liquid can no longer be ignored. The results of part I (paper II) do prepare us to except that shear thinning may or may not show up possibly as all or nothing phenomenon.

Similarly, no obvious effects of elasticity are seen. In part I (paper II), the elastic effects are seen only at high capillary numbers in form of lowered dependence on capillary numbers. Also important is the fact that the Deborah numbers calculated were small but not negligible. Where Deborah numbers were taken to be zero because the first normal stress difference was too small to be measured or measured with accuracy, corresponded well with cases that showed no elastic effects. In the data presented here, we see none of the above elastic effects.

There is a complete shift in the data for the highest concentration in Figure 3.5 (mdHS model and 4M PEO). In Figures 3.6 and 3.7 (Cox's model) and at the higher concentrations, the peak mentioned earlier give way to a maximum and sometimes only show negative slopes and thus were not fitted to the two-Newtonian liquid model. It should be noted that all these unusual results are seen in liquids with high polymer concentrations where elastic effects are significant and not explained by any of the theories.

Like in part I (paper II) we have not included the data for the receding contact angle because of complete scatter. The flow is most likely unstable.

4. CONCLUSION

We find here to a good approximation that the flow of polymer displacing oil is described by a Newtonian liquid with the viscosity given by the zero shear viscosity. Except at high polymer concentrations both mdHS model and Cox's[23] model (see Appendix) can correlate the experimental data. The unknown $\ln\left|\frac{1}{\varepsilon}\right|$ calculated from the data shows good agreement with the viscosity ratio *R*.

APPENDIX

de Gennes[21] made an energy balance that led to a result that viscous dissipation in a wedge containing the contact line equal to the surface work done (less the equilibrium). The viscous dissipation was calculated in a wedge where the interface was given by the equation of a straight line $h = \alpha.x$. If the viscous dissipation is calculated using the fluid mechanical solution by Huh and Scriven[22] for two Newtonian liquids, then we get what we refer to in the text as the modified de Gennes-Huh-Scriven (mdHS) equation:

$$\left(cos\lambda\text{-}cos\alpha\right) = 4.Ca_B.ln\left|\frac{1}{\varepsilon}\right|.\left\{c_B^2\left[\frac{\alpha}{2}+\frac{sin2\alpha}{4}\right]\text{-}c_B d_B\left[\frac{1\text{-}cos2\alpha}{2}\right]+d_B^2\left[\frac{\alpha}{2}\text{-}\frac{sin2\alpha}{4}\right]+R\left(\begin{array}{l}c_A^2\left[\frac{\pi}{2}\text{-}\frac{\alpha}{2}\text{-}\frac{sin2\alpha}{4}\right]\\ \text{-}c_A d_A\left[\frac{cos2\alpha\text{-}1}{2}\right]+d_A^2\left[\frac{\pi}{2}\text{-}\frac{\alpha}{2}+\frac{sin2\alpha}{4}\right]\end{array}\right)\right\} \quad \text{(A-1)}$$

$$c_B = \frac{sin^2\alpha\left[sin^2\alpha-\delta^2+R\left(\delta\alpha-sin^2\alpha\right)\right]}{D} \quad \text{(A-2)}$$

$$d_B = \frac{\sin\alpha\cos\alpha\left[sin^2\alpha-\delta^2+R\left(\delta\alpha-sin^2\alpha\right)-R\pi\tan\alpha\right]}{D} \quad \text{(A-3)}$$

$$c_A = \frac{sin^2\alpha\left[sin^2\alpha-\delta\alpha+R\left(\alpha^2-sin^2\alpha\right)\right]}{D} \quad \text{(A-4)}$$

$$d_A = \frac{\sin\alpha\cos\alpha\left[sin^2\alpha-\delta\alpha+R\left(\alpha^2-sin^2\alpha\right)-\pi\tan\alpha\right]}{D} \quad \text{(A-5)}$$

$$D = \left(\sin\alpha\cos\alpha-\alpha\right)\left(\delta^2-\sin^2\alpha\right)+R\left(\delta-\sin\alpha\cos\alpha\right)\left(\alpha^2-\sin^2\alpha\right) \quad \text{(A-6)}$$

$$\delta = \alpha-\pi \quad \text{(A-7)}$$

R is the viscosity ratio and $R = \mu_A / \mu_o$ where μ_o is the zero shear viscosity in B. Now $\ln\left|\frac{1}{\varepsilon}\right|$ comes out of the fact that the stress at the contact line is infinite and it (and immediate vicinity) is excluded from the calculations. The dimensionless term ε is small and represents the size of the region, that is, cutoff length which in the case of rough surfaces is of the order of surface roughness. Thus mdHS model is the consequence of an energy balance. If we move over all terms in α in Eq. (A-1) to the left, we can rewrite Eq. (A-1) as

$$Y(\alpha) = Ca_B \ln\left|\frac{1}{\varepsilon}\right| \tag{A-8}$$

Similarly Cox's[22] results from approximate solution to the fluid mechanical equations are

$$g(\alpha) - g(\lambda) = Ca_B . \ln\left|\frac{1}{\varepsilon}\right| \tag{A-9}$$

$$g(\alpha, R) = \int_o^{\alpha} \frac{d\theta}{f(\theta, R)} \tag{A-10}$$

$$f(\theta, R) = \frac{2\sin\theta\left[R^2\left(\theta^2 - \sin^2\theta\right) + 2R\left\{\theta(\pi-\theta) + \sin^2\theta\right\} + \left\{(\pi-\theta)^2 - \sin^2\theta\right\}\right]}{R\left(\theta^2 - \sin^2\theta\right)\left\{(\pi-\theta) + \sin\theta\cos\theta\right\} + \left\{(\pi-\theta)^2 - \sin^2\theta\right\}(\theta - \sin\theta\cos\theta)} \tag{A-11}$$

Cox's solution assumes that $|\cos\alpha - \cos\lambda|$ are small. Here, $\ln\left|\frac{1}{\varepsilon}\right|$ represents the effects of slip in alleviating infinite stress at the contact line, where ε the dimensionless slip length

is small. For rough surfaces it is of the order of surface roughness. This result is that from force balance and has the same form as Eq. (A-8).

Next are the Figures A1 and A2 show the experimental data of advancing dynamic contact angles versus capillary number for PEO 300K and 4M respectively they were used as displacing fluid to invade the silicone oil (PDMS) over the PET as substrate.

We have prepared the liquid-liquid system in such way to prevent the diffusion through the experiment, first the solution has been shaken and well mixed and left for one night then we use the centrifuge to separate the oil from polymer. Figure A3 shows mixing the two phases in two systems (oil + water) or (oil + polymer). After centrifugation, the first system (oil + water) shows a clear interface and the other system which contains polymer shows a cloud of emulsion at the interface. Figure A4 illustrates the liquid entrained on the solid surface in presence of other immiscible liquid.

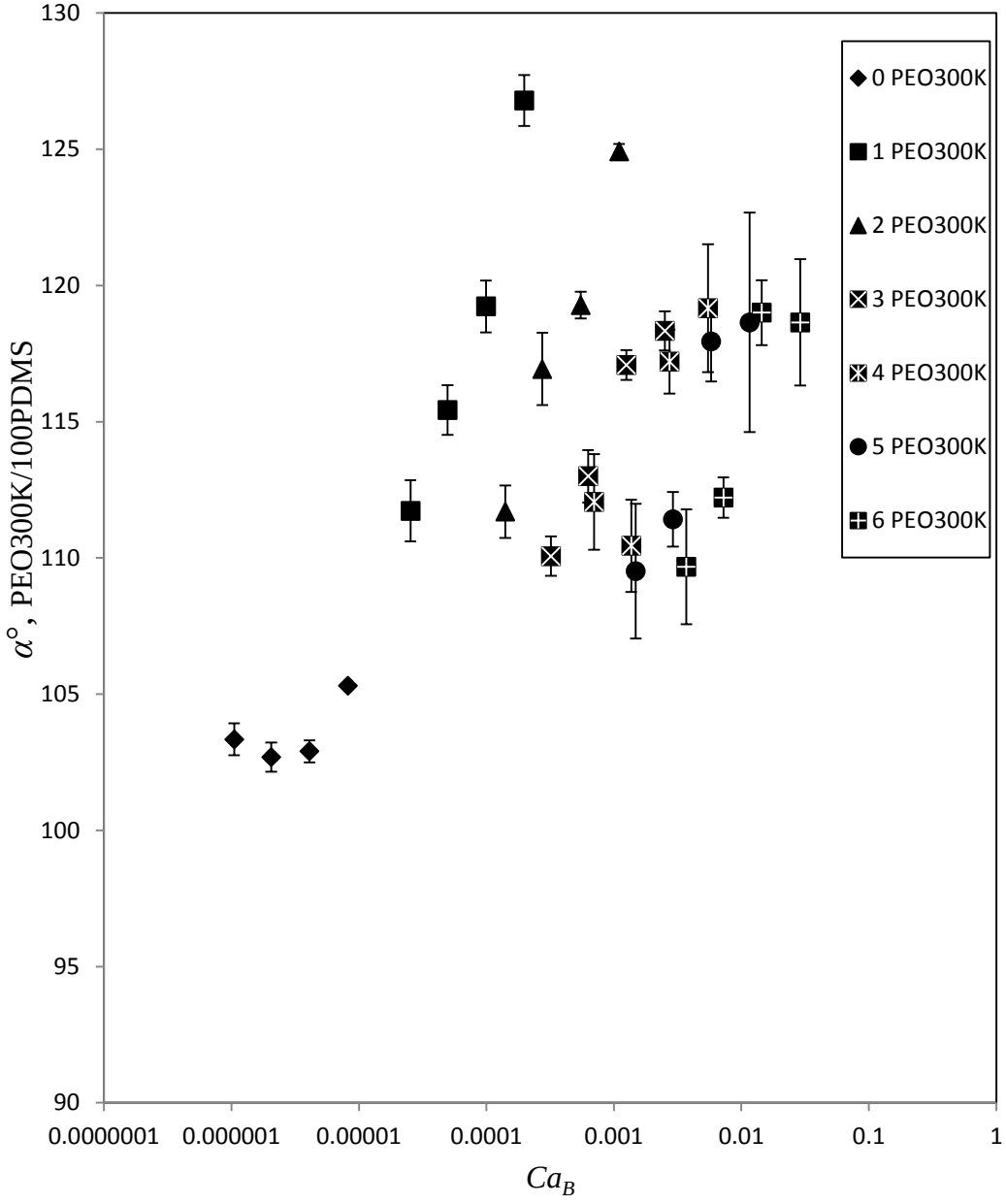

Figure A1. Advancing dynamic contact angles of PEO300K/PDMS/PET vs. Ca_B

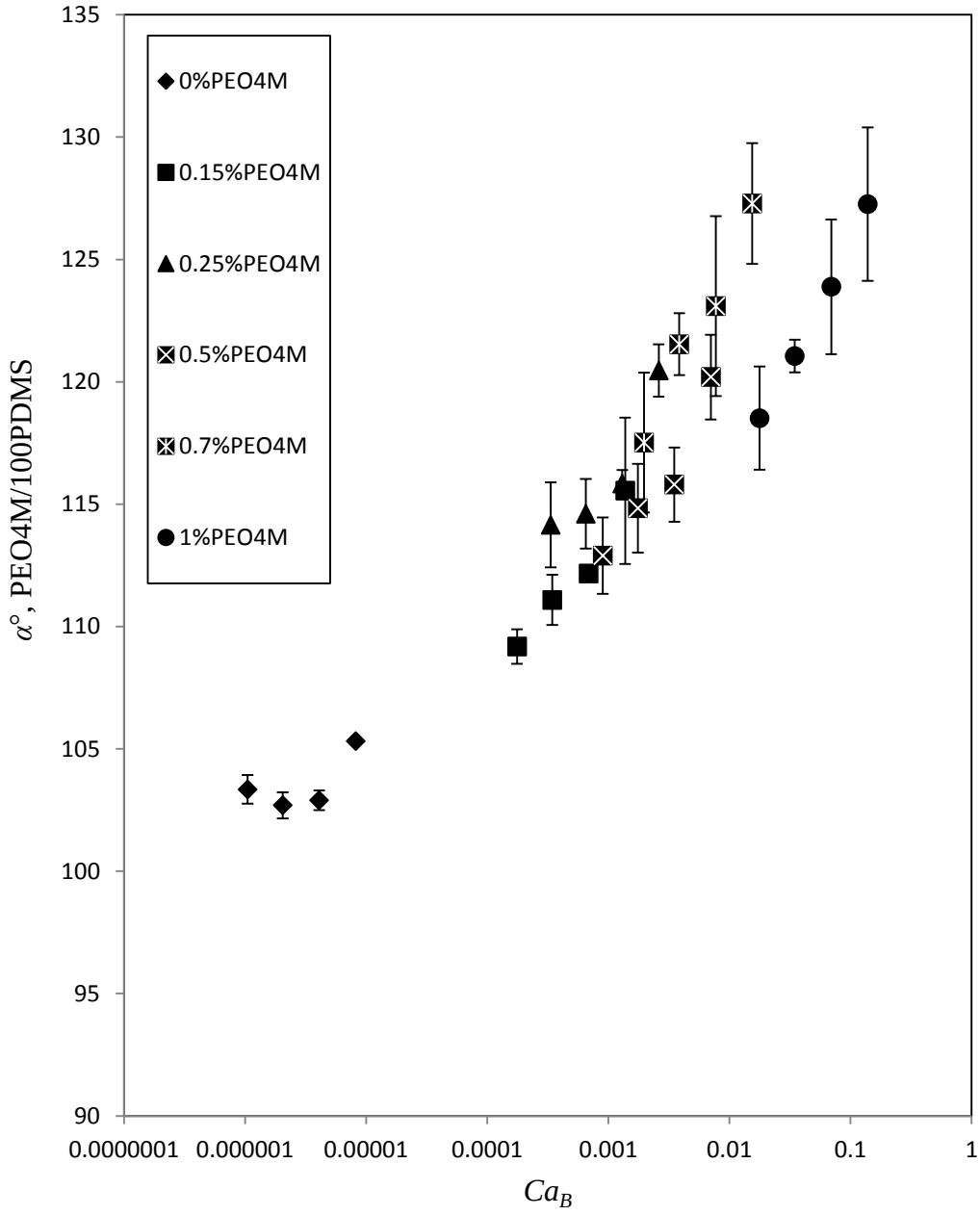

Figure A2. Advancing dynamic contact angles of PEO4M/PDMS/PET vs. Ca_B

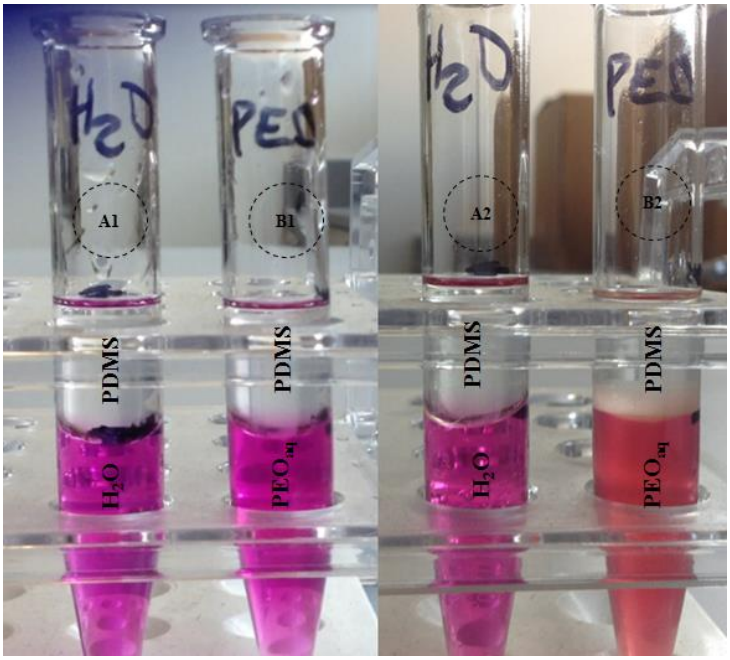

Figure A3. PDMS/PEO solutions were shaking by hand to avoid any mass transfer during the experiment and it is following by centrifugation to separate the phases a part.

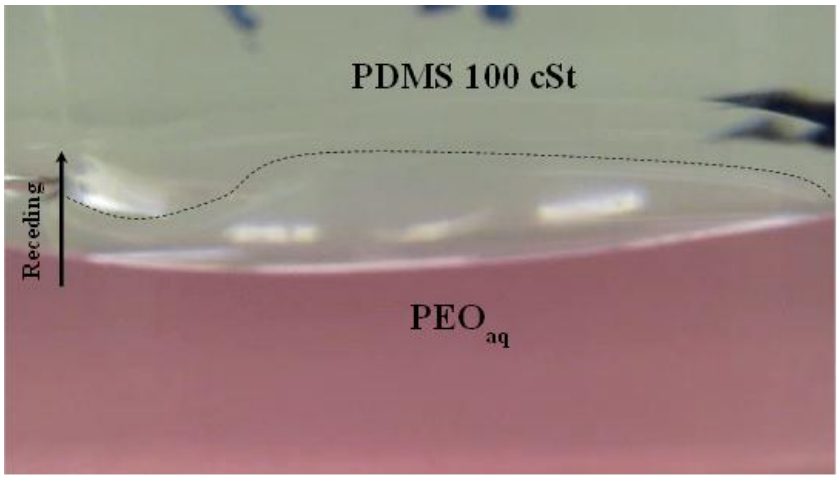

Figure A4. Receding liquid is entrained on the substrate beneath the advancing liquid.

REFERENCES

1. Shah DO, Schechter RS. *Improved Oil Recovery by Surfactant and Polymer Flooding*. Academic Press Inc., New York; 1977. p. 439,487.511.

2. Chang HL. Polymer flooding technology yesterday, today, and tomorrow. *J. Pet. Tech.* 1978;30(8):1113–1128.

3. Littmann W. *Polymer Flooding*. Elsevier Science. 1988.

4. Wang D, Dong H, Lv C, Fu X, Nie J. Review of practical experience of polymer flooding at Daqing. *SPE Reserv. Eval. Eng.* 2009;12(3):470–476.

5. Seright R.S. Potential for polymer flooding reservoirs with viscous oils. *SPE Reserv. Eval. & Eng.* 2010;13:730–740.

6. Dawson R, Lantz R. Inaccessible pore volume in polymer flooding.*SPE J.*1972;12:448–452.

7. Wooding RA, Morel-Seytoux HJ. Multiphase fluid flow through porous media. *Annu. Rev. Fluid Mech.* 1976;8:233–274.

8. Xue HT, Fang ZN, Yang Y, Huang JP, Zhou LW. Contact angle determined by spontaneous dynamic capillary rises with hydrostatic effects: Experiment and theory. *Chem. Phys. Lett.* 2006;432:326–330.

9. Joos P, Van Remoortere P, Bracke M. The kinetics of wetting in a capillary. *J. Colloid Interface Sci.* 1990;136(1):189–197.

10. Craig FF. *The Reservoir Engineering Aspects of Waterflooding*. Dallas: Soc. of Petroleum Engineers of AIME; 1971. p. 142.

11. Al-Shareef A, Neogi P, Bai B. Dynamic contact angles in liquid-liquid-solid systems. Under Journal Rev.

12. Keller A. A., Broje V, Setty K. Effect of advancing velocity and fluid viscosity on the dynamic contact angle of petroleum hydrocarbons. *J. Pet Sci Eng.* 2007;58(1-2):201–206.

13. Neogi P, Ybarra RM. The absence of a rheological effect on the spreading of small drops. *J. Chem Phys.* 2001;115(17):7811-7813.

14. Carré A, Eustache F. Spreading kinetics of shear-thinning fluids in wetting and dewetting modes. *Langmuir*. 2000;16(6):2936–2941.

15. Rafaï S, Bonn D. Spreading of non-Newtonian fluids and surfactant solutions on solid surfaces. *Phys A Stat Mech its Appl.* 2005;358:58–67.

16. Al-Shareef A, Neogi P, Bai B. Wetting kinetics of polymer solutions and force based contact angles. Under Journal Rev.

17. Nieh S-Y, Ybarra RM, Neogi P. Wetting kinetics of polymer solutions. Experimental observations. *Macromolecules*. 1996;29(1):320–325.

18. Ybarra RM, Neogi P, MacElroy JMD. Osmotic stresses and wetting by polymer solutions. *Ind Eng Chem Res.* 1998;37(2):427–434.

19. de Gennes PG. *Scaling Concepts in Polymer Physics*. Ithaca, United States: Cornell University Press; 1979. p. 34 p.

20. de Ryck A, Quéré D. Fluid coating from a polymer solution. *Langmuir*.1998;14(7):1911–1914.

21. de Gennes PG. The dynamics of a spreading droplet. *C R Acad Sci,Ser II Mec, Phys, Chim, Sci Terre Univers*. 1984;298(4):111–115.

22. Huh C, Scriven L. Hydrodynamic model of steady movement of a solid/liquid/fluid contact line. *J. Colloid Interface Sci.* 1971;35(1):85–101.

23. Cox RG. The dynamics of the spreading of liquids on a solid surface. Part 1. Viscous flow. *J. Fluid Mech.* 1986;168:169–194.

SECTION

2. CONCLUSIONS & RECOMMENDATIONS FOR FUTURE WORK

2.1. CONCLUSIONS

In this dissertation, we present a comprehensive comparison to our experimental data of dynamic contact angles with our mathematical models for Newtonian and non-Newtonian fluids. We introduce a solution to the fluid mechanical problem at low Reynold number in a variety of fluid flow systems. We shed light on the dynamic contact angles in a diverse set of multiphase flows. The corresponding applications to the present study involve coating flow problems and enhanced oil recovery (water flooding and polymer flooding).

To draw a conclusion, in paper I, we introduce concept of de Gennes' that states the total viscous dissipation is equal to the surface work done at immediate vicinity of the contact line. We present an algebraic model dHS (de Gennes' Huh Scriven) that predicts the dynamic contact angles in gas-liquid systems and such model shows an excellent fit to the experimental data for advancing and receding dynamic contact angles. Liquid entrainment occurs in the receding dynamic contact angles in the liquid-air systems at sufficiently large speed of the substrate.

In paper II, we present the dynamic wetting of non-Newtonian shear thinning polymer solutions. This study observed the effect of the shear thinning and elastic behavior of two molecular weight polyethylene oxide on the dynamic contact angles under air. The three low polymer concentrations have shown the fitted shear thinning exponent conforms to that measured *n* using Haak rheometer. Conversely, the other three large polymer concentrations have shown shear thinning exponent to be quite different and small. The

present theoretical work shows that the elastic effect becomes important at larger polymer concentrations that reduce the dependence on capillary number. The theory also indicates why the dynamic contact angles follow power law in this example instead of showing Newtonian behavior with zero shear viscosity when the shear thinning effects are considered.

In paper III, we present the water flooding problem to understand the interfacial phenomena at water-oil interface. Different viscosities of silicone oil have been used as upper phase and the lower phase is fixed at water. To the best of our knowledge, the water is displacing the silicone oil over two different substrates PET and PVC. We observed that in the advancing case the comparison of the experimental data to our mdHS (modified de Gennes' Huh Scriven) and theory of Cox show that the length scale is dependent on the viscosity ratio. In the receding case, the fitting has shown a broad range of scattering and can be attributed to the instability of the contact line. Close-up photographs also show that the contact line is unstable.

In paper IV, we have introduced a further treatment process of polymer flooding, which used to minimize the mobility ratio when water flooding fails to recover high viscosity oil from the reservoir. The viscous fingering problems appeared when the oil is much more viscous than that in drive water. Here, we investigate the dynamic contact angles when silicone oil with fixed viscosity is displaced by different polyethylene oxide solutions. We have observed a decline in the IFT and aqueous droplet advancing equilibrium contact angles of the PDMS-PEO system when polymer concentration is increased.

2.2. RECOMMENDATIONS FOR FUTURE WORK

This dissertation provides a comprehensive theoretical and experimental study to the dynamic contact angles in multiphase flow systems. We shed light on the three phase contact line problem and we have established a fundamental base to the contact angle under dynamic conditions in the immediate vicinity of the contact line. We have summarized some points that can benefit future researchers as following:

- ❖ It will be worth if a future study followed this current work to include a surfactant together with PEO to see how that affects the wettability of the solid surface, interfacial tension and dynamic contact angles.
- ❖ The oil displacement here is on the Wilhelmy plate whether in air flooding, water flooding or polymer flooding, in such displacement it would be important if a future researcher conducted this experiment in non-uniform geometry (Non-uniform Hele-Shaw) or microfluidic device. It would be much clearer to observe the contact line and its stability through the oil displacement.
- ❖ Here we extensively cover the fitting of our theoretical models to our experimental data. A simulation study is recommended as a third choice for comparison. For example “Surface evolver” is a promising simulation program could introduce new ideas for contact line problems.

REFERENCES

Adamson W. & Gast, A. (1997) Physical Chemistry of Surfaces, 6th edition John Wiley and Sons, New York, p.352,353,362.

Bai B., Liu Y., Coste JP, Li L. (2007a). Preformed Particle Gel for Conformance Control: Transport Mechanism through Porous Media, SPE Reservoir Evaluation and Engineering. April 2007a, 176-184.

Bai B., Li LX, Liu Y.Z, Liu H, Wang Z., You C. (2007b). Conformance Control by Preformed Particle Gel: Factors Affecting its Properties and Applications. SPE Reservoir Evaluation and Engineering, Aug 2007b, 10 (2), 415-421.

Bascom, W., Cottington, R., Singleterry, C., 1964. Dynamic surface phenomena in the spontaneous spreading of oils on solids, in: Gould, R. (Ed.), Contact Angle, Wettability, and Adhesion. American Chemical Society, Washington, D. C., pp. 355–380.

Blake, T. D. & Ruschak, K. J.(1979). A maximum speed of wetting. Nature 282, 489-491.

Blake, T.D., (1993). Dynamic contact angles and wetting kinetics, in: Berg, J.C. (Ed.), Wettability. Marcel Dekker, Inc., New York, pp. 251–309.

Brochard-Wyart, F., Meglio, J., Quéré, D., de Gennes, P., (1991). Spreading of nonvolatile liquids in a continuum picture. Langmuir 12, 335–338.

Cox, R.G., (1986). The dynamics of the spreading of liquids on a solid surface. Part 1. Viscous flow. J. Fluid Mech. 168, 169–194. doi:10.1017/S0022112086000332

Craig, F.F., Jr. (1971) The reservoir aspects of water flooding, SPE Dallas, TX.

de Gennes PG (1986) Deposition of Langmuir-Blofgett layers. Colloid Polym. Sci. 264:463–465.

Derjaguin,B.V. (1940). A theory of capillary condensation in the pores of sorbents and of other capillary phenomena taking into account the disjoining action of polymolecular liquid films, Zh. Fiz. Khim., 14,137-147.

Fermigier, M., Jenffer, P., (1991). An experimental investigation of the dynamic contact angle in liquid-liquid systems. J. Colloid Interface Sci. 146, 226–241.

Foster, W.R, (1973). A low-tension waterflooding process, *SPE J.*, 25, 205-210.

Frumkin, A.N. (1938). Wetting and adherence of bubbles, Zh. Fiz. Khim., 12,337-345.

Green, D.W., and Wilhite, G.P. (1998) Enhanced Oil Recovery, SPE Dallas, TX.

Gutoff, E.B., Kendrick, C.E., (1982). Dynamic contact angles. AIChE J. 28, 459–466.

Landau, L. & Levich, B.(1942). Dragging of a liquid by a moving plate. Acta Physicochim. (USSR)17, 42–54.

Miller, C. & Neogi, P. (2007) Interfacial Phenomena: Equilibrium and Dynamic Effects. Marcel Dekker, New York.

Neogi P. (1987) Oil recovery and microemulsions, in Microemulsions: Structure and Dynamic, S.E. Friberg and P. Bothorel, eds., CRC press, Boca Raton, Fl., p.197.

Quéré, D. (1991). On the minimal velocity of forced spreading in partial wetting. C.R. Acad. Sci.Paris II 313, 313-318.

Slattery, J.C. (1974) Interfacial effects in the entrapment and displacement of residual oil. AIChE Journal 20, 1145.

Stegemeier. G.L. (1977) Mechanisms of entrapment and mobilization of oil in porous media. Improved oil recovery by surfactant and polymer flooding, D.O. Shah and R.S. Schechter, eds., Academic Press, New York, p.55.

VITA

Amer Mohammad Al-Shareef was born and bred in Al Khums city located on the Libyan coast of the Mediterranean Sea. He received his BS degree in Chemical Engineering from University of Elmergib in 2002. He attended The National University of Malaysia in 2004 and he received his M.Sc. in Chemical Engineering in 2006. He was employed as a lecturer in Chemical Engineering Department at Elmergib University in 2007. In fall of 2011, he joined the Chemical and Biochemical Engineering Department at Missouri University of Science and Technology (Rolla, Missouri, USA) and received his Ph.D. in Chemical Engineering in May of 2016.